Nevis 298

FERMILAB-THESIS-2000-20

Search for Neutral Heavy Leptons in a High-Energy Neutrino Beam

Arturas G Vaitaitis

R-1538
CU-404
Nevis-298

Columbia University
Department of Physics
New York, New York 10027

SEARCH FOR NEUTRAL HEAVY LEPTONS IN A HIGH-ENERGY NEUTRINO BEAM

Arturas Vaitaitis

Submitted in partial fulfillment of the
requirements for the degree
of Doctor of Philosophy
in the Graduate School of Arts and Sciences,
Columbia University

National Science Foundation
NSF PHY 98-13383

2000

SEARCH FOR NEUTRAL HEAVY LEPTONS IN A HIGH ENERGY NEUTRINO BEAM

Arturas Vaitaitis
Columbia University, New York, NY 10027

*Research supported by the National Science Foundation.
†Submitted in partial fulfillment of the requirements for the degree of Doctor of Philosophy in the Graduate School of Arts and Sciences, Columbia University.

Abstract

A search for neutral heavy leptons(NHLs) has been performed using an instrumented decay channel at the NuTeV (E815) experiment at Fermilab. The decay channel was composed of helium bags interspersed with drift chambers, and was used in conjunction with the NuTeV neutrino detector to search for NHL decays. Our search was sensitive to isosinglet type neutral leptons with masses between 0.25 and 2.0 GeV. No evidence of NHLs was found. The experiment took place during the 1996-1997 Fermilab fixed-target run. Collected data were examined for NHLs decaying into muonic final states ($\mu\mu\nu$, $\mu e\nu$, $\mu\pi$, and $\mu\rho$). This analysis places limits on the mixing of NHLs with standard light neutrinos at a level up to an order of magnitude more restrictive than previous search limits in this mass range.

Acknowledgements

> "For me there is only the traveling on paths that have heart, on any path that may have heart. There I travel, and the only worthwhile challenge is to traverse its full length. And there I travel looking, looking breathlessly"
>
> *Don Juan*

With this thesis I am finishing an important chapter in my life and it would not be possible without the help and guidance of many people. It is my pleasure to acknowledge those who made the completion of this dissertation possible.

My foremost gratitude goes first of all to my thesis advisor Michael Shaevitz. My decision to devote the best years of my life to research would not be realized without Mike. In our first conversation five and a half years before these acknowledgements, Mike mentioned the decay channel and the possibility of looking for Neutral Heavy Leptons (NHLs). It sounded like science fiction. Some time passed before I got involved with this project and now, five years later, I am happy to present results of our research. During these years I had a great opportunity to live in the scientific community and experience a life of a scientist. I thank Mike Shaevitz for all of this.

It has been a great privilege to work closely with Janet Conrad. She was the driving force behind this research project, from designing the decay channel to the final analysis. During hard times for the decay channel project, I felt safe and sound knowing that Janet was there. I could not have seen the decay channel without Janet.

I am very grateful to members of the NHL group, who directly or indirectly contributed to the NHL search. When Bob Drucker joined our group, the analysis picked up and we were able to present preliminary results in half a year. His attention to details saved me from many coding pitfalls. Sally Koutsoliotis' work was a big part of this research, and it was a pleasure for me to work with such a nice person. Joe Formaggio, my officemate, was the other graduate student working on the NHL search. He contributed greatly to the NHL search, and he was a very pleasant colleague to work with. Eric Zimmerman joined our group recently and quickly got involved into the NHL search. He helped me to write a PRL article on the NHL search results, and

he gave me some very useful critique of my thesis. Pal Nienaber provided some valuable comments and suggestions. I must also thank the students who helped build the decay channel. I remember just a few names: Dave Cohen, Ali Kinkhabwala, Ben Greenbaum, Tiffany Freitas, but this is for every person that I could have not mention.

I consider myself lucky that I have been a member of the NuTeV collaboration. During the time that I spent at the lab hard working and dedicated people surrounded me, which was the excellent research environment. I could only wish that Fermilab was located in New York City, but that would be too perfect for a graduate student life. Dinners and get-together events, playing on a volleyball court for the NuTeV team or all-nighters during owl shifts, it all created the sense of collaboration in the full meaning of that word. I thank every member of the NuTeV collaboration; it was a pleasure.

I have learned a great deal from people who I worked with at the NuTeV experiment. I'd like to thank Tim Bolton for his suggestions on how to improve my analysis and for his help with Monte Carlo simulations. I am still amazed by his knowledge and expertise, not only of technical matters and physics but also of number of other things (including Lithuanian basketball). I thoroughly enjoyed working with Panagiotis Spentzorious and Donna Naples. I have to thank them for their help in bringing up the decay channel electronics. Bob Bernstein and Debbie Harrison made some useful comments on how to include systematic errors in our limit. (Special thanks to Bob for the collaboration donuts.) Conversations with Lucy deBarbaro and Jae Yu, and their rigorous critique were very important for the NHL analysis.

I had the pleasure of being in the company of fellow grad students at Fermilab (Sergey, Dave, Max, Jesse), and at Nevis (Bonnie, Joe), who helped make my time in graduate school more enjoyable. Extra thanks to Sam Zeller, for looking out for decay channel drift chambers and answering my countless questions.

Again, thanks to all people who reviewed my thesis. Your comments, reviews and suggestions have been of invaluable assistance. I thank Bill Seligman for the his help in preparing my thesis defense presentations.

I'd like to thank Jane for her love and caring. She brought much joy and happiness to me, and she made my life at Fermilab a lot more happy than it would have been without her.

I am most grateful to my family for their caring support and encouragement throughout my life. I was blessed with a friendship with my mother, and even now, from across the ocean, she is a source of inspiration for me. I dedicate this thesis to my mother.

Contents

List of Tables

List of Figures

Chapter 1

Introduction

The current understanding of properties of the elementary constituents of matter and their interactions is summarized in the Standard Model (SM). In spite of its success, it is not capable of predicting nor explaining the fermion masses. In particular, the Standard Model only contains neutrinos that are massless and left-handed, but there is no indication of any fundamental reason that neutrinos should have zero mass or left handedness. It is not known why neutrinos are so much lighter than the rest of the leptons, but the reason may be related to more encompassing theories.

Plausible extensions to the SM allow neutrinos to have mass and to have relatively heavy right-handed partners called Neutral Heavy Leptons (NHL). For example, NHLs naturally occur in "grand unification theories" (GUT), which seek to unify the strong and electroweak interactions. In such extensions to the SM, the NHLs do not couple directly to the Z^0 and $W^{\pm}$ bosons, and can be produced and decay via mixing with SM neutrinos.

If observed, NHLs might provide an explanation for the pattern of fermion masses. A better understanding of the origin of neutrino mass would provide knowledge about the expansion of the universe and early formation of large-scale structure. Observation of NHL decays would also be an unambiguous sign of new physics.

This dissertation presents the results of a search for neutral heavy lepton decays at the NuTeV (E815) experiment at Fermilab during the 1996-1997 fixed-target run. This search combined the capabilities of the high intensity neutrino source with an instrumented decay region. The rest of this chapter briefly describes the history of neutrino physics and presents previous NHL searches from other experiments. The chapter concludes with the outline for this thesis.

1.1 Brief history of neutrino physics

Neutrino physics began with a letter from Wolfgang Pauli (Ref. [1, 6]) in 1930. In order to explain the apparent non-conservation of energy observed in nuclear beta decay, he introduced a new particle, the neutrino ("small neutron"). Pauli postulated that this particle was neutral and had spin 1/2 so that energy, electrical charge, and angular momentum would be conserved in this 3-body interaction.

Enrico Fermi moved further by proposing his theory for the $\beta-$decay through $n \to pe\bar{\nu}$ in 1934. The Lagrangian in this theory is

$$L_F(x) = -\frac{G_F}{\sqrt{2}}[\bar{p}(x)\gamma_\lambda n(x)][\bar{e}(x)\gamma^\lambda \nu(x)] + h.c., \tag{1.1}$$

where the fermion field operators are denoted by their particle names, h.c. denotes hermitian conjugate of the preceding term, and

$$G_F \approx 10^{-5}/m_p^2 \tag{1.2}$$

is the Fermi coupling constant with m_p being the proton mass. The cross section for the interaction of the neutrino with matter was believed to be very small.

The first experimental identification of an electron neutrino was made by Reines and Cowan in 1953 (Ref. [7]) in nuclear beta decay. The muon neutrino was observed by Danby *et al.* in 1962 (Ref. [8]) and the tau from tau neutrinos were observed by Perl *et al.* in 1975 (Ref. [9]).

The discovery of parity non-conservation led to the eventual formulation of the V-A theory in 1958 (work of R.P. Feynman, M. Gell-Mann, see Ref. [2]). It was suggested that the effective Lagrangian

$$L_{\text{eff}}(x) = -\frac{G_F}{\sqrt{2}} J_\lambda^\dagger(x) J^\lambda(x) + h.c. \tag{1.3}$$

describes the weak interactions, where the weak current is of the vector-minus-axial (V-A) form.

Further experimental and theoretical achievements led to the modern weak interaction theories by Glashow, Salam and Weinberg, which eventually became part of the more general framework of the SM. This model describes all of the physics of weak and electromagnetic interactions known so far.

More recently neutrinos have been used to probe the SM in the precision electro-weak measurements (see Ref. [3]) and possibly find hints of a physics beyond it.

Neutrinos themselves could indicate new physics through experimental evidence of neutrino mass. A number of experiments have claimed neutrino

oscillation signals. Neutrino oscillations are a necessary consequence of non-zero neutrino mass and mixing between flavors. In 1998, the Superkamiokande experiment claimed discovery of $\nu_\mu \to \nu_x$ oscillations, where ν_x could be the steril or tau neutrino(see Ref. [5]).

1.2 The production and observation of NHLs

Though the direct measurements of the Z-boson invisible width (see Ref. [11, 12]) proved the existence of only three generations of light neutrinos ($m_\nu \leq m_Z/2$), they could not eliminate the presence of heavy weak isosinglets, that do not couple to the Z^0 directly. The absence of weak, strong and electromagnetic charge makes the detection of these particles a hard task. The only way for them to interact in the detector and be observed is through mixing with SM neutrinos. The mixing could be observed as a particle decay. This will be discussed in more detail in Chapter 2. The search for the heavy isosinglets, called Neutral Heavy Leptons (NHLs), could be conducted in neutrino experiments, such as NuTeV experiment, involving production of neutrinos, with subsequent mixing into the NHLs.

1.3 Outline of the thesis

This thesis reports the results of the search for NHLs conducted at the NuTeV detector. The data were collected during the 1996-1997 fixed-target run at Fermilab.

This thesis is organized as follows:

• Chapter 2 discusses the theory of neutral heavy leptons.

• Chapter 4 describes the experimental apparatus, including the accelerator facilities at Fermilab, the neutrino beam, the decay channel and the NuTeV detector.

• Chapter 5 explains the Monte Carlo simulation used for the background estimate and NHL signal simulation.

• Chapter 6 describes the tracking and vertex-finding algorithms, particle identification method, and analysis procedures; it also describes the cuts used to extract the NHL signal.

• Chapter 7 lists the levels of the various backgrounds.

• Chapter 8 describes the sources of systematic uncertainties and their corresponding magnitudes.

- Finally, Chapter 9 presents the results of the NHL analysis, which are summarized below:
  - No evidence has been found for NHL candidates in the 0.25-2.0 GeV mass range.

- Limits were established on the mixing of NHLs with standard light neutrinos, which are as much as an order of magnitude more restrictive than previous search limits in this mass range.

The results of this thesis were published [26], and Appendix C contains the published article. Appendix A demonstrates the chamber alignment procedure and its results along with discussions of detector performance issues. Appendix B is complimentary to Chapter 6, and contains the computer code with the cuts that were used to select NHL candidates.

Chapter 2

Theoretical background

Neutral Heavy Leptons (NHL) arise in some extensions to the Standard Model (SM). NHLs are also referred to in the literature as heavy neutrinos, right-handed neutrinos, or sterile ν. In the text the symbols L^0, N or NHL will be used interchangeably.

In this thesis I will mainly consider only the models where NHLs are isosinglet partners to the SM neutrinos. Isosinglet particles with no charge, like NHLs, do not couple directly to the Z^0 and $W^{\pm}$ bosons, nor to any carriers of weak, strong and electromagnetic interactions. NHLs only mix with the light SM neutrinos in such a way that the observed mixture becomes massive. To explain the process of mixing we have to review the problem of neutrino mass in the SM and introduce the concepts of Dirac and Majorana particles.

The suggestion that a neutrino could be a Majorana particle comes from the possible explanation of the negligible neutrino mass in comparison with the masses of other SM fermions. The SM does not explain why neutrinos are so much lighter than the charged leptons. If we want the usual left-handed neutrino to be strictly massless then we must believe that there is a new exact symmetry preserved at all orders. From my point of view, there is no decent scheme that could introduce such a symmetry. An appealing alternative is that neutrinos, unlike any other fermions, are Majorana particles and have a unique mechanism of mass generation through mixing with heavy isosinglets. In other words, if neutrinos have a very different mass scale, it may be because they are very different types of particles.

According to the simple see-saw model [32] of mixing, the mass of the neutrino is:

$$m_\nu \approx O\left(\frac{m_D^2}{m_{\mathrm{NHL}}}\right), \tag{2.1}$$

where m_{NHL} is the mass of the heavy neutrino (L^0 or, in this thesis, NHL) and m_D is a typical SM Dirac mass.

In this chapter we will talk about Majorana and Dirac neutrinos, explain

the mixing mechanism in the see-saw model and derive NHL properties, such as mixing and mass.

2.1 Mass in the Standard Model

The Langrangian of a single massive Dirac field could be written as:

$$\mathcal{L}_{\mathcal{M}} = -\frac{1}{2}\int d^4x(\bar{\psi}\gamma_\mu\partial^\mu\psi + m_e\bar{\psi}\psi), \tag{2.2}$$

where $m_e\bar{\psi}\psi$ is the Dirac mass term. The parameter m_e in front of the binominal term $\bar{\psi}\psi$ is the mass of the particle, for example the mass of an electron. To preserve hermicity of the Langrangian, m_e has to be real.

In the SM, particle masses are generated by the spontaneous breaking of the $SU(2)_L \times U(1)$ symmetry of the vacuum, which is commonly called the Higgs mechanism. In the Higgs mechanism, a doublet of scalar Higgs fields, Φ, is introduced $\mathbf{\Phi} = \begin{pmatrix} \phi^+ \\ \phi^0 \end{pmatrix}$. The Higgs bosons interact with other particles, for example with an electron:

$$\mathcal{L}_{\mathcal{M}} \quad = \quad \frac{1}{2}h_e(\bar{\nu}_L\bar{e}_L)\Phi e_R + h.c.,$$

where h_e is the Yukawa coupling constant of the electron to the scalar field.

In the process of spontaneous symmetry breaking, the Higgs field develops a vacuum expectation value $<\mathbf{\Phi}>_0 \equiv <0|\mathbf{\Phi}|0> = \begin{pmatrix} 0 \\ \frac{v}{\sqrt{2}} \end{pmatrix}$, where $v =< \phi^0 >$ is the vacuum expectation value of the neutral component of a doublet of Higgs scalar fields. The value of v could actually be derived by measuring the value of a weak coupling and it is : $v = 246GeV$. The Higgs doublet after the symmetry breaking is $\mathbf{\Phi} = \begin{pmatrix} 0 \\ \frac{1}{\sqrt{2}}(\chi + v) \end{pmatrix}$, where χ is a scalar Higgs field after the breakdown. As the result of the symmetry breakdown the Langrangian acquires mass terms:

$$\mathcal{L}_{\mathcal{M}} = \frac{1}{2}h_e(\bar{\nu}_L\bar{e}_L)\begin{pmatrix} 0 \\ \frac{1}{\sqrt{2}}(\chi + v) \end{pmatrix} e_R + h.c. \tag{2.3}$$

$$= \frac{1}{2}\bar{e}_L m_e e_R + \frac{1}{2\sqrt{2}}h_e\bar{e}_L\chi e_R + h.c., \tag{2.4}$$

where h_e is the Yukawa coupling of an electron to ϕ^0 and $m_e = h_e\frac{v}{\sqrt{2}}$ is the mass of an electron. In our example the binominal term $\bar{e}_L m_e e_R$ is actually a Dirac mass term and m_e is the mass of an electron. The second term describes the interaction between the Higgs and electron. The next section discusses

the Dirac and Majorana types in more detail. It appears that the Dirac mass term is invariant under the global phase transformation $\psi \to e^{i\alpha}\psi$, thus it is associated with a conserved quantum number, called "lepton number".

The SM does not have a corresponding Dirac mass terms for neutrinos. Weak interactions couple only to the left-handed currents so the right-handed neutrino ν_R is not present in the Standard Model Langrangian. As the result it is not possible to form $\nu_L m_\nu \nu_R$ terms in the Standard Model.

2.2 Dirac and Majorana neutrinos

Two types of neutrinos originate from the following question: "Is a particle really different from its antiparticle?" While the answer is obvious for charged particles, since the positive are distinct from negative particles by their electromagnetic properties, it is not clear in the case of neutral particles. Depending on the answer, the neutral particles will be either Majorana or Dirac types.

If the answer to the above question is "yes", then the particle is a Dirac particle. It appears in the familiar Dirac equation:

$$\left(\gamma_\mu \frac{\partial}{\partial x_\mu} + m_i\right)\psi_i = 0.$$

If the answer is "no" and the particle is identical to its antiparticle, then it is a Majorana particle. The concept of the Majorana particle was first introduced by Majorana in 1937 [6]. Examples of the Dirac-Majorana particles are the neutral pion, which is identical to its antiparticle and according to the definition belongs to the Majorana type, and the neutral kaon, which is different from its antiparticle and belongs to the Dirac type.

To put this in mathematical terms, we have to make use of the transformation properties of particles. The charge conjugate to the free neutrino field ψ is defined as

$$\psi^C = C(\bar{\psi})^T,$$

where C is a 4×4 matrix and ψ^T is a transposed field. We define a Majorana field as an eigenstate of charge conjugation.

$$\chi = \frac{1}{\sqrt{2}}\left[\eta_C^* \psi + \eta_C \psi^C\right],$$

where ψ is a free neutrino field which obeys the Dirac equation, and η_C is a complex phase. With the appropriate choice of phase $\eta_C = e^{i\Phi}\lambda_C = \pm 1$ we obtain an eigenstate of charge conjugation with eigenvalue $\lambda_C = \pm 1$.

The above definition is only for free fields. We have to generalize it to the interacting field. Neutrinos interact only via the weak interactions, which are

not invariant to charge conjugation C. An interacting Majorana neutrino cannot be an eigenstate of C. The generalized definition is: "a Majorana neutrino field is an eigenstate of the CP transformation". It follows (see Ref. [6]) that the Majorana field has the CP eigenvalue of $\pm i$, where fields with $+i$ are called even CP states, fields with $-i$ are called odd CP states.

One can visualize the distinction between Majorana and Dirac neutrino if we consider the transformation properties a) under the Lorentz transformation and b) under the CPT transformation. Let's assume that the left-handed neutrino ν_L has a mass. Dirac neutrino ν_L^D transforms under the Lorentz and CPT transformations differently. Lorentz transformation to the faster moving frame of reference turns ν_L^D into a right-handed ν_R^D.

$$\text{Lorentz} \ : \nu_L^D \rightarrow \nu_R^D. \tag{2.5}$$

CPT transformation turns ν_L^D to the CPT mirror image $\bar{\nu}_R^D$

$$\text{CPT} \ : \nu_L^D \rightarrow \bar{\nu}_R^D. \tag{2.6}$$

The Majorana neutrino ν_L is an eigenstate of the CP and CPT and transforms similarly under the Lorentz and CPT transformations. The transformations are shown in Figure 2.1.

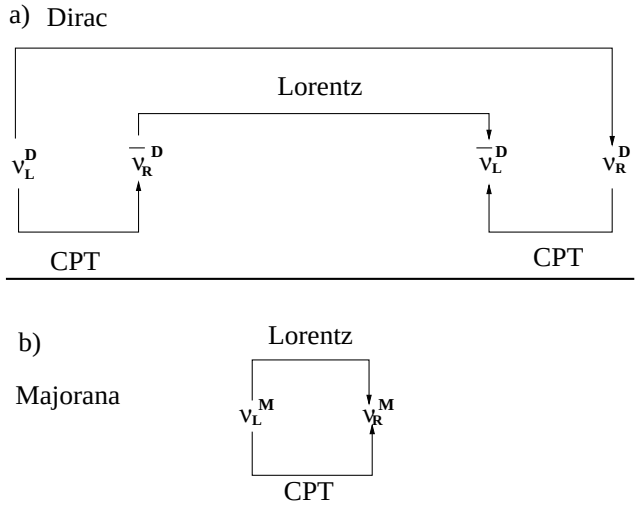

Figure 2.1: Dirac a) and Majorana b) neutrinos transform differently under the Lorentz and CPT transformations. Dirac ν^D with nonzero mass a) has four distinct states, Majorana ν^M b) has two distinct states.

The distinction between Majorana and Dirac neutrinos is not only theoretical. A massive Dirac neutrino has nonzero magnetic and electric dipole moments, that could be observed experimentally, whereas a Majorana neutrino does not.

The Majorana and Dirac particles are different only if the neutrino rest mass is not zero. If the neutrino has no mass and travels at the speed of light, then the Lorentz transformation to a faster moving frame is not possible. The difference between the types disappears smoothly. For Dirac neutrinos, the dipole moments are proportional to mass and vanish for a massless particle.

The Lorentz invariant mass terms in the Langrangian could be the Dirac and/or Majorana terms. The Dirac mass term was mentioned in the previous section in the discussion about SM mass terms. It has the form $(\bar{\psi}_L m_D \psi_L + \bar{\psi}_R m_D \psi_R)$, where the parameter m_D is the Dirac mass.

If we assume that a neutrino mass is solely a Dirac mass, $m_D = g_\nu < \phi^0 >$, then a ν_e mass in the 10 eV range would require an extremely small coupling ($g_{\nu_e} \leq 10^{-10}$). Moreover, g_{ν_e} would have to be smaller by $m_{\nu_e}/m_e \leq 10^{-4}$ than the analogous Yukawa coupling for the electron. My opinion is, that this is not an attractive presumption.

Another possibility is that the neutrino is a Majorana particle and has a Majorana mass. Majorana mass terms are of the form $\bar{\psi}_L m_M (\psi^C)_R$ or $\bar{\psi}_R m_M^* (\psi^C)_L$, where superscript C is the charge conjugate and m_M is the Majorana mass. In a different presentation, the Dirac mass terms could be $\bar{\psi} m_D \psi + \bar{\psi}^C m_D \psi^C$ and Majorana terms $\bar{\psi} m_M \psi^C + \bar{\psi}^C m_M^* \psi$. However the diagonalization of the mass term is more simple if we use chiral projections (from Ref. [6] p.9).

Dirac mass terms are invariant under global phase transformations and this leads to lepton number conservation. The Majorana mass term $\bar{\psi}_L \psi^C$ or $\bar{\psi}_R^C \psi_L$ is not invariant under this transformation and violates the conservation of the lepton number by two units. Also, neutrino oscillations (for example, $\nu_\mu \rightarrow \nu_e$) imply family lepton number violation.

Lepton number violation is possible only in extensions of the SM. Although the SM Langrangian does not have any terms that violate lepton number, there is no intrinsic gauge symmetry that would require that lepton number be conserved.

2.3 General mass term

The most general way to generate a small neutrino mass is to introduce Dirac and Majorana mass terms into the theory. The most general mass Langrangian for the neutrino is (see Ref. [6])

$$\mathcal{L}_\mathcal{M} = \frac{1}{2} M_D (\overline{\nu_L} \nu_R + (\overline{\nu^C})_L (\nu^C)_R) + \frac{1}{2} m_L \overline{\nu_L} (\nu^C)_R + \frac{1}{2} m_R (\overline{\nu^C})_L \nu_R) + h.c.$$

The terms $\overline{\nu_L} \nu_R$, $(\overline{\nu^C})_L (\nu^C)_R$ are Dirac terms and $\overline{\nu_L} (\nu^C)_R$, $(\overline{\nu^C})_L \nu_R$ are Majorana mass terms.

One can rewrite this Langrangian in the matrix form:

$$\mathcal{L}_{\mathcal{M}} = \frac{1}{2}\bar{\nu}^C \mathcal{M}\nu + h.c., \tag{2.7}$$

where $\nu \equiv \begin{pmatrix} \nu_L \\ \nu_R^C \end{pmatrix}$. The matrix in the above equation (Eq. 2.7),

$$\mathcal{M} = \begin{pmatrix} m_L & m_D \\ m_D & m_R \end{pmatrix}, \tag{2.8}$$

is usually to appear if there is some kind of mixing between mass and weak eigenstates.

In this form, the ν vector is a mixture of the Majorana particles ν_L and ν_R^C, which has two mass eigenvalues and two corresponding eigenstates. To find eigenstates we have to diagonalize the matrix $\mathcal{M}$. The eigenvalues of the above matrix are:

$$m_1 = \frac{1}{2}\sqrt{4m_D^2 + (m_R - m_L)^2} - \frac{m_L + m_R}{2}, \tag{2.9}$$

$$m_2 = \frac{1}{2}\sqrt{4m_D^2 + (m_R - m_L)^2} + \frac{m_L + m_R}{2}; \tag{2.10}$$

and the eigenstates of this matrix are given by

$$\nu_L{}' = \nu_L \cos\xi + \nu_R^C \sin\xi, \tag{2.11}$$

$$\nu_R^{C\prime} = -\nu_L \sin\xi + \nu_R^C \cos\xi; \tag{2.12}$$

with $\tan 2\xi = \frac{2m_D}{m_R - m_L}$.

If we make the reasonable assumption about parameters, m_D, m_L and m_R, such that $m_L << m_D << m_R$ then Eq. 2.10 simplifies significantly and leads to the See-Saw model.

The next two section describe several models and consider the underlying physics of the neutrino mass terms.

2.4 Grand Unified Theories

Grand Unified Theories (GUT) unite electroweak and strong forces at energies greater than the mass scale $M_{\rm GUT} = 10^{14} - 10^{16}$ GeV/c^2. Above this mass scale the running couplings of weak, strong and electromagnetic forces merge giving us a "Grand Unification" theory.

GUT theories introduce additional sets of Higgs bosons, which are responsible for the breaking of the symmetry between the strong and weak interactions at the $M_{\rm GUT}$ scale. As the result of this spontaneous symmetry breaking these additional Higgs multiplets, Φ, develop vacuum expectation values and set the

mass scale for both gauge bosons and fermions. In analogy to the SM Higgs, a scalar multiplet Φ, couples with the fermions. The result of this interaction is the fermion mass:

$$m_f = m_D = h_\nu \bar{\nu}_L \Phi \nu_R,$$

where h_ν is the Yukawa coupling of a neutrino to a Higgs field.

GUTs based on groups larger than SU(5) predict the existence of heavy weak isosinglets, N, that couple with the SM neutrinos. In the process of coupling the following eigenstate mixture appears, $\begin{pmatrix} \nu \\ N \end{pmatrix}$. I will call this mixture a weak eigenstate mixture, because ν is the weak eigenstate, even though its eigenstate partner, N, does not have a weak charge.

Mass eigenstates ν' and N' are related to the weak eigenstates ν, N through the mixing matrix in Eq. 2.8:

$$\begin{pmatrix} \nu' \\ N' \end{pmatrix} = \begin{pmatrix} m_L & m_D \\ m_D & m_R \end{pmatrix} \begin{pmatrix} \nu \\ N \end{pmatrix}. \tag{2.13}$$

The mixing matrix enters the neutrino mass Langrangian in the form of Eq. 2.7. The parameters m_D, m_L and m_R appear in the Langrangian as a result of the interaction of ν and N fields with the set of additional Higgs fields, Δ_L and Δ_R. Additional Higgs, Δ_L and Δ_R, couple with Majorana terms in the mass Lagrangian,

$$m_L = h' \bar{\nu}_L^C \Delta_L \nu_L,$$
$$m_R = h' \bar{\nu}_R^C \Delta_R \nu_R;$$

There is an important difference between m_L and m_R terms. Higgs doublet Δ_L must have a small vacuum expectation value. It appears that the coupling of any additional doublet to existing fermion fields in the SM would lead to experimentally observable consequences. For instance, it would violate the experimentally very well confirmed equality $\frac{M_W}{M_Z} = sin^2\theta_W$, unless the vacuum expectation value of the Δ_L doublet Higgs was small. On the other hand, there are no constraints on the vacuum expectation values of a singlet field Δ_R. Its mass scale must be very large because there is no evidence of an additional right-handed gauge boson in the experimentally sensitive range. The GUT predicts the mass of the weak singlet eigenstate to be that of the GUT scale, $10^{14} - 10^{16}$ GeV/c^2.

This leads to the following relation between Dirac and Majorana mass:

$$m_L << m_D << m_R.$$

Under this assumption the eigenvalues in Eq. 2.10 are

$$m_1 \simeq \frac{m_D^2}{m_R}, \tag{2.14}$$
$$m_2 \simeq m_R; \tag{2.15}$$

For example, the $m_D \approx 1GeV$ and $m_R \approx 10^{15}GeV$ yields very heavy and very light neutrinos: $m_1 \approx 10^{-15}GeV$ and $m_2 \approx 10^{15}GeV$.

GUTs predict one of the states in the weak admixture to have very small mass and another to be extremely heavy. The first corresponds to the light left-handed neutrino and the latter to its heavy right-handed partner.

2.5 Left-right symmetrical model

Heavy neutrinos are predicted in left-right symmetrical models as well. Left-right symmetrical model, $SU(2)_l \times SU(2)_R \times U(1)_{B-L}$, states that the basic weak Langrangian is invariant under space reflection, like the electromagnetic and strong interactions. It therefore involves both $V-A$ and $V+A$ charged currents and predicts the existence of a right-handed gauge boson, W_R. The observed predominance of left-handed weak interactions at low energies is understood as the consequence of the fact that the vacuum is not symmetric under space reflection (see Ref. [31]). In these models, both right and left helicities of the neutrino are included and the neutrino has a mass.

Additional Higgs multiplets Δ_R, Δ_L and Φ are introduced. Δ_R is responsible for the breaking of the left-right symmetry: $SU(2)_l \times SU(2)_R \times U(1)_{B-L} \rightarrow SU(2)_L \times U(1)$ via $<\Delta_R> \neq 0$. The subsequent breakdown of $SU(2)_L \times U(1)$ down to $U_{em}(1)$ is achieved via the Standard Model Higgs $<\Phi> \neq 0$. Note that $<\Phi> \neq 0$ is no longer a doublet, rather it is 2×2 matrix.

The neutrino mass Langrangian after the symmetry breaking is

$$\mathcal{L}_{\mathcal{M}} = \frac{1}{2}h'(\nu_L^T v_L C \nu_L - \nu_R^{CT} v_R C \nu_R^C) + \frac{1}{2}h\nu_L^T v1 C \nu_R^C + h.c.,$$

where C is charge conjugation matrix, ν^T is the transposed field, $v_L \equiv <\Delta_L^0>$, $v_R \equiv <\Delta_R^0>$, $v1 \equiv <\Phi>$ are the vacuum expectation values and h is the Yukawa coupling to Φ and h' is the Yukawa coupling to Δ_L and Δ_R (eq. 2.12 in the Mohapatra paper [31]).

In matrix form

$$\mathcal{L}_{\mathcal{M}} = \frac{1}{2}(\bar{\nu}^T N^T)\mathcal{M}\begin{pmatrix} \nu \\ N \end{pmatrix} + h.c., \tag{2.16}$$

where $\nu \equiv (\nu_L N) \equiv C(\bar{\nu}_R)^T$, $\mathcal{M}$ is a mass matrix similar to the one in the equation Eq. 2.8, where $m_D = hv1, m_L = h'v_L, m_R = h'v_R$.

The eigenstates of this matrix are therefore given by

$$\nu' = \nu\cos\xi + N\sin\xi, \tag{2.17}$$

$$N' = -\nu\sin\xi + N\cos\xi; \tag{2.18}$$

with $\tan 2\xi = \frac{2m_D}{m_R - m_L}$.

ν and N happen to be the Majorana spinors, for they are eigenstates of C, the charge conjugation operator.

By diagonalizing the matrix (Ref. 2.8) in Eq. 2.7 we could find the mass eigenvalues of the neutrino ν and its heavy partner N. There are two possible solutions depending on the number of the Higgs bosons in the theory:

- If there is only one Φ in the theory then we obtain

$$m_{\nu'} \approx m_L + m_D^2/m_R, \tag{2.19}$$

$$m_{N'} \approx m_R. \tag{2.20}$$

  In this case the tiny neutrino mass could be attributed to the arbitrarily chosen small Yukawa coupling.

- A better possibility is if the gauge-boson and fermion masses originate from different mass scales. Then we have two Higgs fields, one for the fermion mass scale and another for the gauge-boson mass scale. The main difference from the previous case is that the value for m_L is much smaller:

$$m_{\nu'} \approx m_D^2/m_R, \tag{2.21}$$

$$m_{N'} \approx m_R; \tag{2.22}$$

m_R is related to the mass of the right-handed boson via the Yukawa coupling $\frac{h}{g} = \frac{m_R}{m_{W_R}}$, where h is the Yukawa coupling of the Higgs to the fermions and g is the Yukawa coupling to the gauge bosons.

The left-right symmetry model leads to the same relation of Eq. 2.22 as Eq. 2.15 of the GUT model. The prediction for the mass of the right-handed neutrino N is of the same order as the mass of the right-handed W:

$$m_{N'} \simeq m_{W_R} \approx 10^5 \text{GeV}. \tag{2.23}$$

2.6 See-Saw mechanism

The assumptions made in the previous sections can be generalized in the following way. We assumed that besides the left-handed neutrino, ν_L, which couples to its family charged lepton in weak charged currents, there is also a right-handed partner N, which is a weak isosinglet and does not couple to any fermions or bosons directly. Both neutrinos have mass and the handedness is no longer preserved, thus when I use the term a left or right-handed neutrino, I mean that the state is mostly left or right-handed.

To get the neutrino mass eigenstates of ν and N, we had to diagonalize the general mass matrix M of Eq. 2.8. The two eigenvalues were given in Eq. 2.10

and two eigenstates in Eq. 2.12. Both GUTs and left-right symmetrical models predict the following relation:

$$m_L << m_D << m_R. \tag{2.24}$$

According to GUTs and left-right models, the right-handed neutrino is extremely heavy: $m_R \approx 10^5 - 10^{16}$ GeV. Under those assumptions Eq. 2.10 becomes approximately

$$m_1 \simeq \frac{m_D^2}{m_R}, \tag{2.25}$$

$$m_2 \simeq m_R; \tag{2.26}$$

where $m_2 >> m_D >> m_1$.

This is the "See-Saw" mechanism: as N gets heavier, ν gets lighter. Eq. 2.12 becomes

$$\nu' = \nu(1 - \frac{\xi^2}{2}) + N\xi, \tag{2.27}$$

$$N' = -\nu\xi + N(1 - \frac{\xi^2}{2}); \tag{2.28}$$

where $\xi \approx \frac{m_D}{m_R}$. The parameter m_D is a typical Dirac mass: $m_D \approx m_f$. There is no indication, however, on what fermion mass qualifies to be "typical". The two eigenstates are the heavy neutrino with the mass m_R and the "light" SM neutrino with the mass $\frac{m_D^2}{m_R}$.

In the See-Saw mechanism [32], the neutrino mass is proportional to the square of the mass of a fermion (lepton or quark) and inversely proportional to the mass of its right-handed partner, NHL or N. The See-Saw mechanism naturally leads to neutrino masses much smaller than the masses of the other fermions.

$$m_\nu = \frac{m_D^2}{m_R}$$

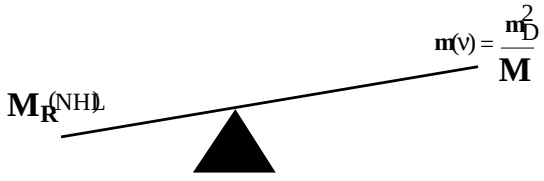

Figure 2.2: See-Saw mechanism: Larger $m_R \rightarrow$ smaller m(ν_L).

2.7 See Saw model for three generations

In this section we extend this result for all three generations.

Instead of 2×2 mass matrix in Eq.2.7, we'll have 6×6 matrix

$$\mathcal{M} = \begin{pmatrix} m_L & m_D \\ m_D & m_R \end{pmatrix}, \tag{2.29}$$

where m_D, m_L and m_R are 3×3 matrices.

If m_R after diagonalization has the form

$$m_R \simeq \begin{pmatrix} 1 & 0 & 0 \\ 0 & 1 & 0 \\ 0 & 0 & 1 \end{pmatrix}, \tag{2.30}$$

then, according to the See-Saw mechanism applied for three generations, the neutrino mass is proportional to the square of the mass of a fermion (lepton or quark) from the same family.

$$m_{\nu_e} : m_{\nu_\mu} : m_{\nu_\tau} = m_e^2 : m_\mu^2 : m_\tau^2$$

or

$$m_{\nu_e} : m_{\nu_\mu} : m_{\nu_\tau} = m_u^2 : m_c^2 : m_t^2.$$

The heavy neutrino mass could follow the family hierarchy as well:

$$m_R \simeq \begin{pmatrix} m_e & 0 & 0 \\ 0 & m_\mu & 0 \\ 0 & 0 & m_\tau \end{pmatrix}, \tag{2.31}$$

Then the quadratic dependence in the equations above is replaced by the linear dependence on m_D:

$$m_{\nu_e} : m_{\nu_\mu} : m_{\nu_\tau} = m_e : m_\mu : m_\tau.$$

2.8 The mixing

NHLs do not have electromagnetic, strong or weak charge and consequently do not interact with matter. They could only be observed or produced through the mixing process with SM neutrinos.

Under the See-Saw model the left-handed neutrino is the mixture of two Majorana neutrinos described in Eq. 2.28.

Let's introduce the mixing constant, $|U|^2 \equiv < \nu_i|N >= -\frac{m_D}{m_R}$, and rewrite Eq. 2.28 as:

$$\nu' = \nu(1 - \frac{|U|^4}{2}) - N|U|^2, \tag{2.32}$$

$$N' = \nu|U|^2 + N(1 - \frac{|U|^4}{2}); \tag{2.33}$$

The mixing between 'mostly' left-handed ν' and 'mostly' right-handed N' in most of the SM extensions on the tree level is shown in Figure 2.3

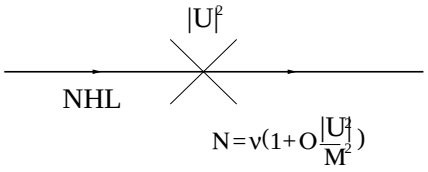

Figure 2.3: Mixing between NHL and left-handed neutrino.

The production and decay of NHLs could happen through the mixing with virtual (off mass shell) neutrinos. The mixing contributes to the processes of NHL production and decay by including the factor of $|U|^2$ into the amplitudes. Both processes are considered below.

2.9 NHL production modes

NHLs could be produced in the semileptonic decays of a charged stable meson. In our analysis we considered $K^{\pm}$, $D^{\pm}$ and $D_S^{\pm}$ decays only, because they could be produced in enormous numbers in the pN nucleon collisions in our neutrino beam and because the CKM suppression of the two-body decay is modest ($K^{\pm}$, $D^{\pm}$) or absent $D_S^{\pm}$ (Ref. [40]). The two-body decay rate is related to $\mu\nu$ rate except for the $|U|^2$ factor (from Ref. [40]):

$$\Gamma(H \to N\mu) = |U|^2\Gamma(H \to \nu\mu)\eta(m_{\rm NHL}/M_H, m_\mu/m_{\rm NHL}), \tag{2.34}$$

where $H = (K^{\pm}, D^{\pm}, D_S^{\pm})$, $|U|^2$ is the mixing constant, $\Gamma(H \to \nu\mu)$ is the decay width of a muon H into $\mu\nu$, M_H is the meson mass, $m_{\rm NHL}$ is the NHL mass, m_μ is the muon mass and η is a kinematic factor that accounts for phase space suppression (Ref. [40] eq.12):

$$\eta(x,y) = \frac{[(1+y^2) - x^2(1-y^2)^2]\sqrt{[1-x^2(1-y)^2][1-x^2(1+y)^2]}}{y^2(1-x^2y^2)^2}. \tag{2.35}$$

The kinematic factor, η, approaches zero as $m_{\rm NHL} \to M_H - m_\mu$. For $m_{\rm NHL} >> m_\mu$, $\eta(m_{\rm NHL}/M_H, m_\mu/m_{\rm NHL}) \to m_{\rm NHL}^2/m_\mu^2(1-(m_{\rm NHL}/M_H)^2)^2$. For NHL masses that follow $m_\mu << m_{\rm NHL} << M_H$, the η factor would be proportional to $m_{\rm NHL}^2$.

The Feynman diagram in Figure 2.4 shows the production of NHL in two-body meson decay.

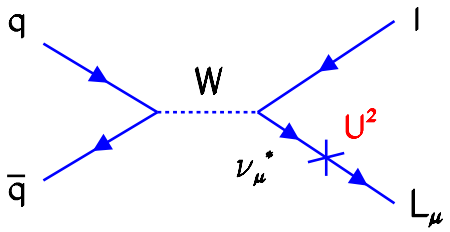

Figure 2.4: Feynman diagrams for the production of neutral heavy leptons (L_μ or NHLs).

NHL were also assumed to be produced in three-body decays of D and D_S mesons. The cross section for D meson production was taken to be $27\mu b$ (Ref. [42] eq.3.4), the average of the E743 and E653 experiments. The production was normalized to the total cross section for NuTeV experiment. More details on this is in section 5 on NHL MC. The average semileptonic branching ratio was measured in e^+e^- annihilations ([42]), $B_{SL}(D) = 8.2 \pm 1.2\%$. Three-body decays and relative rates could be expressed in terms of two-body decays using suppression factors I (I_1 in [42] eq.2.40):

$$I(x,y,z) = 12 \int_{(x+y)^2}^{(1-x)^2} \frac{ds}{s}(s - x^2 - y^2)(1 + z^2 - s) \times \tag{2.36}$$

$$\{[s - (x-y)^2][s - (x+y)^2][(1+z)^2 - s][(1-z)^2 - s]\}^{1/2}. \tag{2.37}$$

Then the three-body averaged semileptonic branching ratio is,

$$B(D \to XNl^+) = B_{SL}(D) \frac{I(m_s/m_c, m_{\rm NHL}/m_c, m_l/m_c)}{I(m_s/m_c, 0, m_l/m_c)} |U|^2, \tag{2.38}$$

where m_s is the mass of strange quark, m_c is the mass of charm, m_l is the mass of lepton, N is a NHL and $m_{\rm NHL}$ is the NHL's mass.

In our experiment the NHL production was divided into 2 modes corresponding to π, K mesons decaying in the meson decay pipe and charmed mesons decaying in the proton dump.

- π, K: Those mesons decayed in the meson decay pipe. Mesons were sign-selected and focussed toward the NuTeV detector and decay channel. The mass of the produced NHL was limited to $m_{\rm NHL} < m_K - m_\mu$.

- $D^\pm$, D^0, D_S: Due to the short lifetime, charmed mesons decayed right away in the primary production target or dump. For this reason, the NHLs were not focussed toward the detector. The primary beam pointed 7.8 mrad away from the detector, because of the design that allowed sign-selection. D mesons were not sign selected. Decays were limited kinematicly to the NHL mass: $m_{\rm NHL} <\simeq 2$ GeV.

Table 2.9 shows NHL production fractions for NHLs produced in decays of charmed mesons and in decays of K mesons per proton on target.

mass, GeV	Br(K$\rightarrow L^0 + X$)	Br(D$\rightarrow L^0 + X$)
0.35	5.4%	- %
0.85	0%	13.6%
1.15	0%	10.8%

Table 2.1: NHL production fractions for NHLs produced in charm decays (1.15 GeV) and in K decays(0.35 GeV) per proton on target.

2.10 NHL decay modes

This analysis searched for NHLs with masses between 0.25 to 2.0 GeV, which decay with a muon in the final state.

In the process of decay, a NHL converts to a virtual neutrino via mixing ($|U|^2$). The neutrino virtually inherits all of the NHL's mass. To get back on mass shell, the virtual neutrino emits an electroweak boson, which then decays into 2 leptons, 2 quarks or 2 neutrinos. Depending on the boson, the NHL could decay via charged or neutral current. The decays are shown in Figure 2.5.

- *Charged current* The decay modes are:
  lepton + $\mu\nu_\mu$, lepton + $e\nu_e$, lepton + $\tau\nu_\tau$, lepton + $q\bar{q}$

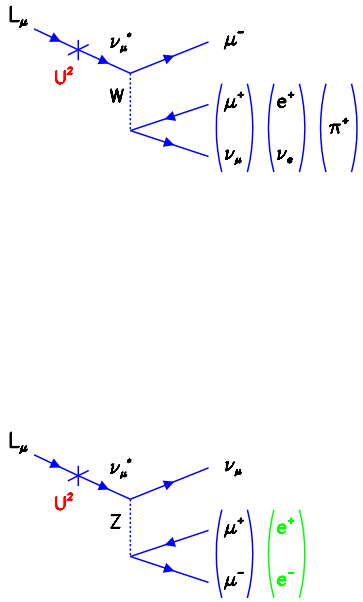

Figure 2.5: Feynman diagrams for the decay of neutral heavy leptons (L_μ or NHLs). Shown are the decays via a W and a Z boson. Tau decay modes are not shown.

- *Neutral current* The decay modes are:
  $\nu e^+e^-, \nu\mu^+\mu^-, \nu\tau^+\tau^-, \nu qq', \nu\nu\bar{\nu}$

The primary NHL decay modes with a muon in the final state were

1. NHL $\rightarrow \mu\mu\nu$
2. NHL $\rightarrow \mu e\nu$
3. NHL $\rightarrow \mu\pi$
4. NHL $\rightarrow \mu\rho$

In the standard mixing model[42, 40], the expected ratio of decay rates for $\mu\pi$: $\mu e\nu$: $\mu\mu\nu$ is 3.5 : 1.6 : 1.0.

Table 2.10 shows NHL decay ratios for different NHL masses. This ratio was obtained from NHL Monte Carlo and reflects the fact that the amplitude

mass, GeV	Br(NHL$\to \mu\mu$)	Br(NHL$\to \mu e$)	Br(NHL$\to \mu\pi$)	Br(NHL$\to \mu\rho$)
0.35	5.9%	9.8%	15.1%	0%
0.85	7.6%	14.3%	22.1%	9.1%
1.15	7.8%	14.2%	22.3%	21%
1.75	7.6%	13.0%	19.2%	18.0%

Table 2.2: NHL branching ratios for different NHL masses.

of a semileptonic decay is bigger than fully leptonic one. The $\mu\rho$ channel is significant only at NHL masses above 1 GeV, where there is enough phase space for it to be produced. Above 1 GeV $\mu\rho$ is comparable to the $\mu\pi$ mode.

The decay rate is

$$\Gamma(L \to \mu + X) = \sum_i \frac{G_F^2 m_{\rm NHL}^5}{192\pi^3} |U_i|^2 \Phi_i(m_{\rm NHL}), \tag{2.39}$$

where $m_{\rm NHL}$ is the NHL mass, i is the index over the possible channels ($\mu\mu$, μe, $\mu\pi$, $\mu\rho$) and $\Phi_i(m_{\rm NHL})$ is a phase space factor.

2.11 The sensitivity of the NHL search

The number of produced NHLs is proportional to the total number of protons, $N_{\rm POT}$ on target and factor $|U|^2 \times \eta$ from Eq. 2.34. The factor η is proportional to $m_{\rm NHL}^2$ for NHL masses away from the edge of the available phase space. The number of decays in the decay channel is proportional to the decay rate (Eq. 2.39), which gives a factor $|U|^2 m_{\rm NHL}^5$, to the length of the decay channel L, and to an extra factor of $m_{\rm NHL}/E_{\rm NHL}$ due to time dilation.

In a combined form the number of observed NHLs, $N_{\rm NHL}^{obs}$, has the dependence (from Ref. [40]):

$$N_{\rm NHL}^{obs} \simeq \frac{N_{\rm POT}}{E_{\rm NHL}} L |U|^4 m_{\rm NHL}^8 \tag{2.40}$$

Thus the sensitivity is proportional to the mixing constant squared $(|U|^2)^2$ and to the NHL mass to the 8th power.

Combining the production and decay amplitudes (Eq. 2.34 and Eq. 2.39) we get the sensitivity for the NHL search as,

$$N_{\rm NHL} = |U|^4 N_H \Gamma(H \to N + X) \Gamma(H \to \text{mode}) \eta_P P(\tau) \epsilon, \tag{2.41}$$

where $|U|^4$ is the NHL mixing parameter, N_H is the number of mesons which decay in the decay pipe, ϵ is the efficiency of the detector, η_P is a kinematic factor, and $P(\tau)$ is the probability that the NHL will decay within the decay channel. This formula for the NHL sensitivity is implemented in the NHL Monte Carlo, which was used to calculate the sensitivity of the experiment.

2.12 Constraints on the mixing and mass

In this section, the upper limits on mixing are estimated assuming different models of NHLs. As will be shown, GUT and left-right symmetries favor extremely heavy NHLs and very small neutrino masses. However one cannot rule out the possibility of a NHL around 1 GeV and mixings of order $10^{-7} - 10^{-8}$, the range of sensitivity of this search.

- GUT predicts the values for the NHL mass to be of the order of the GUT scale $10^{14} - 10^{16} GeV/c^2$. The mass of the muon neutrino according to the see-saw model could be as small as:

$$m_{\nu_\mu} \approx \frac{m_\mu^2}{M_{\rm GUT}} = \frac{(105.6{\rm MeV}/c^2)^2}{10^{14} - 10^{16}{\rm GeV}/c^2} \approx \tag{2.42}$$

$$\times(10^{-13} - 10^{-15}){\rm MeV}/c^2 \tag{2.43}$$

  This is smaller than the experimental indications for the neutrino mass $(1 - 10^{-3}{\rm eV})$ from ν oscillation experiments [10]. The lower limit on mixing $|U|^2$ with the above values for the NHL mass and assuming the see-saw model is

$$|U|^2 \approx \frac{m_\mu}{m_{\rm NHL}} = \frac{105.6{\rm MeV}}{10^{-13}{\rm MeV}/c^2} < 10^{-11}. \tag{2.44}$$

  This is an extremely low mixing value and is beyond the reach of sensitivity of any high energy experiment.

- In the left-right symmetry model $m_R \equiv m_{\rm NHL} \geq 10^5 GeV/c^2$. Using see-saw model one predicts

$$|U|^2 = \frac{105.6{\rm MeV}/c^2}{10^5{\rm GeV}/c^2} > 10^{-15}, \tag{2.45}$$

  also beyond the existing experimental sensitivity.

- *alternatives:*
  However there are models [33] with $m_R << M_{\rm GUT}$. Fine tunings and modifications are possible within the GUT. For example in the framework of O(10)GUT there could be a neutrino mass $(\alpha/\pi)^{-2}$ times larger than the predictions above (from Ref. [34]). Also, it is not clear what to use as the typical Dirac mass: the mass of the fermion or the quark mass from the same family or the fermion/quark masses from other families. Given present bonds on the muon neutrino mass $m(\nu_\mu) \leq 0.5$ keV and taking typical Dirac mass as $m_D = m_e = 0.5$ MeV one could estimate the masses of NHL of the muon family m_R, using the see-saw mechanism:

$$m_R \approx \frac{m_D^2}{m(\nu_\mu)} = 0.5{\rm GeV}.$$

Taking the NHL mass of the order of 1 GeV and the typical Dirac mass of 0.5 MeV the lower limit on $|U|^2$ mixing is about 10^{-7}.

2.13 Few words on the See-Saw mechanism

In summary, both GUT and left-right symmetry provide a mechanism for the neutrino mass generation. The See-Saw mechanism naturally follows from these theories. However both theories predict extremely heavy NHLs; more than $10^{14} GeV/c^2$ for GUT, and a bit better $10^5 GeV/c^2$ for left-right symmetry. Both of these values are beyond the sensitivity reach of any experiment in the foreseeable future. Also, the predictions of GUT and left-right symmetry for the neutrino masses are inconsistent with the experimental indications on the neutrino mass from ν oscillations [10].

There are alternative theories which predict the same mechanism of Majorana masses and see-saw relations and a much lighter NHL. One can assume that the symmetry breaking happens at lower than the GUT and LR scales. In this case, the mass of the NHL could be within experimental reach.

Without strong theoretical indications on the mass range of NHLs, except that it should be relatively heavy, the whole range from 0.1 GeV to infinity is open for the searches. [1]

The formulas for the production, Eq. 2.34, and decay, Eq. 2.39 ,of neutral heavy leptons are implemented into the NHL signal Monte Carlo and then applied to data in the search for NHL signals.

[1] There is a joke about a drunk who lost his keys and decides to look for them only under a lamp post where one can see. This approach actually makes lots of sense and is forced on many exotic searches.

Chapter 3

Previous Neutral Heavy Lepton searches

Searches for Neutral Heavy Leptons (NHLs) began in earnest about 25 years ago. The theoretical predictions for lifetimes and branching ratios were published in 1971 (my birth year :-) in Ref. [13]. The same year M. Davier, B.H. Wiik [14] proposed searching for NHLs at SLAC.

Since then, a variety of experimental searches for NHLs have taken place. Based on the source of NHL production they can be divided into two broad categories:

1. *Meson Decay Experiments:* The NHLs could be produced in neutrino beams via mixing with light neutrinos in meson decays.

2. *Collider Searches:* The NHLs could be produced in W and Z (or any heavier gauge boson) decays in collider experiments. Because NHLs do not couple directly to weak bosons, they are produced through mixing with light neutrinos.

The decay channel search described in this thesis belongs to the first category. So far there has been no experimental evidence for NHL particles, except in a timing anomaly found at the KARMEN detector, which resembles an NHL signature. It is described in the next section among with other decay experiments.

3.0.1 Meson decay experiments

In meson decay experiments, NHLs could be produced in the decays of mesons produced in a target. NHLs are assumed to travel some distance before they decay in a detector. Experiments in which particles travel a long distance to reach the point of detection are called long "baseline" experiments. Experiments probe either longer or shorter NHL lifetime, depending on the ratio

of the distance over the beam energy, L/E. Meson decay experiments are typically long baseline with the relatively low beam energy, and obtain NHL limits in the low lepton mass region (less than $5GeV$) and low values of mixing (above $|U|^2 \simeq 10^{-5} - 10^{-6}$).

There are several types of meson decay experiments depending on how the mesons decay, in flight or at rest, how thick is the target etc. In experiments with a thick meson production target, the secondary mesons are stopped in the target. Those experiments are called beam-dump experiments. Below is the list of the competitive NHL searches with the same order of magnitude mass region as this search.

- *KEK (E89)*, (1982) [15]: The experiment at the KEK synchrotron in Japan looked for the signature heavy neutrinos from K^+ decays using $550MeV$ K beam stopped in plastic counters. The heavy neutrino eigenstates were identified by searching for a separate peak in the energy spectrum of the two-body leptonic decay. If NHLs mass were sufficiently large, they would be well separated from the dominant energy peak. The upper bounds on the mixing parameter were found to be $|U_\mu|^2 < 10^{-5}$ for $m_N = 100\text{MeV}/c^2$ at 90 % confidence level, and $|U_\mu|^2 < 10^{-6}$ for $m_N = 200 - 300\text{MeV}/c^2$, with the range of the mixing parameter varying from $10^{-4} - 10^{-6}$ in the mass range of $70 - 300$ MeV.

- *LBL*, (1989) [16]: This experiment at the LBL Bevatron searched for NHLs produced in $K^+ \to \mu^+\nu\bar{\nu}\nu$ and $K^+ \to \pi^+\nu\bar{\nu}$ decays. This decay could take place if a K meson decays to μ and a NHL, with the subsequent decay of the NHL to neutrinos. No events were found and limits were established on the NHL mixing varying from 6×10^{-7} to 10^{-6} in the mass range $0.2 - 0.3$ GeV.

- *CHARM*, (1986) [17]: In this beam-dump experiment heavy neutrinos may be produced in charmed D meson decays. A search was conducted in both a "prompt" neutrino beam produced by dumping 400 GeV protons on a thick copper beam dump and a "wide-band" horned-focussed neutrino beam (WBB) produced by 400 GeV primary protons from the SPS at CERN. In the prompt neutrino beam NHLs could decay to $e^+e^-\nu_e$, $\mu^+e^-\nu_e$, $e^+\mu^-\nu_\mu$, and $\mu^+\mu^-\nu_\mu$. No candidate events were found and the limits of $|U_{ei}|^2, |U_{\mu i}|^2 < 10^{-7}$ were obtained for NHL mass around 1.5 GeV/c^2. In the wide-band experiment, heavy neutrinos were assumed to be produced by neutral-current interactions in the CHARM calorimeter, and decay into a muon and hadrons. The signature was an in-time double vertex event. This experiment was sensitive to decays of neutrinos with mass in the range 0.5 - 2.8 GeV/c^2 and set limits $|U_{\mu i}|^2 < 3 \times 10^{-4}$ for masses around 2.5 GeV/c^2.

- *WA66 (BEBC)*, (1985) [18]: The decays of heavy neutrinos were searched with the CERN Big European Bubble Chamber (BEBC) in the proton beam dump experiment WA66. Heavy neutrinos could be produced in charmed D meson decays in the prompt neutrino beam produced by 400 GeV protons interacting in the beam dump. No events satisfied the required kinematic constraints and the resulting limits were $|U|^2 < 10^{-6} - 10^{-7}$ for the neutrino masses between 0.5 and 1.7 GeV/c^2, respectively.

- *CCFR*, (1987) [25]: A search by the CCFR collaboration for NHLs was conducted in the iron-scintillation calorimeter 10 years prior to the search described in this paper (The same calorimeter was used in the NuTeV experiment and in this search). The CCFR collaboration looked for the NHL decay modes $N_\mu \to \mu^+\mu^-\nu$ or $N_\mu \to \mu +$ hadrons inside the steel calorimeter. They found no evidence for NHLs and established upper limits on the NHL mixing in the mass range of 0.25 - 14 GeV/c^2.

- *PS191*, (1986) [19]: In this search NHLs may be produced in π and K meson decays at the CERN PS, $K/\pi \to eN$ and $K/\pi \to \mu N$. The best limit for mixing was $|U_e|^2 < 10^{-8}$ for mass around 400 MeV, essentially well covering the mass region < 400 MeV. However the analysis technique of this search has not been generally accepted. According to Ref. [19] they hand-scanned their data sample consisting of "few dozens events" and eliminated them as candidates for various subjective reasons. I do not plot it on the final Figure 9.1.

- *CHORUS/NOMAD*: This group is searching for NHLs in the CERN wideband neutrino beam produced by 400 GeV protons in the mass region 0.5 - 3.0 GeV/c^2. Results are yet to be published.

The combined upper limits for $|U|^2$ are summarized in Figure 3.1

3.0.2 Collider searches

In collider searches, possible sources of NHLs are $W^\pm$ and Z^0 decays, where NHLs are both produced and decay inside the detector. Collider experiments set limits on the branching ratios or cross sections and NHL masses. For comparison, those limits are converted in the corresponding limits on NHL mixing constants and masses. All limits are given at the 95% confidence level.

Collider experiments do not contribute significantly to the upper limits on the NHL mixing in the mass region described in this paper (0.2 - 2.0 GeV/c^2); Instead they cover higher masses and larger mixing regions.

- *L3*, (1996) [20] This search was based on the data collected at LEP with the L3 detector in 1990-1991. A NHL may be produced in the decay

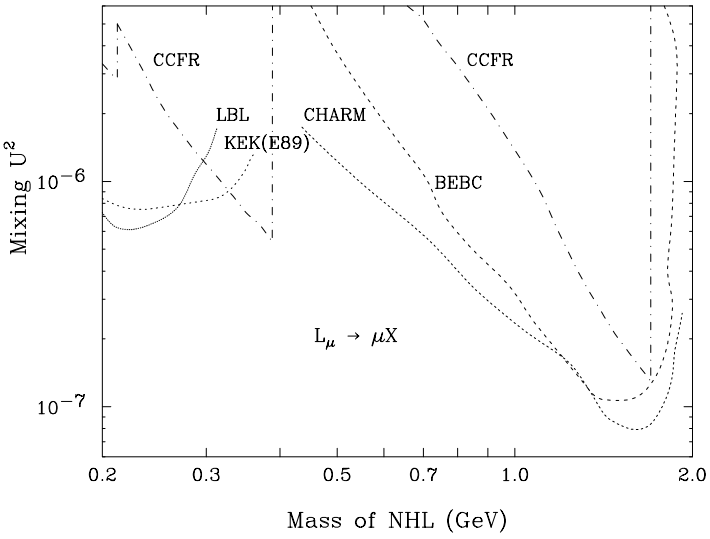

Figure 3.1: Experimental limits on the NHL–ν_μ mixing in the mass range 0.2 - 2.0 GeV/c^2, excluding results of this search.

$Z^0 \rightarrow \bar{\nu}_l + NHL$. The search covered the NHL mass range from 1 GeV/c^2 up to m_Z. In this search, isosinglet neutral lepton would decay via the neutral or charged weak current

$$N_l \rightarrow Z^* \nu \text{ and } Z^* \rightarrow ee, \mu\mu, \tau\tau, \nu\nu, qq,$$
$$N_l \rightarrow W^* \begin{pmatrix} \mu \\ e \\ \tau \end{pmatrix} \text{ and } W^* \rightarrow e\nu, \mu\nu, \tau\nu, \nu\nu, qq',$$

which could be identified in the detector as a displaced vertex. Among 424,000 hadronic Z^0 decays no such events were found. Limits of the order of 5×10^{-4} were set on the mixing term $|U|^2$, corresponding to limits of the order of 3×10^{-5} on the branching ratio $Br(Z^0 \rightarrow \nu_l \text{NHL})$ for NHL masses from 3 GeV/c^2 up to $\simeq 85$ GeV/c^2.

- *ALEPH*, (1996) [21] This collider experiment at LEPII searched for the pair production of heavy leptons at the center-of-mass energies, $\sqrt{s} =$ 130 and 136 GeV. No candidate events were found and upper limits were established on a NHL mass of 63 GeV/c^2 for $|U|^2 < 10^{-10}$ for Dirac neutrinos and $m_{\text{NHL}} > 54.3$ GeV/c^2 for $|U|^2 < 10^{-10}$ for Majorana neutrinos.

- *DELPHI*, (1997) [22] Weak isosinglet NHLs have been searched for using data collected by the DELPHI detector corresponding to 3.3×10^6 hadronic Z^0 decays at LEP1. No indication of the existence of these particles has been found, leading to an upper limit for the branching ratio

$BR(Z^0 \to NHL\overline{\nu})$ of about 1.3×10^{-6} at 95% confidence level for NHL masses between 3.5 and 50 GeV/c^2. This corresponded to the upper limit on the $|U|^2$ of $2.2{\times}10^{-5}$. Outside this range the limit weakens rapidly with the NHL mass.

3.1 KARMEN anomaly

The KARMEN experiment [23, 24] is a neutrino experiment, which used a pulsed proton beam to generate pions. The pions are stopped and decay to a muon and a neutrino, with the muon subsequently decaying and yielding muon and electron neutrinos. Neutrino interactions are observed and their timing spectrum is characteristic of the muon lifetime. However, there is an excess of events seen by KARMEN in the ν timing distribution, which can be interpreted as the decay of a slow moving particle, $v \approx 0.016c$, arriving 3.6 μs after the pulse. A possible explanation is the existence of a 33.9-MeV NHL lepton produced in the pion decay $\pi \to \mu$ NHL. The potential NHL is on the edge of the available phase space, and therefore travels slowly in the π rest frame, making this type of detection possible.

The search described in this thesis cannot address the anomaly directly since an outgoing muon in the decay is required. Another search using the decay channel data has been performed by the same group. The results gave no indication of such NHL and excluded part of the KARMEN allowed region (see Ref. [62]). Our experiment is sensitive to the decays of NHLs in the mass range 0.2-2.0 GeV for the mixing constants above 10^{-8}.

Chapter 4

The Experimental Setup

In order to detect NHL decays, an instrumented decay region ("the decay channel") was constructed 1.4km downstream of the production target. The decay channel was designed to track and identify NHLs decaying to two charged particles. There were four basic elements of the experimental setup

1. *The SSQT beamline*
   NHLs may be created in the NuTeV SSQT beamline by the decays of π, K and D mesons.

2. *The Veto Wall*
   It rejected charged particles entering the decay channel from the upstream region

3. *The decay channel*
   In this region NHLs could be detected if they decay. It was composed of

   - 6 drift chambers
   - Helium bags

4. *The NuTeV sampling calorimeter*
   It provided particle identification (ID), energy measurements, and triggering.

The relative layout of the veto wall, the decay channel and a part of the NuTeV calorimeter is shown in Figure 4.1 (the drift chambers were named as shown for various real and fictitious people). Each of these elements is discussed in more detail below in this section.

4.1 Neutrino beamline

In this section, I describe the production of NHLs in the NuTeV SSQT beamline. This beamline was supplied by 800 GeV protons from the Tevatron Accel-

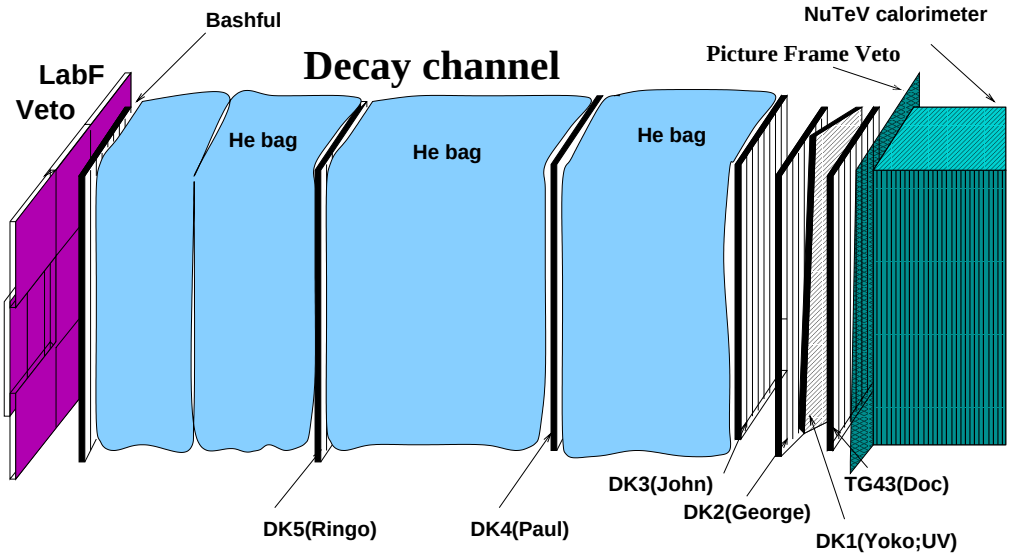

Figure 4.1: The decay channel, veto wall, picture frame veto wall and part of the calorimeter. Beam direction is from left to right of the picture. Decay channel chambers are marked with DK# and with names in parenthesis. Bashful chamber was not used in the NHL analysis. DK1 was a tilted "UV" chamber.

erator. The protons struck a BeO target producing π, K and D mesons. The long lived charged mesons (pions and kaons) were directed toward the detector and focussed using a series of magnets called the sign-selected quadrupole train (SSQT). Below I consider each step of the production process, beginning with the acceleration of the protons.

The primary proton beam was created in the Tevatron accelerator at Fermilab. The production and acceleration of protons occurred in stages as shown schematically in Figure 4.2.

First, H^- ions were produced by a cesium cathode immersed in a hydrogen gas. Then the H^- ions were collected from the source and accelerated to 750 KeV by multiple electrostatically induced potential drops. The energy of H^- ions was increased further to 200 MeV by a Linac. Ions were stripped of their electrons as they passed through a carbon foil at the exit of the Linac. In the 70m radius Booster ring the protons were accelerated to 8 GeV and passed to the Main Ring. The Main Ring consists of the 1km radius synchrotron, which accelerated the protons to 150 GeV. A superconducting proton synchrotron was designed to accelerate protons to 1 TeV. For fixed-target running, the protons were accelerated to 800 GeV. Every acceleration cycle of 60.1 secs, protons were extracted into the fixed-target beamlines. There were three fixed-target beamlines (meson, neutrino and proton) and the extracted protons were split between all of them by magnets located in the switchyard facility. The

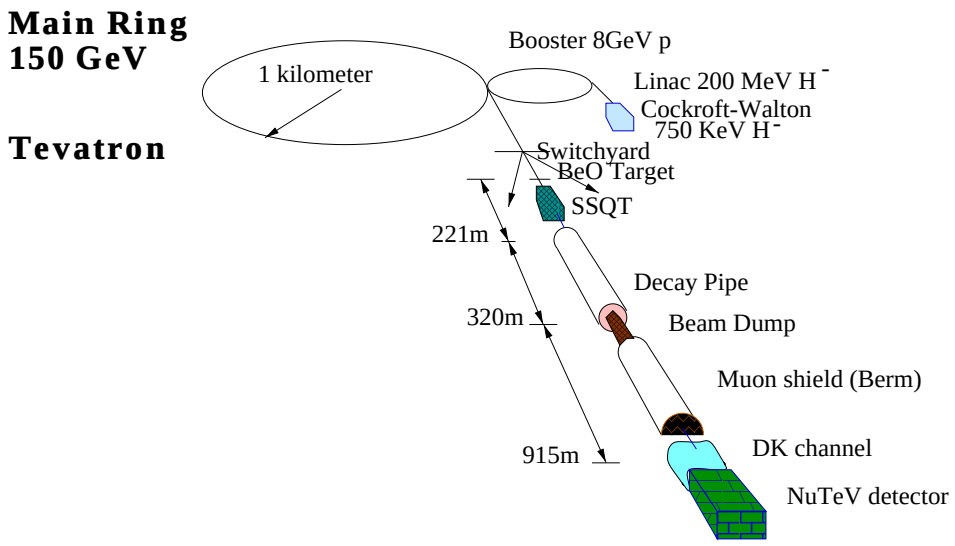

Figure 4.2: Fermilab Tevatron and neutrino beamline.

switchyard transfered special proton bursts ("pings") of 5 msec width to the neutrino line only. Every cycle there were five special pings, each containing up to 3×10^{12} protons.

In the neutrino area, the protons would strike a 30.5 cm beryllium oxide target producing a secondary wide-energy beam of hadrons. The sign-selected quadrupole train (SSQT [37],[35]) with alternating focusing directions provided net focusing and sign selection of the secondary mesons of the right charge ("right-signed"). The SSQT consisted of 6 focusing quadrupole magnets, 2 bending magnets (dipoles) and 2 beam dumps.

SSQT dipoles (described in Ref. 4.3) focused the π and K mesons down a beamline 7.8 mrad from the primary proton beam direction but directed towards the Lab E/F neutrino detector. "Wrong-signed" π, K and the secondary protons were bent in different directions and dumped into blocks, mostly made out of aluminum.

The sign selection of the SSQT was critical to certain measurements by the NuTeV experiment, such as $sin^2\theta_W$. For this analysis sign selection was not required. A consequence of the sign selection was the 7.8 mrad bend of the secondary beam, which reduced the sensitivity of the search for NHLs from D meson decays. This effect was taken into account when calculating the resulting limits.

The SSQT elements were aligned so that the the magnetic center of each quadrupole was along the path of forward-produced secondaries at the central momentum of the SSQT, which was 250 GeV. A schematic view of SSQT is shown in Figure 4.4. The detailed description of the SSQT alignment can be found in Ref. [35]. To test the alignment of SSQT elements, a test run on

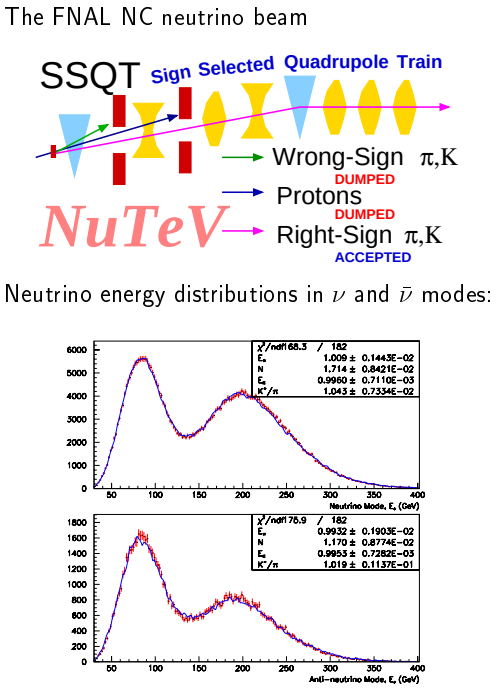

Figure 4.3: The figure of NuTeV Sign Selected Quadrupole Train and neutrino energy distributions in neutrino and antineutrino modes.

straight-through protons was performed during 1995.

During the 1996-1997 fixed-target run, while the decay channel was taking data, 1.13×10^{18} protons were received with the magnets set to focus positive mesons, and 1.41×10^{18} protons with negative meson focusing. After focusing, the mesons entered a 541m long decay region. K mesons were assumed to decay via two body decays producing NHLs with masses from 0.25 to 0.4 GeV/c^2. NHLs in the mass range of $0.4 < m_{\mathrm{NHL}} < 2.0 GeV/c^2$ could be produced in two- or three- body decays of D-mesons in the proton dump or primary production target. The production rate of D_S mesons was taken to be 54% of the D production rate (Ref. [39]). NHL production from π decays was not considered this analysis.

Table 4.1 shows the number of K and D decays that contributed to the NHL production. That was our flux.

Approximately 3% of π mesons and 17% of K mesons decayed in the decay pipe and the rest of the beam was dumped into a 6m block of aluminum. Only the neutrinos and muons from these decays would penetrate the downstream aluminum beam dump. The muons ranged out in the 915 m of earth "berm"

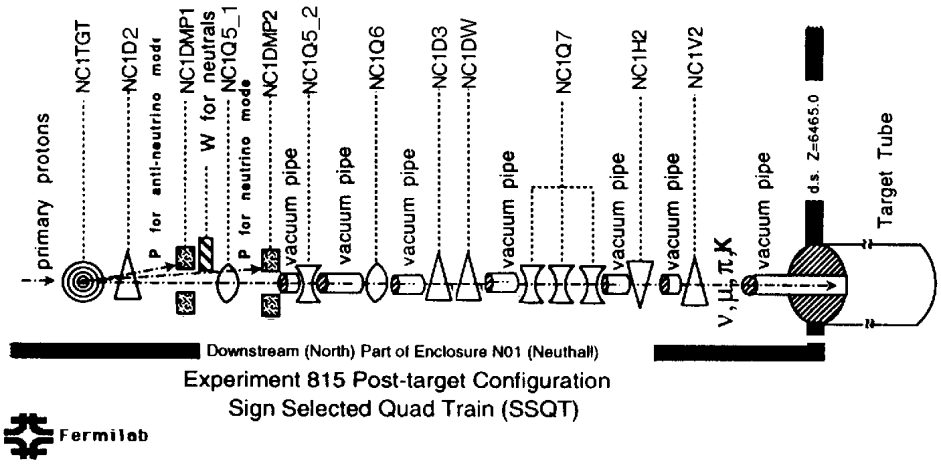

Figure 4.4: A schematic view of SSQT elements. energy distributions in neutrino and antineutrino modes.

mode	number of K decays	number of D decays
ν	2.18×10^{15}	2.12×10^{12}
$\bar{\nu}$	8.03×10^{14}	2.64×10^{12}
total	2.98×10^{15}	4.76×10^{12}

Table 4.1: Meson decays contributing to NHL production.

downstream of the dump and only neutrinos could penetrate into the experimental area. However, some of the neutrinos interacted in the berm creating muons that entered the experimental hall. Events with muons produced in the muon shielding were identified by the veto wall and discarded.

4.2 The veto wall

The veto wall array marked the most upstream part of the decay channel. It's purpose was to identify the beam related backgrounds caused by charged particles produced by neutrino interactions in the soil shielding in front of detector called "berm".

Charged particles could enter the detector hall after being produced by neutrino interactions in the berm. Any charged particle had to go through the veto wall before entering the decay channel. A veto signal was used to form triggers for the decay channel and for other measurements as well (described in Ref. [60, 61, 37]).

The veto wall was located in "LabF", upstream of the decay channel and NuTeV calorimeter. It consisted of two adjacent planes of scintillation counters. The counters were assembled on unistrut frames. Each plane had three rows and three columns. The veto wall lay-out is shown in Figure 4.5

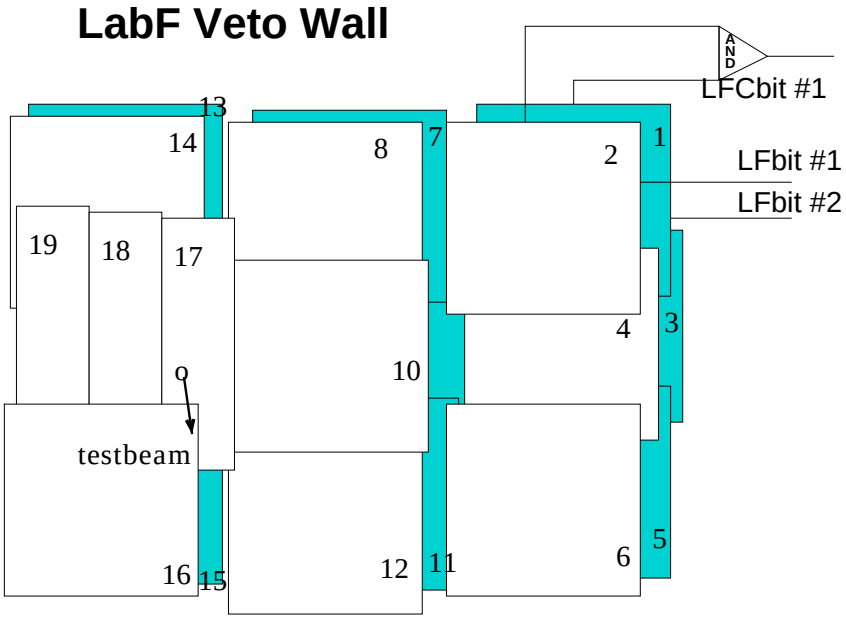

Figure 4.5: Picture of the veto wall located in LabF. Each counter had a corresponding flag in the software called LFbit. Two neighboring counters form a coincidence flag, LFCbit. An arrow shows the direction of the NuTeV testbeam going downstream toward the viewer.

There were 19 scintillation counters assembled in two $4.6m \times 4.6m$ veto arrays, completely shielding the decay channel and NuTeV calorimeter. The second array was placed immediately downstream of the first wall of counters. A charged particle going through the veto wall would fire counters in both arrays in coincidence. The counters were one-inch thick, enveloped in black plastic preventing any optical leaks. More than 2 inches of overlap of adjacent counters was made to ensure that either veto plane contained cracks and the entire face of the Decay Channel was covered. Two out of three columns had 60"×60" counters placed one after another. The counters on top and on the bottom of the third column had similar layout and same make and size.

Special considerations were needed for the center section of the east–most column; this was to accommodate the NuTeV testbeam which passed through that region. To minimize any interference with the testbeam, only a single layer of thinner, 1/2" detectors was used. These are labelled Paddles 17, 18, and 19 in Figure 4.5. It consisted of three counters placed with their vertical edges overlapped by only 2 inches. The counters were covered in thin black

isolation paper. They were 20 inches wide, 90 inches high and 1/2 inch thick. Monte Carlo studies indicated that there were no significant interactions of the testbeam with material of the veto wall. The positions of the center of lab F veto wall counters were measured by surveyors and are given in Table 4.2. [1]

Lab F veto wall counter	X pos. of center in inches	Y-center in inches	Z-center in inches
lfbit 1	56.56	49.56	-2410.97
lfbit 2	56.56	49.56	-2382.47
lfbit 3	56.56	5.0	-2405.22
lfbit 4	56.56	5.0	-2388.22
lfbit 5*	56.56	-41.56	-2410.97
lfbit 6	56.56	-41.56	-2382.79
lfbit 7*	0.11	47.56	-2365.72
lfbit 8	0.11	47.56	-2337.28
lfbit 9*	-1.23	5.21	-2361.53
lfbit 10	-1.23	5.21	-2343.03
lfbit 11	0.0	-41.56	-2365.72
lfbit 12	0.0	-41.56	-2337.28
lfbit 13*	-53.56	63.31	-2399.91
lfbit 14	-53.56	63.31	-2375.41
lfbit 15*	-51.58	-48.31	-2423.16
lfbit 16	-51.58	-48.31	-2415.16
lfbit 17	-40.28	-8.06	-2403.41
lfbit 18	-58.28	-8.06	-2404.41
lfbit 19	-77.28	-8.06	-2405.41

Table 4.2: Positions of the centers of lab F veto wall counters in the NuTeV lab frame in inches. Counters are marked by a corresponding lfbits. The positions marked with * were measured by the Fermilab surveyors (counters 5,7,9,13 and 15). Positions of the rest of the counters was measured based on the surveyor's measurements.

The scintillation counters work by the following principle: A charged particle excites the scintillator, producing light in the blue and UV range. The light is then shifted into the blue-green range by wave guides. They also direct the light to phototubes (PMT's) which convert the light to an electronic signal. For each of the 5ft×5ft counters, there were two HAMMAMATSU R2154-05 phototubes (phototubes A and B in the discussion below) located at opposite corners. Counters 17, 18 and 19 each had a single phototube.

[1] Survey measurements were conducted for counters 5, 7, 9, 13 and 15.

The high-voltage to the phototubes was provided by a "cow", a high-voltage divider system set to 1900 Volts. The non-amplified Bicron scintillator phototubes were source-balanced to determine their voltages. The three counters in the testbeam region, had special phototubes with a maximum voltage of 1600 Volts and a nominal operating voltage of 1460 Volts.

The veto signal was formed following the logic shown in Figure 4.6. For

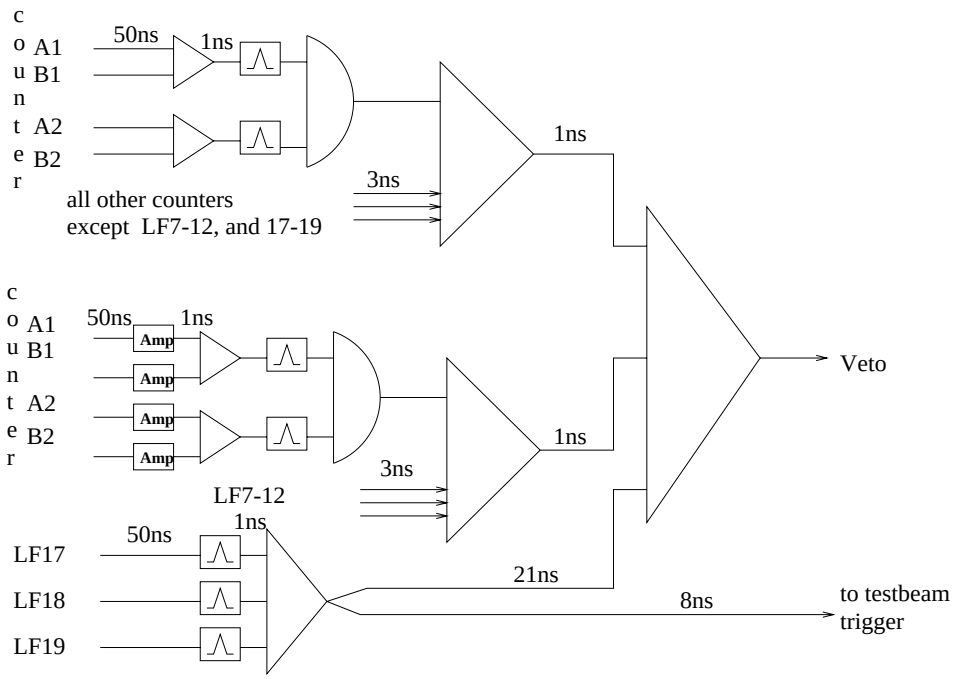

Figure 4.6: Lab F veto wall logic.

each counter, the signal from phototube A and phototube B were combined via a logical Fan-in module and discriminated at a level which isolated particle signals from noise in both tubes. The signals from counters 17, 18 and 19 were logically 'OR'd. Delay cables were used for time synchronization as shown in Figure 4.6. The combined and discriminated signal from each counter provided the input to the veto wall logic. The logic used in forming the veto was based on the NIM standard. The veto required a coincidence of the signals from the counters at the same transverse position in both planes. Counters 1 and 2 would form a coincidence signal (LFCbit), which would result in veto, however the coincidence of counters 1 and, say, 6 would not produce a veto, because the counters were too far apart. This scheme reduced the veto rate from cosmic ray showers and other noise sources. The veto signal was relayed to the trigger logic via fast, hard-line cable. The total time it took for a signal to propagate from the phototube to the end of the hardline in the trigger room was 130 ns.

Along with the single veto signal, the combined and discriminated signals from every counter were recorded as software flags for later studies (for example

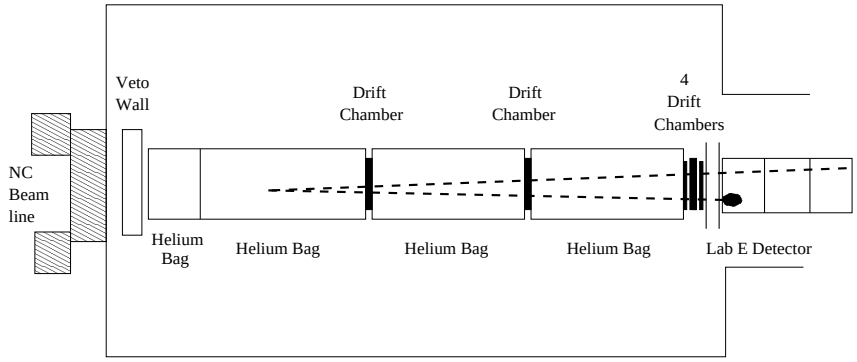

Figure 4.7: A schematic diagram of the decay channel. The beam enters from the left; at the far right is the Lab E calorimeter. An example NHL decay to $\mu\pi$ is also shown. The event appears as two tracks in the decay channel, and a long muon track and a hadronic shower in the calorimeter.

for studying a veto wall efficiency). They were converted from NIM to TTL standard (standard used by TDC logic) and passed to TDC modules via twist-N-flat wire. The signals from the individual counters were called 'LFBits'. The coincidence signals from adjacent counters were stored as 'LFCbits'. There were 19 LFbits, one for each counter, and 10 LFCbits. 16 veto wall counters formed 8 LFCbits. Signals from the counters 17, 18 and 19 were connected via a logical OR, just as for the hard line veto, and formed the 9th LFCbit. The hard line veto constituted the trigger level veto signal. The 10th LFCbit signal was OR of the other 9 LFCbits, and repeated the trigger signal in the software.

4.3 Decay Channel

The purpose of the decay channel was to register the products of a possible NHL decay. It was instrumented in the region in front of the NuTeV calorimeter and downstream of the Lab F veto wall. The basic elements of the decay channel were helium contained in the plastic bags and 6 drift chambers formed a particle tracking system. The layout of the decay channel in the Lab F is shown in Figure 4.7.

4.3.1 Drift chambers

Drift chambers provided the tracking of the charged particles in the decay channel. They were placed at 15.4m, 25.2m, 35.5m, 36.8m, 38.5m and 40.0m with respect to the downstream edge of the veto wall array. The following table, Tab. 4.3, lists positions of drift chambers. Names, DK1, DK2, DK3, DK4 and DK5 were assigned to the chambers, DK5 being the most upstream

Chamber Name	Z position	
	in Lab E, in inches	to Veto, in meters
TG43	-819.50	40.0
DK1(UV)	-877.97	38.5
DK2	-887.22	36.8
DK3	-939.63	35.5
DK4	-1343.61	25.2
DK5	-1729.32	15.4
BASHFUL	-2300.94	0.9

Table 4.3: Z positions of the chambers in the labE frame (shown in inches) and relative to the veto wall (in meters). The XYZ positions of the first wire for every chamber could be found in the standard E815 specfiles (see Ref. [50]). The zero point for in the Lab E frame was 60.8m from the veto wall.

chamber. DK5(DK1) was at a distance of 26.2(3.08)m from the front face (FF or upstream edge) of the calorimeter. An additional drift chamber called TG43 was also used in the decay channel tracking. It was located 1.59 m from the FF of calorimeter (40 m from the veto wall). For some period during the run (it corresponded to approximately 10TG43 was shifted by 18" to the right of the beam (east of NC) if looking in the beam direction. For run numbers 5653–5707 (tape numbers 320–338) TG43 was shifted by 18" to the east and for runs 5708–5947 (tapes 339–475) by 9". The TG43 chamber movements are reflected in the alignment periods in Table A.1. The Bashful chamber, which was not part of the decay channel, marked the end of the decay channel volume at 39.2 m from the calorimeter FF or 0.9m from the veto wall. It was also shifted to the right of the beam (east side of the detector) by about 1.34 meters.

The decay channel drift chambers had two planes for X- and Y- position measurements. The X plane was located upstream of the Y plane. Combining the hit information from two orthogonal planes provided the determination of the particle's position in the "XY" plane. However in the case of two or more tracks passing through the chamber, there was an ambiguity for matching tracks between X and Y views. The question was: "Which X hit belonged with which Y hit?" To provide the matching of tracks between X and Y views, one of the chambers was tilted by 47 mrads clockwise in the beam direction and was called the "UV" chamber. The hits registered in this chamber would be referenced in a tilted frame of UV coordinates, hence the chamber name. The hits in the UV chamber combined with XY position of a measured track from the rest of the decay channel chambers can be used to resolve the ambiguity

and match the tracks.

The decay channel drift chambers were taken from the most downstream region of the neutrino detector. The chambers were originally used in the toroid-spectrometer system to measure the outgoing muon momentum. A MC study showed that removing 6 drift chambers would not appreciably affect the precision of the NuTeV spectrometer measurements (see Ref. [39]). Three drift chambers were removed from the downstream part of the detector ("blue cart") and three from the toroid. Drift chambers were supported by unistrut stands mounted to the floor. Due to its low cost and ease of use, the unistrut material was used extensively in the decay channel construction.

Each drift chamber had an active area of 10 square feet and consisted of 24 horizontal and 24 vertical cells. Each cell was 5 inches across and 0.75 inches thick. The chambers were constructed of Hexel covered aluminum walls. Parallel aluminium strip, I-beams were spaced five inches apart and defined the drift chamber cells. The chambers were filled with a 50-50 mixture of argon/ethane gas. The material content of a drift chamber is described in Table 4.4 (based on Ref.[60]). When a charged particle passed through a chamber, the argon atoms in the gas were ionized. The free electrons drifted toward the anode wires. The drift velocity of electrons in the chamber is around 50 μm/nsec. The total drift time to cross 2.5 inches inside a cell is 1.3 μsec. An avalanche of electrons was produced when electron reached the anode "sense" wire. Excited argon could produce X-rays, but ethane atoms de-excited it. The ethane acted as a quench gas, absorbing electrons and limiting the size of avalanche and the amount of charge that would otherwise smear the signal pulse. The cascade of electrons induced a "signal" voltage on the sense wire, which if it was large enough to fire the discriminator was registered by the DAQ. In this thesis the registered signal is called a "hit". The hit was then recorded by a readout system.

Five of six drift chambers were "single wire" chambers. They had one sense (anode) wire per cell and thus had an ambiguity for which side the particle went through. Sense wires were made of 30 μm diameter gold-plated tungsten threads and were kept at +1750 Volts. The high voltage for the sense wires in a drift chamber was provided by a "Droege" power supply. The drift field was produced by strips of copper clad on a G-10 cover, held at voltage to create a 690 V/m uniform electric field. The G-10 cover was supported by parallel aluminum I-beams, which were the cathodes of the system and were kept at -4500 Volts by a Bertan high voltage power supply. A single Bertan supply in each rack served several drift chambers. Single-wire chambers measured the drift time of the ions created by the passing charged particle, but could not detect on which side of the wire a particle passed. The left-right ambiguity was resolved in the offline analysis by the tracking algorithm. Drift chamber cells were numbered from 1 to 24, with the cell X24 in the X plane on the left,

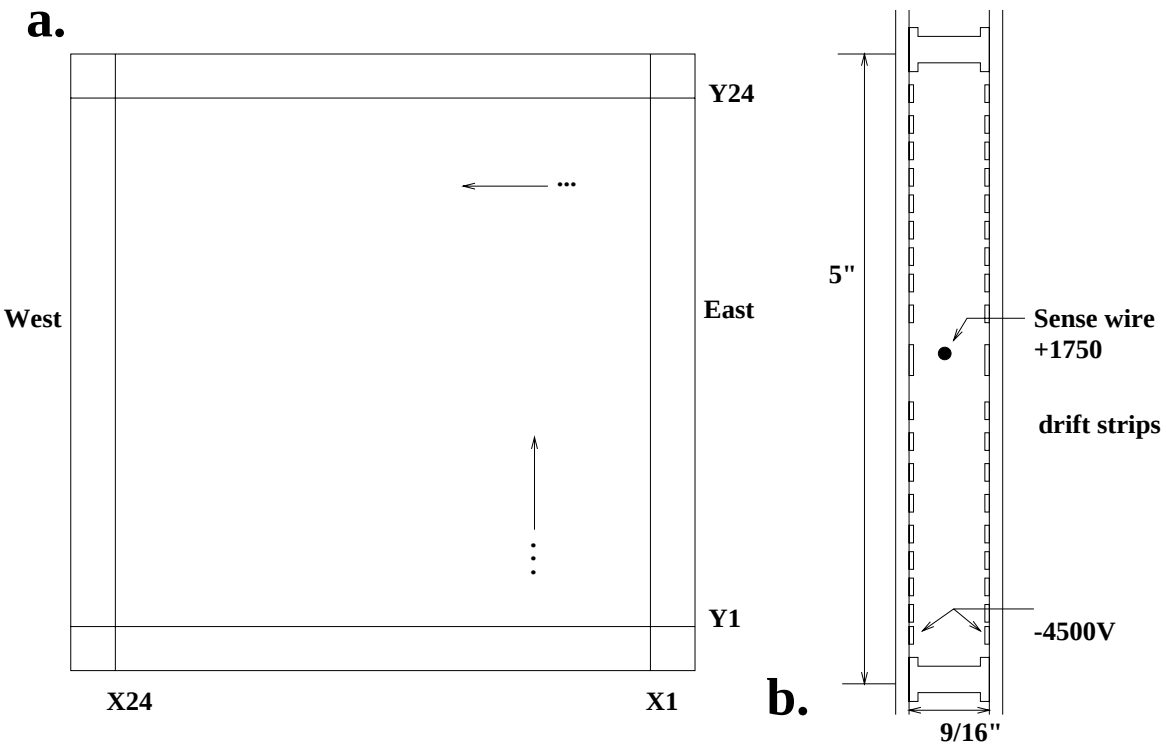

Figure 4.8: **a)** A drift chamber had 24 cells numbered, so that cell 24 of Y and X (X24, Y24) plane was in the upper left corner if looking downstream. **b)** Diagram of one cell of a "single wire" chamber. X plane was located upstream of Y plane.

if looking in the beam direction, and the cell Y24 on the top of the chamber as shown in Figure 4.8.

The sixth decay channel chamber, TG43, was a three-wire chamber. It was also used as a spectrometer chamber for the NuTeV testbeam and belonged to the calorimeter read-out branch.

Three-wire chambers had two sense wires and one field wire per cell. An extra sense wire made it possible to determine the side of the cell a passing particle traversed. In other words, the two sense wires in the cell removed the left-right ambiguity for a hit. Each cell had the field shaping wire kept at +350 Volts between the two sense wires to keep the system in electro-mechanical equilibrium. Nylon spacers placed every 12 inches maintained the 2mm separation between the sense and field wires. Figure 4.9 shows a picture of the drift chamber and the three-wire cell. The drift chambers were staggered in the transverse direction to help to resolve the left-right ambiguity, so that the dead regions between cells would not line up.

The leading and trailing edge times of input signals were stored for readout. After the trigger, this time history was read out by the TDC (time-to-digital

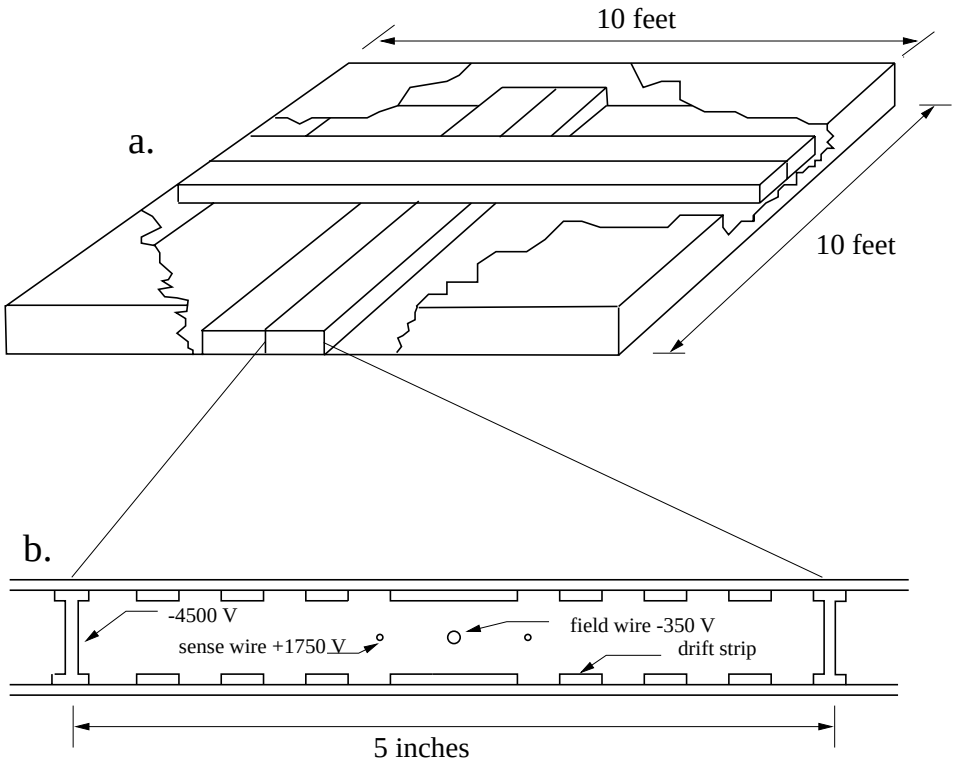

Figure 4.9: **a.** The diagram of a three-wire drift chamber. There are two orthogonally-oriented planes consisting of three-wire cells.**b.** A three-wire cell had two sense wires and a field wire between them.

converter) system. The signal from the decay chambers was transfered to the TDC modules by flat-and-twisted cable. The cables were accurately cut in length so that the signals from the same plane would arrive at the TDC modules in time. In the middle of the run (December 1996), TG43 had 2 bad cables that were replaced with new ones. The replacement cables had significantly different length, so the alignment procedure for the drift chambers had to be adjusted accordingly. The data readout was controlled by the DAQ (data acquisition), which transfered data onto the tapes. The readout is described in more detail in Sec. 4.6.2.

4.3.2 Helium – the fiducial volume of the decay channel

The decay channel was designed to minimize the background without significant loss of acceptance. Neutrino interactions in the material of the decay channel contributed most to the NHL background. The rate of ν interactions depends on the number on nucleons per volume. A material with the lowest possible density could reduce the NHL background. In the case of the NHL searches, helium gas was the most reasonable choice. A vacuum region of this

size would be impractical and hydrogen was too dangerous to handle. The helium was contained in four plastic cylindrical bags, 16 feet in diameter and 34 feet long. The helium bags were connected to the Fermilab helium supply system.

The helium flow in the lab supply system was subjected to changes due to fluctuations in air temperature and pressure. The uncontrollable expansion and contraction of helium bags could lead to mechanical deformation of the drift chambers located between them, and as a result, to high voltage trips and losses in detection efficiencies. To regulate and maintain the pressure in the supply system, a rack with a monitoring system was mounted in lab F, beside the decay channel. It served as a buffer between the lab supply and the decay channel helium. The monitoring system consisted of a helium pressure gauge and 4 smaller flow controllers, one per helium bag. Four small plastic tubes, one per helium bag, were branched out of the helium supply flow and went through a volume filled with mineral oil. If the pressure in the external supply system and/or in the helium bag was over the limit the extra helium would push through the mineral oil and "bubble" out into the atmosphere. The pressure level was maintained by the level of the oil in the bubblers. However, the flow rate through the bubblers was small and, due to the vast volume, it could take several hours for the system to reach equilibrium in the severe case of a rapid change in temperature.

Helium was put into the bags after the tracking system was assembled and mounted in place. The helium bags were held down by soccer nets attached to the floor of the laboratory in between decay channel drift chambers. Having helium in the fiducial volume of the decay channel lowered the neutrino interaction background by about an order of magnitude with respect to air.

4.4 The Neutrino Detector

The labE neutrino detector consisted of an iron-scintillator sampling calorimeter, that served also as a neutrino target, and a toroidal magnet spectrometer, which measured the momentum of the outgoing muon.

Figure 4.10 shows the picture of the NuTeV detector.

4.4.1 Target Calorimeter

The NuTeV calorimeter consisted of 168 10ft$\times$10ft$\times$2" steel plates interspersed with 42 drift chambers and 84 scintillation counters. It had a mass of 690 tons and was 17.7 m long. The calorimeter was longitudinally divided into six identical movable carts. Each cart had a repetitive structure with a sandwich-like unit Fe–SC–Fe–DC–Fe–SC–Fe repeated 7 times, where DC stands for a drift chamber, SC for a scintillation counter and Fe for iron plates.

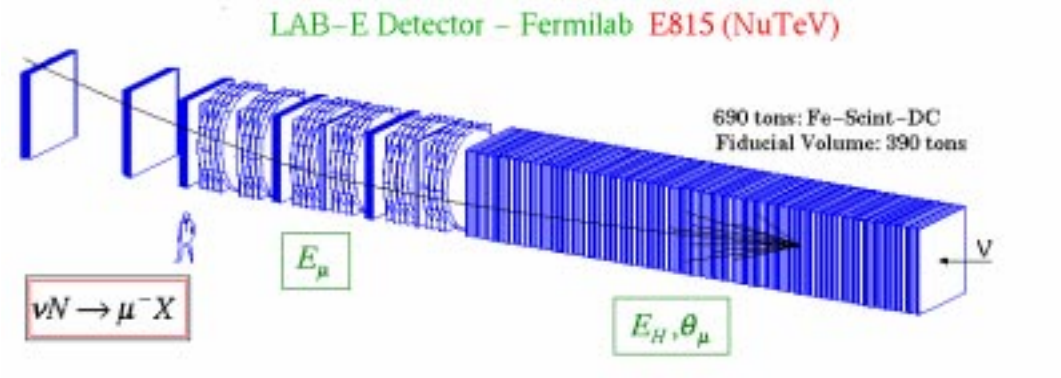

Figure 4.10: A picture of the NuTeV detector, The neutrino beam enters from the right. The two leftmost sets of drift chambers are known as the blue cart. The decay channel upstream (right) of the NuTeV calorimeter is not shown on this figure.

There were two plates of steel between every two consecutive scintillation counters and one drift chamber between every other set of counters. Table 4.4 gives the composition of the NuTeV calorimeter subunit. The mean density of the target was 4.2 g/cm^3 (Ref. [60]).

Neutrinos interacted in the calorimeter and the energy of the interaction was sampled by the scintillation counters every 10cm of iron. The scintillation counters were made of 10' $\times$ 10' acrylic tanks filled with scintillator (mineral) oil. The oil was provided by the Bicron corporation and had an admixture of scintillating fluorsin mineral oil. A charged particle passing through the counter excited the primary fluors, which would radiate ultraviolet light. The secondary fluors absorbed the ultraviolet and emitted visible blue light. At the edges of the counter there were one half inch thick BBQ doped plastic bars that absorbed the blue light and re-emitted green light. The green light was guided to the ends of the bars in photo multiplier tubes.

Four photo-multiplier tubes at the corners collected the light output of the counter. They were HAMMAMATSU R2154-05 10-stage gree-extended phototubes operating with a potential drop of 1400 volts across the cathode. A photon striking the cathode has about a 20% chance of knocking out an electron. It is accelerated in a electrical field of the tube, knocking more electrons out of the tube dynodes and producing an electron shower. Each dynode emits on average four electrons for each one absorbed. Ten stage phototubes produced a signal of about 0.25 pC from a single initial photoelectron.

The phototube signal was digitized by a LeCroy 4300 FERA Analog to Digital Converter (ADC). The digitized signal (pulse-height) was read out by the DAQ system and written on tape. The total light output from the counters was approximately proportional to the total energy of the sampled hadron

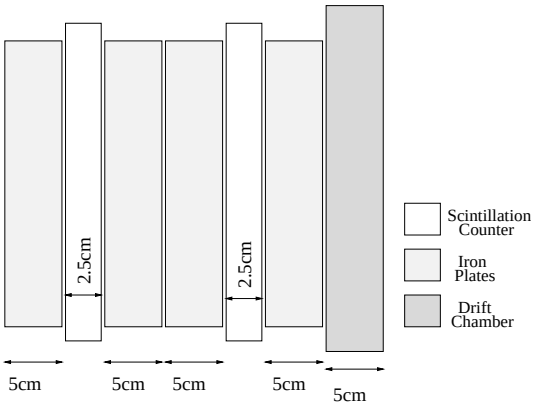

Figure 4.11: A unit of the calorimeter. It consists of 4 steel plates, 2 scintillation counters and 1 drift chamber. It is repeated 42 times to make up the entire calorimeter.

shower. The coefficient of proportionality was determined in the calibration procedure, described in more detail in Ref. [37]. An absolute calibration was established with the testbeam particles by measuring the energy deposited by beam particles with known momentum.

The hadronic energy resolution of the calorimeter was $\frac{\sigma}{E} = 0.022 \oplus \frac{0.86}{\sqrt{E}}$, and the electromagnetic energy resolution was $\frac{\sigma}{E} = 0.042 \oplus \frac{0.50}{\sqrt{E}}$. The response to electrons and pions was similar with an $\frac{e}{\pi}$ ratio of about 1.08 .

4.4.2 Muon spectrometer

A toroidal spectrometer measured the momentum of the outgoing muon by determining its bend in the magnetic field.

The muon spectrometer was located downstream of the neutrino target calorimeter and consisted of three large toroidal iron magnets (toroid carts), acrylic counters and an array of single-wire drift chambers. Each toroid cart was segmented into eight cylinders, called washers, which were 8 inch thick, 140-inch in diameter and with a 10 inch diameter hole in the center. Each washer was divided horizontally into semicircles separated by 0.95cm to allow installation of the coils. This also made it possible to insert the Hall probes for measurements of the magnetic field of the washer during the run. Each washer was supported by two iron legs on movable platforms. A current of 1200 A produced a magnetic field ranging from 1.9 tesla near the center of the toroid to 1.55 tesla near the outer edge. The muon traveling the length of the calorimeter received a 2.4 GeV transverse momentum kick from the magnetic

item	component	formula	length (cm)	density (g/cm^3)	mass (g/cm^2)
1 drift chm.	Al hexcel	Al	0.32	2.70	0.86
	Al I-beams	Al	0.06	2.70	0.15
	G10(1 of 2)	60% SiO_2	0.64	1.7×0.6	0.67
	G10(2 of 2)	40% CH_2O	0.64	1.7×0.4	0.45
	copper	Cu	0.08	8.96	0.74
	gas	ArC_2H_6	1.91	0.0016	0.00
total			3.65		2.87
4 iron plate	Fe plate	Fe	20.68	7.874	162.53
2 counter	scint. oil	CH_2	5.08	0.8	4.06
	lucite	$C_5H_8O_2$	1.28	1.18	1.51
	water	H_2O	5.08	1.00	5.08
	mylar	$C_5H_8O_2$	1.52	1.39	2.11
dead space	air	$N_0.79O0.21$	6.05	0.0012	0.01
TOTAL			43.34		178.17

Table 4.4: Components of the NuTeV calorimeter subunit with their molecular formulae and masses, including drift chamber materials.

field.

Five sets of single-wire drift chambers provided the tracking of the muon passing through the spectrometer. The two most downstream sets of drift chambers behind the toroid magnet were used to improve the measurements of the outgoing muon momentum. They were located in the downstream part of the NuTeV detector ("blue cart"). To resolve the drift direction ambiguity, called the left-right ambiguity, the chambers were staggered by 1.25inches (1/4 of the cell). In addition there were two UV drift chambers rotated 5 degrees about the beam axis.

The resolution of the energy measurement by the toroid spectrometer was $11\%/\sqrt{E}(GeV)$.

4.5 The decay channel particle ID and energy measurements

Decay channel particle ID and energy measurements were done using the downstream neutrino target-calorimeter and toroid.

The tracks were identified as muons if the reconstructed track was long and thin. The details of particle ID are discussed later in Chapter 6. Here I give only a brief overview. Hadrons and electrons were identified as short

and fat clusters with many hits. The analysis algorithms tried to match tracks reconstructed in the decay channel with the clusters of hits in the calorimeter.

The momentum of the muon track was measured by the NuTeV calorimeter or toroid muon spectrometer. A toroidal spectrometer measured the momentum of the outgoing muon by measuring its bend in the magnetic field.

In the case of a "range-out" muon (one that stopped in the calorimeter), the momentum was determined by the distance measured in the number of calorimeter blocks that the muon traveled. The calorimeter block was described above in Table 4.4. The energy resolution of the range-outs was 155MeV, and was limited by the size of the calorimeter segments.

If the muon exited from the side of the calorimeter, its momentum was determined by a fit to the amount of multiple scattering in the calorimeter steel. Using this method, the energy resolution for momenta lower than 85 GeV was 25%.

The energy of clusters was measured in the calorimeter scintillation counters and assigned to the matching decay channel tracks. The particle ID, energy and momentum determination will be discussed later.

4.6 Trigger, readout, and Data Acquisition (DAQ) systems

The trigger selected events to be digitized and recorded. A set of readout systems digitized drift chamber hits and scintillation counter pulse heights. The digitized data were written to 8mm Exabyte tapes using a VME-based data acquisition system (DAQ). This section describes these systems.

4.6.1 Gates and Triggers

In the high intensity, the detector beam responded with vast quantity of signals, that simply could not be processed by the DAQ due to the processing speed and data volume limitations. To get around this limit, one had to separate and classify events to record only those that satisfy the basic requirements or "triggers". The trigger system, in a very short period of time, identifies events and forms a trigger signal if the events passed the requirements. This signal causes the DAQ to accept the event and record the responses of the detector for that particular event. The trigger system is composed of the detector subsystems that respond very quickly. Usually, it is based on the scintillator signals, that could be produced and processed faster that drift chamber data.

Events were classified and recorded during time windows called "gates". Decay channel triggers happened during gate 1, or a "fast gate", when the beam was present and during gate 7, "cosmic ray gate". The cosmic ray gate was used for background studies and for studies of the veto wall counter noise.

Shown below is the list of the relevant triggers for the NHL analysis. Triggers 1,2,3,9 were used in the NHL analysis. Trigger 5 was used for the NuTeV testbeam. Trigger 6 logged straight-through muons used for alignment.

- **Trigger 1** (Charged Current): selected events in which a muon originates in the target and penetrates into the toroid. The trigger could be satisfied by either of two requirements. The first one required at least two of the last four counters (counters 1 through 4) be active (to fire their s-bits, s-bit defined later in the text), and both T2 (toroid gap 1) and T3 (gap 2) to measure at least a minimum ionizing signal. The second definition of the trigger did not require the muon to penetrate as far as T3, but instead demanded two out of four s-bits in counters 9 thorough 12 together with a signal in T2 and two out of four s-bits in counters 1 through 4. Additionally, no signal in the veto was required.

- **Trigger 2** (Neutral Current): selected events which deposit more than 8 GeV of energy shared between any eight adjacent scintillation counters, coincident with twice minimum-ionizing energy deposited in two out of the four most downstream counters in the group of eight and no veto signal.

- **Trigger 3** (Penetrating Muon): required 16 counters in the target (not necessarily consecutive) to fire their s-bits, no veto signal, and at least 4 GeV of energy deposited in any 8 consecutive counters (not necessarily the same ones that fired their s-bits).

- **Trigger 5** (Test Beam): used for test beam running, when muon and hadron beams are incident directly onto the detector.

- **Trigger 6** (Straight Through Muon): selected muons produced upstream of Lab E which traverse the whole detector. It requires a veto signal and at least one s-bit in each of the target carts.

- **Trigger 9** (NHL): read out events which have the characteristics of a NHL decay. It had two paths: a muon trigger looking for the signature of the muon (μe, $\mu\mu$ and $\mu\pi$) or electron/hadron trigger (ee and $e\pi$). It is described in more detail below.

The NHL analysis used events selected by the triggers 1,2,3 and 9. Trigger 9 was especially designed for the NHL search. The muon part of this trigger had the following three requirements:

- Three out of first four counters (81-84) must fire since there will always be two particles travelling through these counters and

- Four out of the next seven counters (74-80) must fire because there will always be one particle (pion or muon) going through these counters and

- At least thirteen counters in all must fire, because of the penetrating muon.

The first requirement was implemented by summing sbits from counters 81 to 84 in the logical unit, called "3/4(81-84)", which required at least three of the sbit signals coming in to be in time (coincidence level 3). The second part took the sbits for counters 74 to 80 and required at least four of the sbits to be in time. The third requirement used a multiplicity logic units which gave out 50mV for each sbit that fired. These signals were summed in a fan-in module and sent to a discriminator module, whose threshold was set up to produce a pulse only if more than twelve sbits that fired. The discriminator was called the "P>12" module (penetration greater than 12). The outputs of all three modules were required (coincidence level 3) and formed the muon mode trigger signal.

The electron path of the trigger required a deposition of more than 5 GeV in the first four counters (81-84). That was achieved by summing the pulses of all four tubes in a counter (these signals were called "combination lows"); then the summed pulses of four consecutive counters were added to form the "energy sum" for these counters. The ">5 GeV" discriminator module took the output of the energy sum for counters 81 - 84 and discriminated it. The threshold was set to 0.45V, which corresponded to 5 GeV of deposited energy.

Trigger 9 had significant overlap with trigger 1 and 2 in terms of requirements and was used to ensure high efficiency of onlt NHL candidates. The charged current triggers 1 and 3 were very similar to the muon part of the decay channel trigger. Trigger 2, "The Neutral current" trigger, had a stricter energy requirements than the electron part of trigger 9 (8 GeV energy deposition in 8 consecutive counters instead of 5 GeV in the first 3 counters).

Veto signals were included in the trigger logic and formed the veto part of the trigger. The "picture frame" veto was designed to reduce the cosmic ray background. It surrounded the front face of the calorimeter along with the mounted steel plate. The cosmic rays were vetoed if they came at a high angle such that they missed the top portion of the "picture frame" while still hitting counter 83 and twelve other counters below (or deposit more than 5 GeV in one of the first 3 counters). The electron and muon paths were OR'd in the final fan-in module, along with a veto anti-coincidence requirement, set on coincidence level 3 and formed the trigger 9 or NHL trigger. The trigger logic is shown in Figure 4.12.

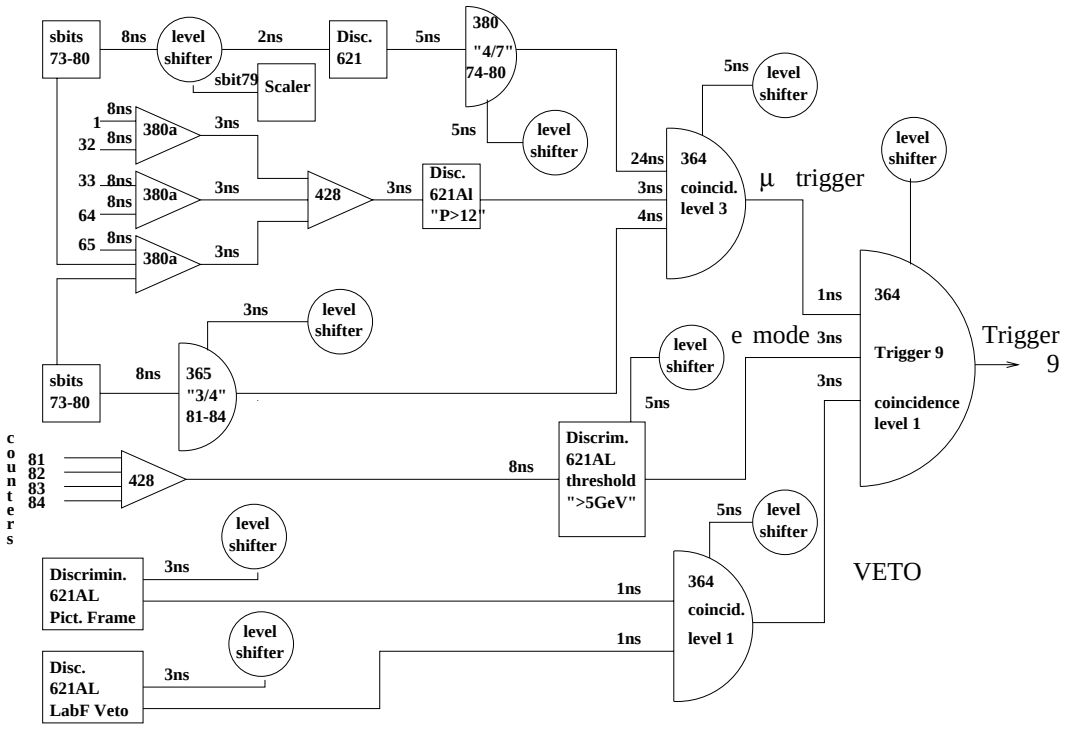

Figure 4.12: NHL (trigger 9) Logic diagram. "3/4" logical module required three out of first four counters, 81 through 84, to fire. "4/7" corresponded to the sbits for counters 74-80. Discriminator "P>12" module required more than 12 s-bits to fire.

4.6.2 TDC Read-Out

The signals from drift chambers were amplified and sent to time-to-digital converters (TDC). The TDC system had three branches: two for the calorimeter and toroid, and the third branch was for the decay channel and the NuTeV testbeam spectrometer. There were two racks with 18 TDC boards. A TDC board took inputs from 16 channels on two 8-pair ribbon cable headers at the front of the board. Single wire chambers had two planes with 24 sense wires per plane, providing 48 channels for 3 TDC boards. To read out signals from 5 decay channel chambers, 15 TDC boards were used, leaving 3 TDCs for the read out of the LabF veto wall bits. The signals from all the modules in the crate were read out and sparsified by the data link (DL). The DL and TDC boards in the crate were controlled by the control link (CL) module. The decay channel CL received commands from the DAQ, issued a read command to TDCs in the crate, and passed the commands to the next crate. The TDC rack was located in LabF, roughly in the middle between the testbeam and calorimeter branches. Due to its location, it served as a repeater and synchronized the CL

commands to the testbeam rack [2].

The data were received as ECL differential signals; each signal was transported over a twisted pair. The 8ns TDC write clock signal was split into two clocks 180 degrees out of phase. With the two clocks, the circular buffers were clocked alternately at 8 ns for a total sampling of the signals at a 4 ns rate. Thus the coupled TDC digitized the time of the pulse in 4 ns bins. The TDCs were capable of buffering hits in 512 bit words. The total live time window was thus 4 ns/word $\times$ 512 words = 2 μs. The maximum drift time was 1.3 μs, so the time window could buffer the full drift range of the cell. The arrival time of the drift chamber pulse on one wire relative to the event time (the trigger) allows the determination of the particle position in one dimension with much more precision than the size of the drift chamber cell. The buffer memory was shared by all 16 channels on one TDC card. The write clock was provided by the external clock generator module. Clocks were synchronized and fanned out to all TDC modules, thus ensuring that the time recording would happen in sync. The TDC read out was activated by the trigger received by the clock/trigger module. Upon the system trigger arriving the clock module stopped the TDC clock called in TDC specifiction "write clock". Stopping of the clock signals prompted the TDCs to transfer the data from 16 circular buffers into the global first-in-first-out (FIFO) buffer memory. It took 8ns to transfer each TDC words into a FIFO buffer. The FIFO buffer could store 32 events per spill. The FIFO buffer was read out by the data acquisition system (DAQ) system. The decay channel TDCs had a buffer size of 256 words.

The data read out of the TDC was initiated by a READ command from the DAQ, and continued until the last word was read out from the main buffer. The data were transfered to the backplane bus to the data link module, which sent data to the DAQ.

4.6.3 ADC Read Out

The pulse height information, which corresponded to the energy deposited in the calorimeter was read out by the FERA system, which comprised one DAQ branch. The FERA system was a fast buffered readout system used by LeCroy 4300 ADCs (analog-to-digital converters) with 11 bit-range. ADCs were placed in the CAMAC crates handled by VME CAMAC branch drivers (CBD 8210). The digitization was done by measuring the time required for the charge collected on the capacitor to dissipate through a resistor (RC chain). The total dead time of the FERA electronics was 11.7 μsec. In the absence of a signal, the FERA was recording random electronic noise originating in

[2]direct connection from the calorimeter CL to the testbeam CL was not possible, because the length of the cable was too large and the direct signal was arriving too late to the testbeam rack with a delay outside of TDC system's acceptable range

phototubes, electronic modules, cables, and gave a signal called the pedestal. Pedestals were measured cycle before the first ping and were later subtracted in the software from the measured pulse height. Ideally this would provide the real energy deposited by the particle without the electronic noise.

The FERA was read out using a CAMAC system connected to a VME-bus readout processor. After the gate a "clear" pulse reset all FERA bits to zero, making the system ready for another event.

4.6.4 VME System

The data acquisition system was based on a VME-bus system build around a Motorolla MVME167 68040 processor board (Ref. [36]), which used "VxWorks" software. The pulse height information and TDC timing was written to 8mm Exabyte tapes. With normal intensity ($10^{13} protons per spill$) there were around two tapes written per day.

4.7 Data Collected

During 1996-1997 fixed-target run at Fermilab, with the decay channel operating, the NuTeV collected 2.54×10^{18} 800 GeV protons on the beryllium oxide production target. This was not the entire data set collected by the NuTeV calorimeter, because the decay channel started taking data a few months after the fixed-target run began. During the run, 1.13×10^{18} protons were received with the magnets set to focus positive mesons, and 1.41×10^{18} protons with negative meson focusing.The decay channel trigger was live for runs 5583 and higher.

Chapter 5

Monte Carlo simulations

The Monte Carlo (MC) simulations have been used to estimate the size of the background, to simulate the signal, to calculate event rates and to test the normalization factors and reconstruction efficiencies used in the analysis. It was based on a well defined model of the decay channel and NuTeV sampling calorimeter. The decay channel MC for this analysis consisted of the following parts:

- The Beam MC
- The ν Deep Inelastic Scattering MC
  - LUND event generator
  - Quasi-elastic and resonance event generator
  - GEANT detector description
- Modeling the noise
- The NHL signal MC
  - The NHL production
  - The NHL decay
- other MC
- K_L neutral punch-through MC

Beam, DIS and K_L Monte Carlo simulations were used to estimate NHL background. The most significant background to the analysis came from deep inelastic neutrino scattering. The neutral (K_L) punch-throughs and ν interactions in the material were next biggest, though not being a very large backgrounds for this analysis. Background sources and level are discussed in more detail in the Chapter 7.

The NHL MC produced the sample of events that were treated as a NHL signal. Each of the MC simulations is described in details below. The output of the simulation was written in the same format (ZEBRA [58]) as the real data, allowing detailed comparisons with full reconstruction.

5.1 Beam Monte Carlo

The beam MC produced the flux of incident neutrinos interacting in the decay channel and NuTeV calorimeter. The flux was used in the simulations of neutrino DIS events and in the NHL Monte Carlo. Incident neutrinos were generated from simulated decays in the secondary beam of pions and kaons upstream of the detector. The production of secondary kaons was simulated using the parameterization by A. Malensek [43] to the K production measurements [45] from 400 GeV protons striking a beryllium target at the CERN SPS. The momentum and angle distribution of charged Ks were selected according to the parameterization. Pion decay were simulated by Turtle MC [44] (Trace Unlimited Rays Through Lumped Elements). Secondary mesons decayed in the beam pipe producing a wide-band beam of neutrinos, directed towards the NuTeV detector. The Decay Turtle program, version 4.0 [44], simulated the propagation of charged particles through the beam line.

The Turtle MC assumed 800 GeV protons hitting the beryllium oxide target 1.4 km upstream the decay channel. K and π mesons were produced in those interactions. Energies of the incident neutrinos varied from 20 to 400 GeV. The beam diameter was around 60 inches. Energy and vertex distributions of ν flux are shown in Figure 5.1

The Turtle flux was checked in a past experiment CCFR [46]. The integrated ν_μ and $\bar{\nu}_\mu$ fluxes reaching the detector were measured using the low hadron energy CC event samples, with the absolute normalization fixed by the total neutrino cross section:

$$\sigma^{\nu N}_{\rm TOT} = 0.676 \times 10^{-38} cm^2/GeV \times E(GeV).$$

The data versus MC comparison showed disagreements less than 10%. The output of the Turtle were the neutrino flux files with the neutrino energies and transverse positions of interaction vertices. Neutrino flux files were used both by the background (LUND/GEANT) and NHL MC simulations.

5.2 The Deep Inelastic Scattering Monte Carlo

The DIS Monte Carlo simulated the most important background in this analysis, ν DIS scatters. A typical DIS event is shown in Figure 5.2. To reduce the rate of neutrino interactions the fiducial volume of the detector was filled with the helium.

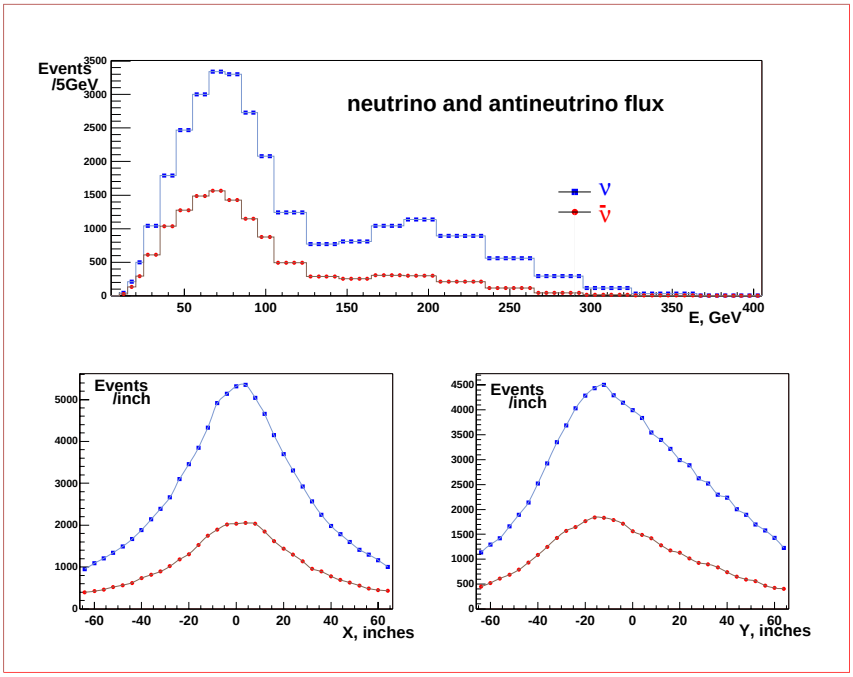

Figure 5.1: Energy and transverse vertex distributions of the incident neutrino beam in the ν mode.

The DIS background in this analysis was generated via the LUND/GEANT MC. The NuTeV detector, including the decay channel, was described in details in the McNuTeV, GEANT-based, customized simulation package [48]. McNuTeV provided an interface to the lepton-nucleon scatters event generator, LUND. The event generator and GEANT are described in detail later.

5.2.1 The ν interactions event generator – Lepto 6.51

The event generator was based on Lepto 6.51 [47], which uses the Lund string model for hadronization process. I'll use terms Lund events generator and Lepto in this section interchangeably.

Lepto/LUND simulated complete ν scattering events, based on the electroweak cross sections. A complete event meant that its description was close to one of the real DIS interaction with the correct kinematics and multiplicities. The ability to check the tracking and identification of individual particles (PID) was essential for tuning the tracking and PID algorithms in this analysis. The DIS events simulated by Lepto showed good agreement with the data. Lepto was interfaced to the detector simulation program, McNuTeV, that was also the driver routine.

In the DIS Monte Carlo every simulated neutrino was forced to interact in the decay region and all Monte Carlo DIS events were unweighted. The DIS

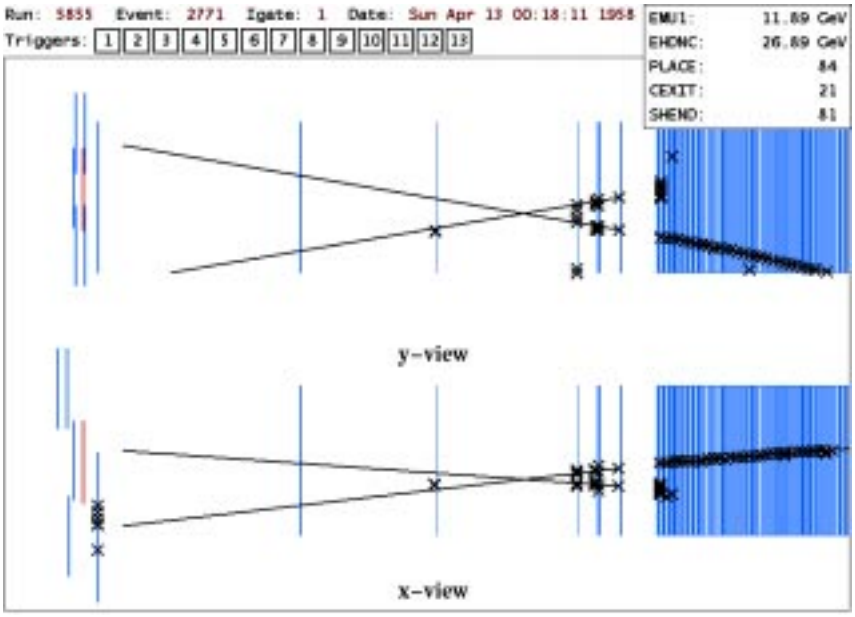

Figure 5.2: DIS background event generated in the DIS Monte Carlo simulation. On the left there is a veto wall array, which is followed by decay channel chambers and the NuTeV calorimeter on the right. On top there is a run,gate, trigger information.

MC events were normalized outside of the simulation program "by hand" and the weights were assigned to events based on the neutrino cross section and flux. For a given number of generated MC events $N_{\rm MC}^{gen}$, the weighting factor W would be

$$W = \frac{N_{\rm data}^{measured}}{N_{\rm MC}^{gen} \times \epsilon_{\rm rec}}, \tag{5.1}$$

where $N_{\rm data}^{measured}$ is the number of neutrino interactions in the data measured in the fiducial volume of the detector and $\epsilon_{\rm rec}$ is the measured reconstruction efficiency of Monte Carlo events. The normalization is described in detail in Chapter 6.

The neutrino and antineutrino energy spectrum used by LUND came from the flux files, generated by the Turtle beam Monte Carlo. The kinematics of the event was chosen according to the electroweak differential cross section given the energy of the incident neutrino. Lepto used a parton description (tree level) on large energy scales (small distances) and the LUND string hadronization model on small energy scales.

Simulation of QCD effects in hadronic final state was done to first order of the QCD matrix elements for gluon radiation and boson-gluon fusion. Jetset libraries were used for the hadronization [51]. The internal pdf library used

was CTEQ2L (the best leading order fit; Ref. [49]). All weak decays, including K and π decays, were not processed in Lepto. Weak decay were done later in the GEANT Monte Carlo.

Before evaluation of the cross section formulae and structure functions, the cuts on the kinematic variables $Q^2_{\rm gen}$ and $W^2_{\rm gen}$ were applied. This decreased the size of the available phase space for generation and significantly shortened generation time per event. The cuts were the following:

- $1.0 GeV^2 < Q^2_{\rm gen} < 10^8 GeV^2$
- $4.0 GeV^2 < W^2_{\rm gen} < 10^8 GeV^2$,

where $Q^2_{\rm gen}$ is a generated momentum transfer squared, and $W^2_{\rm gen} \equiv m_p^2 + 2m_p\nu_{\rm gen} - Q^2_{\rm gen}$, where m_p is the mass of the proton, and $\nu_{\rm gen}$ is the generated hadron energy.

There were two issues which led to the lower limits in $Q^2_{\rm gen}$ and $W^2_{\rm gen}$.

- *First*, the low $Q^2_{\rm gen} < 1.$ GeV region was excluded in the generation. Deep inelastic scattering cross section models stop being valid at $Q^2_{\rm gen} < 1.$ GeV, where the nonperturbative effects take place and QCD predictions fail.

- *Second*, the process of quark formation into the hadrons, hadronization, was not correctly simulated in the low region of $W^2_{\rm gen}$. The number of hadrons produced and their energy strongly depends on the termination process. The hadron shower was stopped if the quark energy was below some cutoff, which determined the size and energy of the shower. The termination process was not tuned well enough for small $W^2_{\rm gen} < 4 GeV^2$ [52]. Thus lepto could not go into the low region of $W^2_{\rm gen}$.

The region below $Q^2_{\rm gen}$ of 1 GeV and with lower values of W^2 was covered by another MC, the quasielastic/resonance simulation.

A summary is given below of what happens on the event generation phase.

1. Neutrino energy E_ν is read from the flux file
2. Lepto/Lund chooses two independent scaling variables out of x, y, Q^2, W^2 and randomly selects their values, using defined cuts and settings. For example x and y.
3. Event kinematics are calculated according to the values of x,y and E_ν.
4. Lepto simulates a complete DIS neutrino interaction

The tracks, their energies and particle ID, along with the vertex were stored into the proper data structures and were processed further by the full detector Monte Carlo, McNuTeV.

5.2.2 Quasi-elastic and resonance production event generator – Quasimodo

The kinematic region below $Q^2_{\rm gen}$ of 1 GeV and W^2 of 4, the region that was not covered by deep-inelastic Monte Carlo, but was simulated with the "Quasimodo", quasi-elastic and resonance Monte Carlo. Neither quasielastics nor resonance production were a large background to this analysis.

The Quasimodo event generator [30] generated the resonance events and single muon quasi-elastics based on the cross sections calculations by Rein and Sehgal [29]. "The scattering model was approximate, but it reflected the right quasi-elastic kinematics." (comments in the program from Ref. [30]). The kinematics were chosen according to Ref. [29], but the final state was limited to the set containing a pion, baryons and a muon.

Two kinematic variables were thrown randomly: W^2 was chosen uniformly in the interval from the user defined range and Q^2 according the quasi-elastic cross section in Ref. [29]. Quasimodo generated events over a flat energy range and W^2 range.

Quasielastic events were generated at low values of $W < m_\pi + m_B$, where m_π is the mass of a pion, and m_B is the mass of a baryon. For big values of W the routine produced a two-body final state, baryon and pion, with isotropic decay in W in the center-of-mass system.

The two-body final states were πp, πn and $\pi^0 p$ in 1:1:1 ratio. The generated pions and baryons were processed further by the GEANT-based detector simulation program, McNuTeV, described below.

5.2.3 A GEANT hit-level detector description – McNuTeV [30]

McNuTeV, a "hit-level" Monte Carlo package for NuTeV, simulated geometry and hit digitization for the NuTeV detector. A hit is a digitized response of the detector to a passing particle. A hit-level Monte Carlo produced simulated data events in the same format as the real data, using the same analysis algorithms for the data and Monte Carlo, thus making possible detailed comparisons between the two. In McNuTeV hits were written in the Zebra format [58] by the same decoding algorithms as the data analysis package "e815_analysis" [63]. This setup was motivated by the need to make the McNuTeV data as close as possible to the real data. Nominal values for counter gains, hi-to-low ratios, photoelectrons per mip, pedestals and drift chamber constants were read from the spec files area specified in the card file (*nucrnch.srv*). McNuTeV provided interfaces to several event generators, to a geometry routine and to digitization routines. Program control occurred through a single card file. McNuTeV was based on "Geant", the standard CERN detector simulation package [48].

The geometry of the decay channel was simulated according to the real experimental setup. It was described in terms of volumes as models of real

detector parts. A volume can be declared to have contents and become a mother volume. The contents then are positioned inside the mother volume. There has to be a unique volume matching the outside boundaries of the entire setup. The reference frame attached to this volume becomes the master reference frame.

Decay channel volumes were:

- the decay channel volume
- 5 drift chambers
- the veto wall counters array
- the floor
- Tohoku, 2 steel blocks outside the decay channel

The geometrical descriptions of the Monte Carlo volumes are stored in the MC spec files ("McNuTeV/spec/target_geant.spec").

The decay channel volume served as a container for other decay channel volumes. It was positioned inside the NuTeV mother volume, whose size was correspondingly increased. The length of the mother volume was 120 meters. The decay channel volume was 37 meters long (bigger than the length of the real decay channel, 34 meters). Each volume in the simulation had a medium number associated with the material in the volume. The decay channel volume was filled with the helium medium. Drift chamber volumes placed in the decay channel had different medium numbers. They were defined by a set of parameters describing materials composing the decay channel chamber. Drift chamber volumes were filled with the argon-ethane gas medium. There were five sensitive drift chamber volumes in the decay channel. If the volume is declared as a sensitive, the information about the hit will be recorded in the proper data structure whenever a particle would interact in the volume. Each chamber consisted of two 3m×3m 0.6" thick rectangular volumes, one with horizontal wires called a X-plane and one for vertical wires, a Y-plane. Drift chamber volumes used in the decay channel model were not different from the drift chambers in the NuTeV calorimeter module. There was a drift chamber upstream of the decay channel. which simulated the Bashful chamber and a veto wall volume. The veto wall arrays were modeled by two 4.6m×4.6m arrays of plastic scintillators volumes. There were 2 walls of 3 columns and 3 rows of the scintillation counters placed right next to each other, total 18 counters. The upstream drift chamber, Bashful, was not used in the analysis. One drift chamber positioned near the calorimeter was tilted to represent a UV-chamber corresponding to the one in the real experimental setup. Figure 5.2 shows a graphical representation of the decay channel with the described above setup.

Transverse coordinates, X and Y, of the of the interaction vertex were given by the distributions in the Turtle flux files, that were read by the 'McPipe' program. The Z-position was specified in the input card file as an external parameter. The event propagation strongly depended on the vertex position and in what material the neutrino interaction happened. For example if the vertex is outside the detector volume there would be no activity in the detector.

The DIS background studies were conducted on the events in the helium, in the drift chambers and in the material surrounding the decay channel. For the DIS background simulations the Z-positions were chosen accordingly:

- inside the decay channel fiducial volume, Helium
- in the drift chambers
- in the floor
- in the steel blocks outside the decay channel, Tohoku.

To assure that the interaction vertices were generated at the right place an interactive version of Geant, xgint, was used. It allowed to zoom in on the particular volume and visually check the positions of vertices.

Two new volumes were introduced to study the background from the neutrino interactions in the material surrounding the decay channel. The floor volume was 120m long and 1m deep just underneath the decay channel and calorimeter volumes.

There were two blocks of steel on the east and west sides of the decay channel. These were remnants of the bubble-chamber magnet upstream of the NuTeV calorimeter, called the Tohoku, used in a previous experiment. The Tohoku blocks were away from the beam center, with helium bags touching them. Taking into account that the neutrino beam was wide, we had to put the Tohoku steel into the simulation and study how it affected the NHL analysis. In McNuTeV [30], the Tohoku blocks were represented by two volumes, $182\times414\times584$ cm, one on the left and another on the right of the decay channel at approximately 25 m downstream from the veto array.

Plastic bags containing helium were simulated by three 0.1cm thin cylindrical volumes placed in between drift chamber volumes.

The vertex, momentum and particle ids of generated tracks were transfered from the event generator common blocks to the kinematics routines. McNuTeV then would propagate and perform the decays of all the particles that were not decayed by Lepto, all weak decays including π and K meson decays. In the specified geometry of the experimental setup the tracking routines then propagated particles through the material of the detector. This was achieved by integrating the equations of motion over successive "steps" and applying

corrections due to the presence of the matter. The volume detected the passing particle if it was marked as a sensitive volume.

For each tracking step hits were stored into Geant's HITS data structures. Digitization algorithms were called at the end of every event. The modeling of the drift chamber hits was simple. Each hit produced a 50 ns wide electronics pulse. A drift time corresponded to the chamber position and x, y, z location of the hit within the chamber was then smeared by a Gaussian distribution with a 0.04 cm sigma (sigma was also varied in the studies of the systematic error on the resolution, see Chapter 8). Precise wire locations, drift velocity, time offset constants and electronic modules addresses were read from the NuTeV spec files. The digitization routine kept track of the energy deposited in a calorimeter counter in a Geant "*HITS*" counter for each produced track. The energy then was corrected ("map-corrected") for the track position dependence of the counters and stored in the form of ADC words. The output of McNuTeV was a ZEBRA data file, the same format as the raw data.

5.3 Modeling drift chamber noise

The drift chamber noise was stripped from neutrino events in the beam gate (trigger 1), with place ≤ 20. The noise effect on the reconstruction efficiency was studied. It was found that the chamber noise caused a 5% loss at the highest transverse masses in the $\mu\pi$ sample and that the effect of additional noise was negligible in the μe and $\mu\mu$ samples. TDC hits were stored on the noise files, which were merged later with the MC files by the noise-combining program ("*noise_combine/nhl_noise*" [63]).

5.4 The NHL/signal Monte Carlo

The NHL and background acceptances and reconstruction efficiencies were calculated from the hit-level Monte Carlo (MC) simulation. The signal Monte Carlo was a combination of detector GEANT simulation, NHL production MC and NHL decay MC. Unlike the background Monte Carlo, the signal events were weighted on the generation stage by their decay and production probability. The simulated raw data events were processed using the same analysis routines as those used for the data. A simulated $\mu\pi$ Monte Carlo NHL event is shown in Figure 5.3. The $\mu\mu$ and μe NHL decays simulated by the MC are shown in Figures 5.4 and 5.5 respectively.

A lengthy memo describes the Neutral Heavy Lepton production and decay simulations [39]. Therefore I will only briefly summarize the process here.

The Neutral Heavy Lepton were produced and decayed according to the

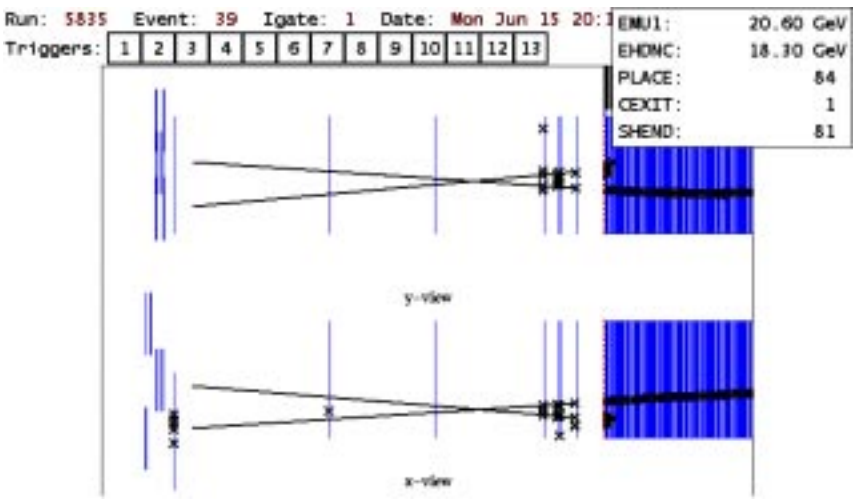

Figure 5.3: Signal Monte Carlo. NHL decays into $\mu\pi$.

model of Gronau, Leung and Rosner(GLR) [42]:

$$N_{L^0} = |U|^4 N_H BR\left(\frac{H \to l + L^0}{H \to l + \nu}\right) BR\left(\frac{L^0 \to \text{mode}}{L^0 \to \text{All}}\right) P(\tau)\epsilon, \tag{5.2}$$

where $|U|^4$ is the NHL mixing parameter, H is the decaying meson (π, K, D, D_S), N_H is the number of meson decays, ϵ is the efficiency to detect the event and $P(\tau)$ is the probability that the NHL will decay within the decay channel,

$$P(\tau) = (1 - e^{-\frac{z_{\text{beam}}}{\gamma c\tau}})e^{-\frac{z_{\text{decay}}}{\gamma c\tau}}, \tag{5.3}$$

where τ is the lifetime of the NHL, z_{beam} is the distance from the production point to the decay channel, and z_{decay} is the length of the decay channel.

Generation of NHLs was a multi-step procedure. Many NHL masses from 0.25 to 2.0 GeV were simulated in stages. The output generated by each particular stage of the simulation process was stored into an intermediate file and used as an input by the next stage. The structure of the signal Monte Carlo and the flow chart of data files is shown schematically in Figure 5.6

5.4.1 The NHL production

The primary source of NHLs for this analysis was the semileptonic decay of K mesons and charmed mesons. K-mesons were produced at the BeO target and transported to the point of decay in the decay pipe. The position and momentum at the target, of produced neutral kaons were recorded in files ("*k0.dat*"). The Turtle Monte Carlo [44] produced files ("*kpos.dat*" and "*kneg.dat*") with charged kaon fluxes, containing the following information:

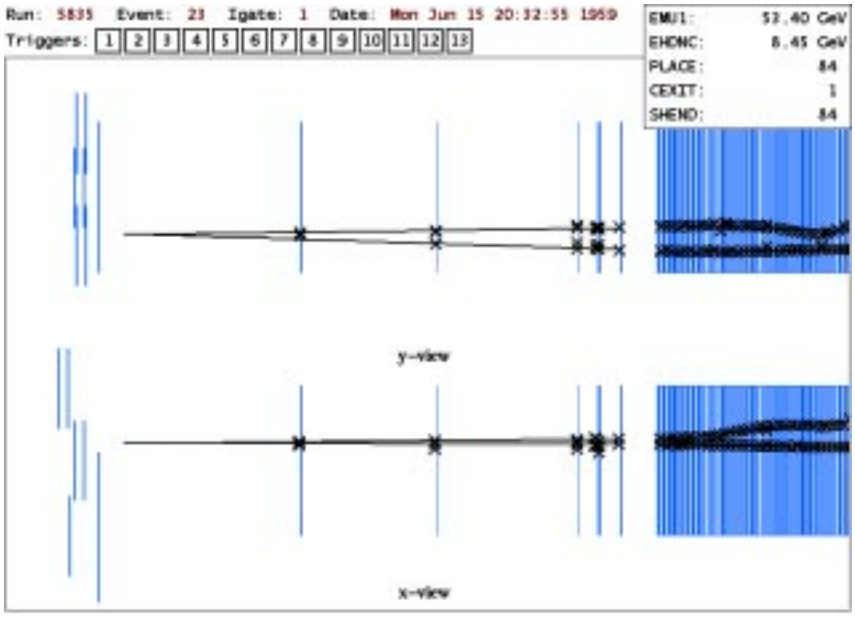

Figure 5.4: A $\mu\mu\nu$ NHL decay.

- x and y coordinates at the beginning of the decay pipe
- θ_x and θ_y angles
- the particle momentum
- the weight

Entries in the file were weighted according to the probability of the observation of a kaon with the given angle and momentum.

The NHL production routine ("*nhl_prod*" [63]) read in the generated turtle file containing the proper weight, energy, position, and angular distribution of kaons in our beamline. D-mesons were simulated according to a parameterization (see next paragraph). Files corresponding to both neutrino and anti-neutrino running were read in. In "*nhl_prod*", the NHLs were produced with a weight per proton on target. Later in the analysis, the weight was multiplied by the correct number of protons on target for the particular running (neutrino or antineutrino). The relative proton on target ratio for neutrinos versus antineutrinos was 45%:55% respectively.

D mesons were also simulated as well as D_S. The D-production Monte Carlo was based on the parameterization in *Frixione et al.* [55] of heavy flavor production data. It used data from two fixed-target experiments E653 and E743 in addition to the data from lower energy experiments(Ref. [55] p.6). D-mesons were produced according to $(1-x_f)^{8.36}$. The p_T^2 distribution was $e^{-0.635p_T^2}$ for low p_T^2 and $\frac{1}{(Am_C^2+p_T^2)^\beta}$ for high p_T^2 where $A = 1.966$, $m_c = 1.5GeV$

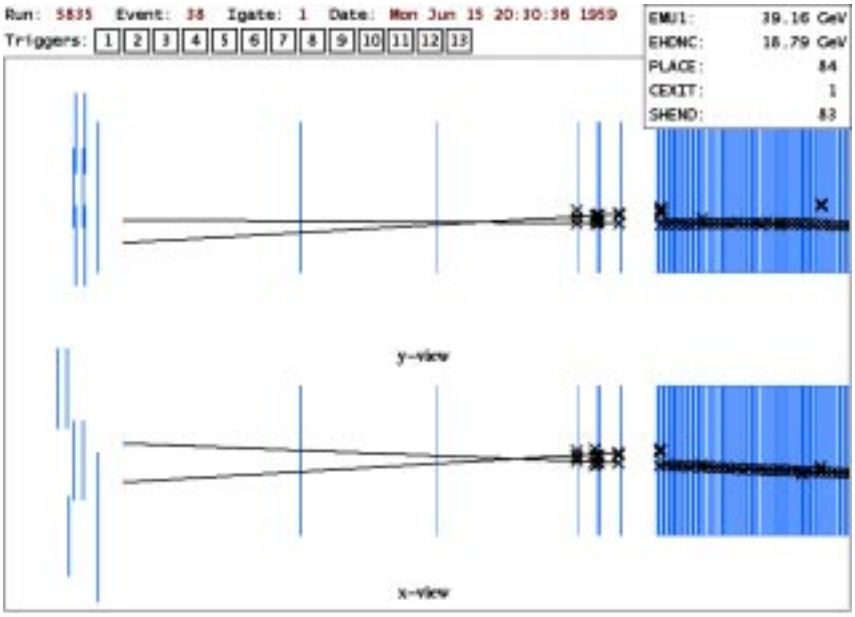

Figure 5.5: A decay of a NHL to $\mu e \nu$.

and $\beta = 5.540$. The total cross section for D meson production was taken to be $27\mu b$, the average of the E743 and E653 experiments. The production was normalized to the total cross section for 800 GeV fixed-target proton-nucleus scattering given by 43 mb. The production rate of D_S mesons was taken to be 54% of the total D-meson production rate. D and D_S mesons could then decay via two- or three- body decays. Other sources of D-production were re-interactions of secondaries in the target and proton dumps and secondaries interacting in the beam line.

Each type of meson was transported separately to the point of decay and given an appropriate weight. Mesons were assumed to decay via two and, in the case of kaons, via three body decays with a range of possible masses. The NHL from the decay was then projected to the 1.5m×1.5m area on the front face of the decay channel. The allowed meson decays included the following channels:

- $\pi \rightarrow l+$ NHL
- $K \rightarrow l+$ NHL
- $D \rightarrow l+$ NHL
- $K \rightarrow \pi + l+$ NHL
- $D \rightarrow K + l+$ NHL

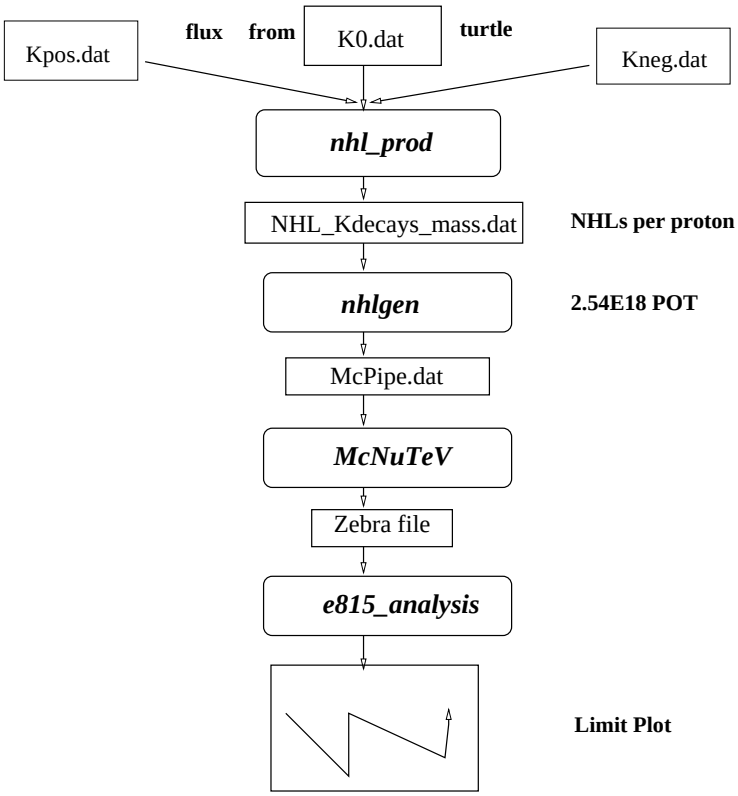

Figure 5.6: The structure of the signal Monte Carlo. Routines are shown in boxes with round corners. Regular boxes show the data files.

- $K^0 \rightarrow \pi + l +$ NHL

The branching ratio for each rate was calculated. These branching ratios come from Ref. [42], and were similar to the fully-leptonic decay branching ratios to neutrinos and charged leptons apart from the extra factor of $|U|^2$, the NHL mixing constant,

- *for the two-body:*

$$Br(A \rightarrow N\ell) = Br(A \rightarrow \nu\ell)\eta(x,y)|U|^2, \tag{5.4}$$

where $x \equiv m_{\rm NHL}/m_A$, $y \equiv m_l/m_{\rm NHL}$, $\eta(x,y)$ is a kinematic factor in Eq. 2.35 (also in Tim Boltons paper [40] eq.12.):

$$\eta(x,y) = \frac{[(1+y^2) - x^2(1-y^2)^2]\sqrt{[1-x^2(1-y)^2]\,[1-x^2(1+y)^2]}}{y^2(1-x^2y^2)^2}.$$

- *for the three-body decays:*

$$Br(A \to BN\ell) = Br(A \to B\nu\ell) I(m_A, m_B, m_{\rm NHL}, m_\ell)|U|^2,$$

where A is the heavy quark, B is the next lighter quark, N is a NHL, ν is a neutrino and ℓ is a charged lepton. The function I which depended on the masses of the quarks and leptons, was given in Eq. 2.37 (also in [42], in equation 3.39 and 2.40 as function I_1):

$$I(x,y,z) = 12 \int_{(x+y)^2}^{(1-x)^2} \frac{ds}{s}(s - x^2 - y^2)(1 + z^2 - s) \times$$
$$\{[s - (x-y)^2][s - (x+y)^2][(1+z)^2 - s][(1-z)^2 - s]\}^{1/2}.$$

The function I and η highly suppressed semi-leptonic decays for NHL masses approaching the mass of the decaying particle. Near the boundary of the limit set by each meson decay, it was the fully-leptonic decays that mainly contributed.

"The D_S branching fraction exceeded the D branching fraction by almost the same factor as the D_S production was suppressed with respect to the D. As a result of this effect, the D and D_S contribute approximately equally [39]".

The purely leptonic decays of D and D_S were parameterized according to Eq. 2.34 and entered into NHL Monte Carlo:

$$B(D \to Nl) = (1.57 \times 10^{-2})|U|^2 (m_{\rm NHL}/1GeV)^2 \times (1 - m^2_{\rm NHL}/m^2_D)^2, \quad (5.5)$$
$$B(D_S \to Nl) = 10^{-1}|U|^2 (m_{\rm NHL}/1GeV)^2 \times (1 - m^2_{\rm NHL}/m^2_{D_S})^2. \quad (5.6)$$

Figure 5.7 shows examples of the momentum distribution of NHLs produced in the NuTeV beamline. For NHLs of mass 1.45 GeV from D meson decay, the average momentum was ∼100 GeV; for the 0.35 GeV NHLs coming mainly from K decay, the average momentum was ∼140 GeV.

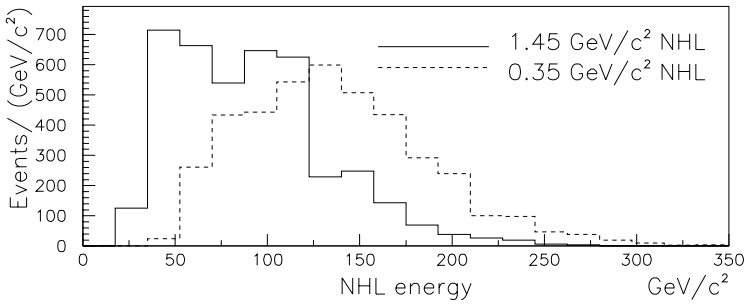

Figure 5.7: Monte Carlo NHL energy distributions for masses 1.45 GeV and 0.35 GeV.

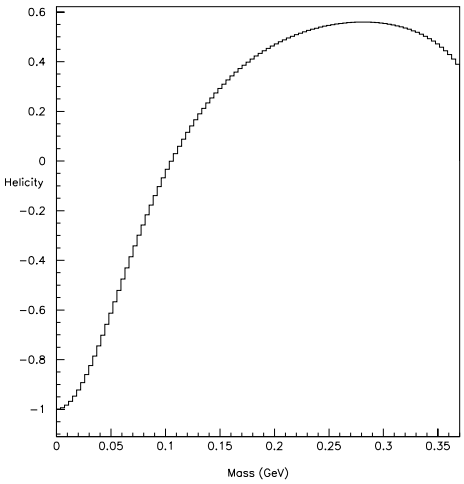

Figure 5.8: Polarization of the NHL as a function of the NHL mass in decay $K^+ \to \mu^+ +$ NHL.

The polarization of the NHL decay was also calculated. This calculation has been described in the separate publication ([41]). The polarization effects the decay distributions of the NHL. The differential decay rate including the polarization effects are given by Eq. 5.7:

$$\begin{aligned} \frac{d\Gamma}{d\cos\theta} &= \frac{G_F^2 f_M^2 m_{L^0}^3 \sqrt{S}}{16\pi}[(1-\delta_l)^2 - \delta_M(1+\delta_l) \\ &\quad -\frac{\sqrt{S}}{2}(1-\delta_l)\cos\theta], \end{aligned} \tag{5.7}$$

where δ_M, δ_l, and S are defined as

$$\delta_M = (\frac{m_{Meson}}{m_{L^0}})^2$$

$$\delta_l = (\frac{m_{lepton}}{m_{L^0}})^2$$

$$S = 1 + \delta_M^2 + \delta_l^2 - 2\delta_M - 2\delta_l - 2\delta_M\delta_l$$

Figure 5.8 shows the helicity of the NHL as a function of its mass.

Each kaon was allowed to decay within the beamline decay pipe, with the proper weight assigned to each decay. Kaon decays were spread over the length of the beamline and D mesons decayed in the production target and dumps. The weights and decay parameters were written to separate K and D mesons NHL files. Each line in the file contained the following:

- mass
- energy
- vertex x and y position at the channel start
- weight
- distance of travel to the decay channel channel start.
- polarization

Each produced NHL was then projected to the decay channel about 1300 meters downstream. Events projecting within the fiducial volume of the decay channel were written out for data analysis. Thus, the final output of "nhl_prod" is a file which contains the NHL kinematic distributions and production weights per proton on target. The output file with NHL kinematic distributions and production weights was then passed to the NHL decay MC [39, 56] ("nhlgen"), which simulated the decay kinematics of the neutral heavy leptons.

5.4.2 The NHL decay

Files with NHL kinematics were read in and processed by NHL decay routine, "nhlgen" [63]. Nhlgen decayed NHLs through two and three body decays. Angular distribution of products took into account the NHL polarization. For this analysis we required one of the decay products to be a muon. Each particle was decayed to a selected mode ($\mu\mu\nu, \mu\pi, \mu\rho$ or $\mu e\nu$). The model for the NHL lifetimes was based on calculations from Ref. [42] (GLR). In this model, the NHL lifetime was depended on $|U|^2$ and m_{NHL}. The matrix elements for the decay amplitudes of particular NHL channels were taken from Ref. [40] and Ref. [41]. The conclusions from these two papers agreed. Branching ratios for the particular channel were then calculated as the ratio of a decay width for the particular channel, based on the matrix element, over the total width, taken from Ref. [42].

The branching ratios of the NHLs follow from the equation:

$$\frac{\Gamma_N}{\Gamma_\mu} = \sum_l |U_{lN}|^2 \left[\frac{M_N}{M_\mu}\right]^5 \Phi_l(M_N), \tag{5.8}$$

where Γ_μ is a decay rate of a muon and Φ is an effective number of unit-strength charged current channels. The total lifetime was given in Ref. [42] as:

$$\tau_{N_\mu} = (4.15 \times 10^{-12} s) \left(\frac{M_N}{1GeV}\right)^{-5.17} |U|^2. \tag{5.9}$$

The lifetime of the NHL was proportional to the NHL mass and inversely on the mixing constant $|U|^2$, whereas the branching ratio was proportional to the mixing. The overall rate of NHL decays depended on the product of those two quantities.

The weights from production, decay, and branching ratios were combined and gave the number of neutral heavy leptons produced per proton on target. The number of protons on target was then folded in to yield the total number of events during the run expected for a given mixing constant.

The program wrote out the NHL events to a text file ("mcpipe" format) to be used for the detector simulation and efficiency estimates and fed to the GEANT [48] detector MC, McNuTeV, which was described above. The generated weight based on the NHL decay and the meson production probability was stored into the event weight array. In addition, a noise file was combined with the GEANT output (using the routine "*noise_combine*" [63]). This GEANT+noise file was analyzed in the cruncher with the same algorithms, as those used for the data reconstruction and analysis.

5.5 Other Monte Carlo studies

Simulation studies were conducted to check on the veto wall influence on the testbeam. They showed no significant interaction of the testbeam with the material of the veto wall. Studies were done using the GEANT MC. More details are in Ref. [39, 56].

5.6 Neutral punch-through Monte Carlo

This MC [39] simulated production of K_L and K_S, by νs just upstream of the decay channel that could decay in the decay channel and mimic the NHL signature. This section is a summary of this MC.

K_L and K_S could be produced in neutrino interactions in the berm, or the shielding material upstream of the decay channel (Lab F) veto wall. There was no significant contribution to the NHL background from K_S, which always decayed before reaching the decay channel. The berm is split in half, with the upper half ending 30 m and lower half ending 5 m before the Lab F veto wall. The ten most downstream interaction lengths of the berm were considered. The veto wall was assumed to be $4.57m \times 4.57m$ and to consist of 5 cm of steel. The efficiency of the veto wall was conservatively taken to be 99%. For particles with showers reaching the veto wall, including muons, 1% of the particles were rejected. The channel was located 6 m downstream of the veto wall.

The Z-position of the vertex was chosen uniformly along the berm within the 10 interaction lengths. The x and y position of the event was chosen

according to the Turtle flux within a 5 m radius, which extends well beyond the edges of the veto wall (hence neutral particles could enter the channel from the side).

Each neutral kaon produced by the Lund program was assigned a weight which was the probability of survival from the point of interaction to the end of the berm multiplied by the probability of survival in the $5cm$ of steel and by the probability of decay before entering the channel.

The Hadron shower and the leading muon of the interaction were generated. Events with showers, which extended beyond the berm and which were within the fiducial region, were considered to be vetoed.

The muon was projected to the veto wall. If it was within the fiducial volume and was of sufficient energy as to not range out in the berm material, then it would fire the veto wall. In the end, 38% of the charged current events had a muon which failed to hit the veto wall. The large number was not surprising considering that the transverse position of the vertex was allowed to extend well beyond the edge of the veto wall.

Based on the relative fiducial volume of the berm and the detector, and scaling from the observed number of events in the detector, including both NC events and CC events with no vetoing muon, 5×10^5 berm events were expected for 2.54×10^{18} protons on target. For the sake of being conservative, this number will be doubled to 1×10^6 events.

Chapter 6

Data analysis

This section describes the algorithms used in the search for neutral heavy leptons (NHL) in the decay channel. We tried to make this search a "closed" analysis, meaning that cuts used in filtering the data were tuned on Monte Carlo without looking at the actual data events. NHL decays were simulated in the signal Monte Carlo and background simulations were performed as well. Cuts were developed to isolate decay topologies specific to NHL decays and to remove background while maintaining high signal efficiency.

The chapter is structured as follows:

- The NHL decay modes and data selection
- Decay channel tracking
- The NHL analysis cuts/requirements
- The neutrino event rate and Monte Carlo normalization
- Studies of the acceptance and reconstruction efficiency
- Comparisons between the data and Monte Carlo distributions

The NHL analysis code was located in the "*e815_analysis*" directory [63] under the "*nhldk*" branch. [1]

6.1 NHL decay modes and data selection

This analysis searched for the decays of a NHL with a muon in the final state. Muonic modes were selected due to the clear signature. The muon, unlike charged hadrons produced in the neutrino interaction, traversed meters of

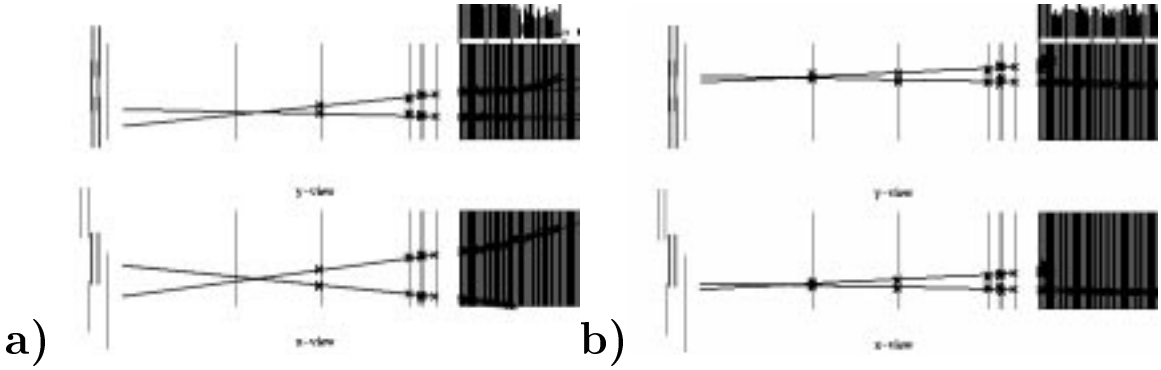

Figure 6.1: Monte Carlo 1.15 GeV NHL decay (a) to $\mu\mu\nu$ and to (b) $\mu\pi$.

steel and was easily identified in the NuTeV calorimeter. Typical $\mu\mu$ and $\mu\pi$ MC events are shown in Figure 6.1.

The search was performed on the data collected during the 1996-97 fixed target run. 2.54×10^{18} protons hit our production target when the decay channel was on. The data were read out and written on tapes using the format based on the "ZEBRA" [58] sequential Input/Output format.The ZEBRA system was created to overcome the lack of dynamic data structures in Fortran 77. It provided facilities to manipulate data structures dynamically, to write them to the external storage medium (in our case Exabyte tapes) and to recover them. About 400 'Exabyte' 8mm SONY QG112M tapes worth of data were written.

To save I/O time this vast quantity of data went through three stages of selection, with each stage progressively reducing the size of the event sample and the cuts getting more and more selective. The three stages were:

- The splitting
- The stripping
- The closed box analysis

The first stage, called "splitting", divided the raw data into streams according to event type. The data streams were written onto Exabyte tapes in the same format as the raw data. Decay channel data were contained in the neutrino stream consisting of events during the fast spill, when the neutrino beam was hitting our detector. The neutrino stream comprised 1/4 of the total tapes.

Next, data from the neutrino stream was filtered with preselection cuts. This process was called "stripping". Events with a muon candidate in the

[1]NHL analysis was done on the pass3 data located in "/calusr/1/dkout_strip/pass3/" on the NuTeV computing cluster at Fermilab.

final state with hits in the decay channel were selected. Events were identified as having a muon if one of the reconstructed tracks penetrated through one meter of steel into the calorimeter. The strip required trigger 1,2,3 and 9 to have been fired. There was also a requirement of activity in the decay channel drift chambers or demanding that 3 out of 4 drift chambers had more than 1 hit. Additionally for the $\mu\mu$ modes, one of 2 most upstream calorimeter chambers was required to have more than one hit. The $\mu\pi$ and μe modes were required to have at least 2 GeV energy deposition in the first 4 counters. Stripping of the NHL data were done in parallel with making DSTs for the NuTeV analysis. The goal of the stripping was to reduce the size of the data so that it could be stored on disk and analyzed. The size of the NHL stripped sample was about 1.5 Gbytes of 87 files. The stripped data were stored in the "/calusr/1/dkout_strip/pass3" at NuTeV computing cluster.

In the analysis, events were processed and more restrictive cuts were applied. The NHL analysis was based on the reconstruction of particle paths, called tracks.

6.2 The decay channel tracking

This section describes how the decay channel software formed tracks and vertices. The driver routine of the tracking called "*run_torgap_dk*" was the part of the NuTeV analysis software ("*e815_analysis*" [63]).

Tracking process consisted of the following steps

1. *Tracking:* Track Reconstruction
    - read out and store drift chamber hits
    - form a track based on hits in chosen seed chambers, see Fig. 6.2
    - form straight tracks by picking hits along the track
    - reject bad quality tracks
2. *Vertexing:* Vertex Reconstruction
    - match tracks between views
    - link tracks to a single event vertex
3. *Clustering:* Cluster Reconstruction
    - form clusters of hits in the calorimeter
    - identify calorimeter clusters
    - determine energy of the cluster
    - assign clusters and energies to tracks in the decay channel

4. *Final fit*

   - perform a multiple-scattering vertex-constrained fit
   - form event vertex

Each step will be described in details in the sections below. The quality of the tracking and vertex reconstruction will be demonstrated at the end of the section in Figures 6.5, 6.6 and in Fig. 6.7.

6.2.1 Forming tracks

This section describes how the tracks were formed in separate (X and Y) views. The decay channel tracking algorithm combined drift chamber hits and reconstructed straight tracks, under the assumption that the particles traveled in straight lines. This assumption is reasonable due to the absence of any strong magnetic field or large multiple scattering in the decay channel detector. Due to the small amount of material in the decay channel volume (mostly drift chambers) there was some multiple scattering. The effect of multiple scattering was simulated in the MC, and shown to be small, and was incorporated into the systematic error on the resolution (see Chapter 8).

The initial tracking used hits from the downstream chambers, TG43, DK1 DK2 and DK3, that were grouped together less than 2 meters apart. Two upstream drift chambers, DK4 and DK5, were not included initially, because the error in tracking would be too large due to the large distance from the other chambers. The error on tracking was proportional to the amount of multiple scattering $\delta x = \theta \times L$, where θ is the angle of deviation due to multiple scattering effects and L is the lever arm. Hits from the chambers DK4 and DK5, located far upstream and far apart, were included later during the final vertex fit, that handled the multiple scattering properly.

The description of the initial tracking algorithm follows. The algorithm drew a straight line through a pair of drift chamber hits. First, the code looped over all pairs of drift chambers. Two selected drift chambers, called seed chambers, provided hits for the initial track. Then the code looped over all possible pairs of hits in the seed chambers connecting two hits in any given pair with a line. Then it searched through the drift chamber hits within a certain distance DIFMIN from the line as shown in Figure 6.2. This the value of the window was DIFMIN $= 10 \times \sigma_{\rm DC}$, where $\sigma_{\rm DC}$ was an internal resolution of the drift chamber (see Chapter A), equal to 0.12 inches. The distance in drift chamber view was calculated as an absolute value of:

$$\Delta_{\rm HIT} = |x_i - (intercept + slope \times z_i)|,$$

where x_i and z_i are coordinates of the ith hit.

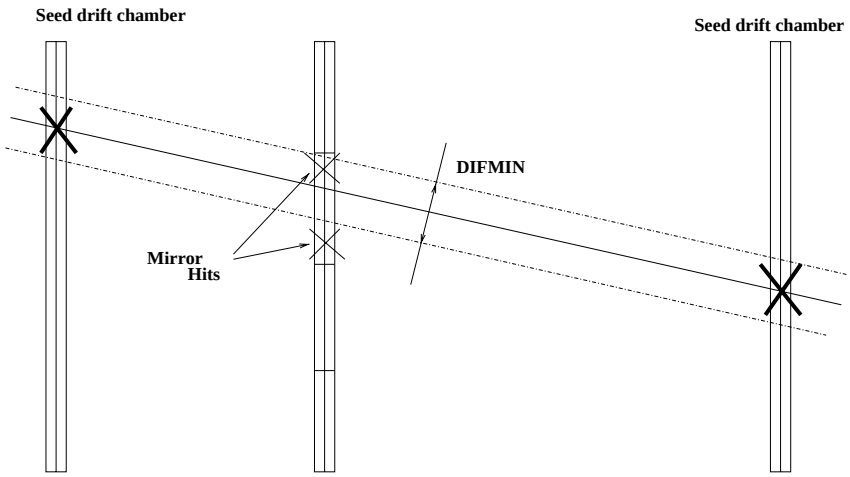

Figure 6.2: Tracking algorithm; pick any two chambers and make them seeds, draw a line, find hits on the track between seed chambers. Hits was assigned to the track candidate if they were within the DIFMIN distance from the track.

If there were more than three hits on the line they were stored and the line was promoted to a track candidate, the line was assigned a track number and stored into the tracking array.

Five of six drift chambers in the decay channel were single-wire chambers and had a left-right (drift direction) ambiguity. It meant that the single-wire chambers could not detect on which side of the wire particle passed (see Chapter 4). In this case, the tracking algorithm placed a hit on both sides of the wire, postponing the resolution of this ambiguity untill later. Therefore, each registered hit had a corresponding "mirror" hit. To resolve the left-right ambiguity the tracking had to identify and reject false mirror hits. The quality parameter for accepting or rejecting a hit was the distance of this hit from the trial track, $\sigma_{\rm HIT} = \Delta_{\rm HIT}$.

After all possible tracks were formed the tracking looped over all tracks and made a 2 parameter fit to a straight line. The two parameters of the fit were the slope and intercept of the track. Another parameter that described the quality of the track was T_0' (in the reconstruction code it was refered as $T0$). It is different from the alignment parameter T_0, even though it's related to it. The parameter T_0 was related to the track timing. It was small for forward-going tracks coincident with the trigger (2,3 or 9). If the track was backward-going, the T_0 value was large ($> 0.1\mu s$), for instance a cosmic ray going upstream through the decay channel, or if the event did not belong to a real trigger. The T_0 value was found from a 3-parameter fit to a straight line with the overall timing of the track being the additional third parameter. Two other parameters were track slopes and intercepts. If the T_0 value was greater than 48ns (12 TDC counts) the track did not belong to the event time frame

set by the trigger and was removed.

The quality of a track "QUAL" was formed as the difference between the number of hits in the track and the value of the sum of hit qualities squared:

$$\text{QUAL} = n - \text{sig\_factor} \times \sigma^2, \tag{6.1}$$

where n was the number of hits in the track, $\sigma^2 = \sum(\text{hitquality})^2$ was the sum over hit qualities and sig_factor was a parameter tuned so that the track with bigger number of hits had bigger quality (sig_factor=5). The typical value of σ^2 was 0.75 . The track quality served as a filter, all tracks with negative quality were removed.

The quality of the decay channel tracks (QUAL), hits (σ_{HIT}), and timings (T_0) were recorded and kept in the quality common block, "dkseg.com".

All drift chambers in the decay channel were assumed to have the same reference frame (XY), with the exception of the UV chamber (DK1). The UV chamber was used to match the tracks between the two different views (the X and Y views). It was tilted in the clockwise direction by 47.71 mrad. The rotation introduced one more ambiguity into the system. To add a hit one had to know the distance from the hit to a track projection on the UV plane of the chamber. However to make a correct rotation to the UV frame one had to know the both X and Y coordinates of the hit to be projected, which needs linked tracks in case of more than two tracks. Thus, a vicious circle is formed: To match the tracks one had to know their position, and to determine the track position one had to match them. The solution to this was to loop over all possible UV combinations and find the best one. The best UV hit that is close enough to the track projection (distance is less than the 20×DIFMIN, which was 2.4 inches) was added to the track.

The tracking candidates were sorted according to their quality, so that the first element of the array would have the largest quality, QUAL. The code descended from the top of the array storing the hit indices in a list, rejecting duplicate ("mirror") hits and erasing bad tracks. If a hit was already taken by a track with a bigger quality, it was subtracted and the number of hits in the track was decreased accordingly. This ensured that there were no hits owned simultaneously by two different tracks and that the track with the bigger quality had a greater priority for hits. The quality was forced to negative number (-1) if the number of hits in the track was less than 3 or if the track had a T_0 less than 12 TDC counts (48 ns). A track with a negative quality (QUAL< 0) was considered to be bad and it was erased from the list. If the list of track candidates was too big (more than 200) then the sorting routine would be called again to compact the candidate list and reduce number of tracks.

In the end of the program, refitted tracks for the track timing and all tracks with negative quality were deleted and the array was re-sorted and compacted.

6.2.2 Matching tracks

X and Y planes of the NuTeV drift chambers were read out separately. As a result, the hits and tracks were also reconstructed separately for each view. A matching procedure was developed to combine two-dimensional tracks in separate views and formed three-dimensional tracks.

Two methods were used for matching tracks between X- and Y-views.

- UV matching
- Matching to the NuTeV calorimeter

The methods were used consecutively. The code first attempted to use UV matching, and if it failed tracks were matched with the calorimeter views.

To provide information for the view matching, one of the decay channel chambers (DK1) was tilted clockwise by 47.71 mrad and called a UV chamber. After the tilt, the UV drift chamber cells were no longer parallel to the cells in the other drift chambers and by combining information from the UV and regular drift chambers one could match tracks between different views as shown in Figure 6.3.

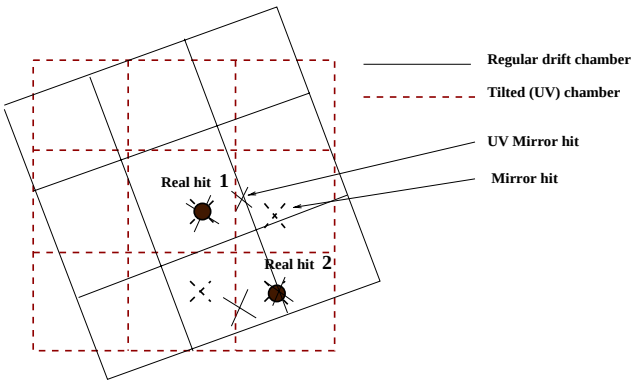

Figure 6.3: Using hits from the tilted (UV) drift chamber to match X-view and Y-view hits. In the case of two real tracks going through the drift chamber the combination of 2 hits in X plane and 2 hits in Y plane would yield 2×2 hit combinations with only two hits belonging to the real tracks. The choice of 2 real hits in this case is ambiguous. Ambiguity is resolved by combining information recorded in the tilted (UV) chamber. Figure shows that there would be only two overlaps of hits from UV and regular chamber, which corresponds to two real hits. Four other hits are not real hits and would be discarded.

If however there are lots of tracks then the rotational transformation from UV frame to the Lab becomes very complicated. In this case the matching is available by looping over all possible combinations and finding the one that

matches tracks the best. There is still a possibility of an error. The resulting ambiguity was resolved further in the final fit.

If the UV matching failed then the decay channel code attempted to link the decay channel tracks to already XY-paired tracks in the calorimeter. There was another UV chamber in the downstream end of the calorimeter. The calorimeter analysis code ("*e815_analysis/calcode*" [63]), which in this thesis will be called "cruncher", used this UV chamber to match its tracks with the advantage over the decay channel that it had more chambers and no left-right ambiguity. In the special case of just two tracks in the decay channel and one muon track in the calorimeter one could match one pair of the decay channel tracks in X- and Y-views with the calorimeter three-dimensional track. The matched pair would belong to the muon track and the second pair of decay channel tracks would form the second track. Events with one calorimeter track and two tracks in the decay channel corresponded to $\mu\pi$ and μe NHL decay modes and happened in the NHL data sample quite often. Matching in the calorimeter was also possible if one track exited the side.

6.2.3 Vertex reconstruction

The vertex reconstruction code linked three-dimensional tracks in the decay channel to a common event vertex. Since this analysis was a search for a single NHL decay in the decay channel, only one vertex in the decay channel volume was assumed.

The vertexing routine looped over all pairs of the decay channel tracks, and calculated the distance between two lines as the distance of closest approach (dclap). Two given tracks formed a vertex if their dclap was less than 4.0 inches. Indices of tracks in the vertex and the corresponding values of dclap were saved into the list of candidate vertices. They were called dclap vertices to distinguish them from a real event vertex.

To find a real event vertex the code clustered dclap vertices by looping over the list of dclap vertices and taking each vertex as a seed. Each seed vertex was assigned a quality based on the number of tracks in the vertex and on the value of dclap. Always the vertex with the most tracks, or if in a tie, the one with the smallest dclap, had the best quality. Next the new seed position was recalculated as the average of all vertex's positions in the cluster and a new quality was calculated. The program looped until it converged on a vertex or it reached 2000 loops.

After vertices were clustered and the event vertex was found, the code formed a list of tracks used in the event vertex. The dclap vertices could have overlapping tracks, it was possible for 3 three-dimensional tracks to form two 2-track vertices. The code then removed any tracks from being listed more than once.

The program returned the list of tracks in the event vertex and its position.

The vertex finding was improved later by the algorithm of a constrain vertex fit. The current found vertex was good enough for the further tracking.

6.2.4 Cluster finding and particle identification

When particles hit the calorimeter they produce clusters of energy deposited by electromagnetic or hadronic showers. The reconstruction algorithm takes the hits in the calorimeter and associates them into "clusters". The energy deposited in the calorimeter is distributed between the clusters, which are then linked to the tracks in the decay channel. The energy assigned to the cluster is proportional to the number of drift chamber hits in this cluster and scaled by the pulseheights in the scintillation counters.

The purpose of the cluster finding algorithms was to estimate the energies of the tracks and assign a particle ID to each track. The energy assigned to the track was used later in the multiple-scattering and kinematic fits. The kinematic cut variables ($x_{\rm eff}, W_{\rm eff}$) were formed from the four-vectors of the tracks. This would not be possible without knowing the energies of the clusters associated with those tracks.

The main clustering driver routine ("cluster") was called from the tracking after the tracks in the decay channel were linked to a common event vertex. The clustering algorithm looped over the X- and Y- views and over the 42 drift chambers in the calorimeter. In each particular view and drift chamber, the code grouped hits into one-dimensional clusters. It then merged one-dimensional clusters from the different chambers into a two-dimensional, XZ or YZ, cluster. Finally it combined the clusters in two views, XZ and YZ, into one true three-dimensional XYZ cluster.

The set of hits within a view was associated with a cluster if the hits within the set were separated by less than 6 inches. Each group was referred to as a "one-dimensional cluster". A hit separated by more than 6 inches from the found cluster formed a new one-dimensional cluster. The one-dimensional clusters in each chamber were grouped in Z-position forming clusters in either XZ or YZ views. In the code, these clusters were called three-dimensional clusters, a misnomer since we still have separate X and Y views, however in this thesis I will call these "two-dimensional clusters". The code looked for overlays based on the upstream and downstream hits. One dimensional clusters were grouped if the center of the upstream cluster was within 12 inches of the downstream cluster. Two-dimensional clusters could begin at any chamber within the calorimeter. For example the hadron shower could have started with one big cluster in the upstream part of the calorimeter and then emerging from the hadron shower muons could start small clusters. For two-dimensional clusters, the "start", "midpoint", "length", and "width" were determined.

The code then looked for two clusters that could be merged together. Usually this was a muon track and a hadron shower in a CC ν event. The algorithm determined if a muon track was sitting on top of a hadron shower by taking the average width and length and the up- and downstream width averages for the cluster. In the case of a muon merged with a hadron shower, the two clusters were separated, one cluster entry corrected and the other added to the bottom of the cluster list. The average width and length of a cluster were determined again after an overlay was found.

The next step was to connect together the decay channel tracks, the tracks in the calorimeter and the separate clusters in the calorimeter together. First, the decay channel tracks were matched to cruncher-identified calorimeter tracks by linking the closest decay channel track to the calorimeter track. Comparisons of positions were made at chamber TG42 (most upstream chamber in the calorimeter). The decay channel tracks were then matched to clusters found by the clustering code in the calorimeter. The matching of a cluster to a track was based on the distance between them. If the track projects to the cluster within some defined window (2×7 inches) then the track was considered to be matched (or linked) to that cluster. Tracks had to either point to the cluster or be within 7 inches of either edge. Clusters which began 6 or more chambers downstream were not considered, because it was unlikely that they were caused by the decay channel tracks. Finally cruncher-based calorimeter tracks were matched to the calorimeter clusters with the same requirement: Tracks had to either point within the cluster or be within 7 inches of either edge.

The algorithm then assigned a particle identification number, *clusid* for each two-dimensional cluster (still separately in the x and y view) based on the length and width. Three values were assigned for the particle id : muon, hadron or noise (hadrons and electrons were separated later in the code).

- *muons (*$0 < clusid < 10$*):* The easiest to identify were muons. They traversed deep into the calorimeter and left long and thin tracks. The muon ID had the values of 1, 2 or 3. If the length of the cluster was more than 20 chambers it was immediately identified as a muon with the cluster ID of 1 ($clusid = 1$). If the cluster was shorter than 20 chambers the requirements for it to be identified as a muon were tightened. It was required to have a small number of hits per chamber per view (< 2 hits) and small width of the cluster (< 1 inch) both downstream and upstream. If the cluster satisfied these requirements, it was assigned a cluster ID. If the cluster was short, less than eight chambers, the width and hit requirements were tightened further. The width should be greater than 0.3 inch and the average number of hits more than 1.1 and the cluster ID was set to three ($clusid = 3$). A cluster shorter than three chambers was not identified as a muon

- *hadrons/electrons (*$10 < clusid < 30$*):* If the length of the cluster was greater than one chamber and it was not identified as a muon, the code set the cluster PID to a hadron: $clusid = 15$. 1 hit hadron showers (length of the cluster was 1 chamber) were allowed if they happened in upstream chambers (chamber 38 and less) with the $clusid = 16$.

- *noise (*$clusid > 30$*):* If the cluster was not identified as a muon and its length was less or equal 1 chamber and it was downstream (less than chamber 38), it was identified as noise and given a $clusid = 30$.

The hadrons were separated from the electrons later in the code by a likelihood method. At this point the code would end looping over the views.

Next, two-dimensional clusters in separate views were linked together. In that procedure, the information about the matched decay channel tracks and calorimeter tracks was used. First, the code linked clusters that were matched to the calorimeter track and to the decay channel track. Only the decay channel tracks linked together in X- and Y-views were used. This was the best matching case when all three parts of the track, the calorimeter track, the decay channel track and the cluster, were linked together. The next best case was the match of a decay channel track to hits in the NuTeV calorimeter. One cluster could be linked with up to 4 tracks, so the code searched for the best match both in terms of nearness of the linked tracks to the center of each cluster and in comparison of cluster properties (start, length, width, averages). If the calorimeter or decay channel tracks were matched in XY-views, the corresponding clusters were matched in the XY-view as well. The clusters could be matched only to calorimeter tracks, but this happened rarely. The worse case was when clusters did not have any associated tracks. Attempts were made to match these again by comparing the cluster properties, like cluster "start", "length", "width" and particle ID number. There are several loops which gradually loosen the requirements comparing the clusters.

Then the clusters were sorted, and the code tried to match the rest of unmatched clusters to the decay channel tracks. The match was easy if the cluster was actually a cruncher-identified muon. The cluster finding code associated the remaining decay channel tracks to the paired clusters. Hadrons were not yet separated from electrons at this point.

The energy of the cluster, E_i, was determined according to the fraction of calorimeter energy assigned to each cluster. The hadronic energy found by the calorimeter code using the scintillator pulseheights was parsed out among the clusters according to ratio of hits. The energy of a cluster, E_i, was proportional to the number of drift chamber hits: $E_i = E_{\rm tot}\frac{N_i}{N_{\rm tot}}$, where $E_{\rm tot}$ is the total energy measured in the calorimeter, and $\frac{N_i}{N_{\rm tot}}$ is the fraction of hits in the ith cluster. If there was a muon cluster merged with the hadron shower the muon energy was subtracted. If the muon went through the toroid its momentum

was measured from its bend in the magnetic field. Otherwise the length of the muon and the most probably dE/dx was used to get the muon energy. The calorimeter rangeout code worked best only above 3 GeV, energies less than that were estimated by multiplying 320 MeV/chamber and track length in chambers. Then the pulseheight for the muon track was properly subtracted from the hadron energy cluster.

The final particle identification algorithm used a likelihood method to distinguish between muon, pion, and electron clusters. There were 6 PID values for the 6 types of clusters:

1. ERROR -1
2. UNKNOWN 0
3. MUON 1
4. ELECTRON 10
5. PION 20
6. NOISE 30

The choice type depended on the distributions of hits and the cluster widths in the chambers and on the total cluster energy and width. The code looped over the all matched pairs of clusters found in the calorimeter extracting the total energy of the cluster, number of hits and cluster width in the calorimeter drift chambers. Hit and cluster width distributions were divided by the total number of hits and total width respectively. Using the normalized distributions and total cluster energy and width, the code attempted to identify the particle, unless the cluster was not identified already as a muon or as a noise. The identification was based on the likelihood of a particle being either a muon, a pion or an electron. The algorithm compared the hit density and width of each cluster to expectations based on single particle Monte Carlo simulations. There were three values of the likelihood corresponding to the three particle types. The particle type with the biggest value of likelihood was chosen. The likelihood was formed from the values of chi^2:

$$L_j = \frac{\chi_j^2}{\sum_i \chi_i^2}, \tag{6.2}$$

where L_j is the likelihood for type j, the summation is over 3 PID types, the χ^2 values were based on the parameterizations of hits and width distributions for the given cluster energy. The parameterizations depended on the total energy of the cluster. The χ^2 was formed as the sum of differences between hit/width distributions squared:

$$\chi^2 = \sum_i \left(w_i - w_i'\right)^2 + \left(n_i - n_i'\right)^2, \tag{6.3}$$

where $w_i(n_i)$ are width(hit) distributions and $w_i'(n_i')$ are parameterizations of width(hit) distributions. The w_i' and n_i' parameterizations were extracted from the Monte Carlo simulation of single particles using McNuTeV MC. The particle ids were stored in the "clpairpid" variables. The efficiency for correctly identifying single clusters was good (96% for muons and electrons, 70% for pions). The Table 6.1 shows the PID efficiency for NHL MC events passed the NHL cuts.

Mode	Rec. μe	Rec. $\mu\pi$	Rec. $\mu\mu$
Gen. μe	$96 \pm 4\%$	$13 \pm 3\%$	$0^{+0.4}_{-0}\%$
Gen. $\mu\pi$	$20 \pm 5\%$	$70 \pm 5\%$	$0^{+0.4}_{-0}\%$
Gen. $\mu\mu$	$0^{+0.4}_{-0}\%$	$0^{+0.4}_{-0}\%$	$96 \pm 4\%$

Table 6.1: Particle Identification Efficiency for NHL MC Events

6.2.5 The final fit

The final fit routines basically repeated track fitting, clustering and particle identification with better tracks and vertices. Using better tracking parameters the code then found the event vertex. At this point, the code have already found good tracks, pairs of tracks in different views have been matched and three-dimensional tracks in the decay channel have been formed and linked to a common vertex. The final fit tried to add more hits to the existing tracks and redo fitting, taking into account the particle energy and multiple scattering in each decay chamber. Figure 6.4 shows the flow chart of routines in the final fit. The output values of the multiple scattering fit were calculated through an error matrix. Elements of this matrix were functions depending on the positions of material in the decay channel relative to the reference point. The multiple scattering fit was done at three "reference" points: at the position of the closest approach of two trial tracks, at the chamber that was the closest to the calorimeter (for linking to clusters) and at the UV chamber to add uv hit.

The final fit routine did the following:

- Added hits in DK4 and DK5 using multiple scattering fit ("msfit")
- Corrected the UV information for linked tracks
- Added better hits in other decay channel chambers using the multiple scattering fit
- Filtered out bad tracks using timing and quality.

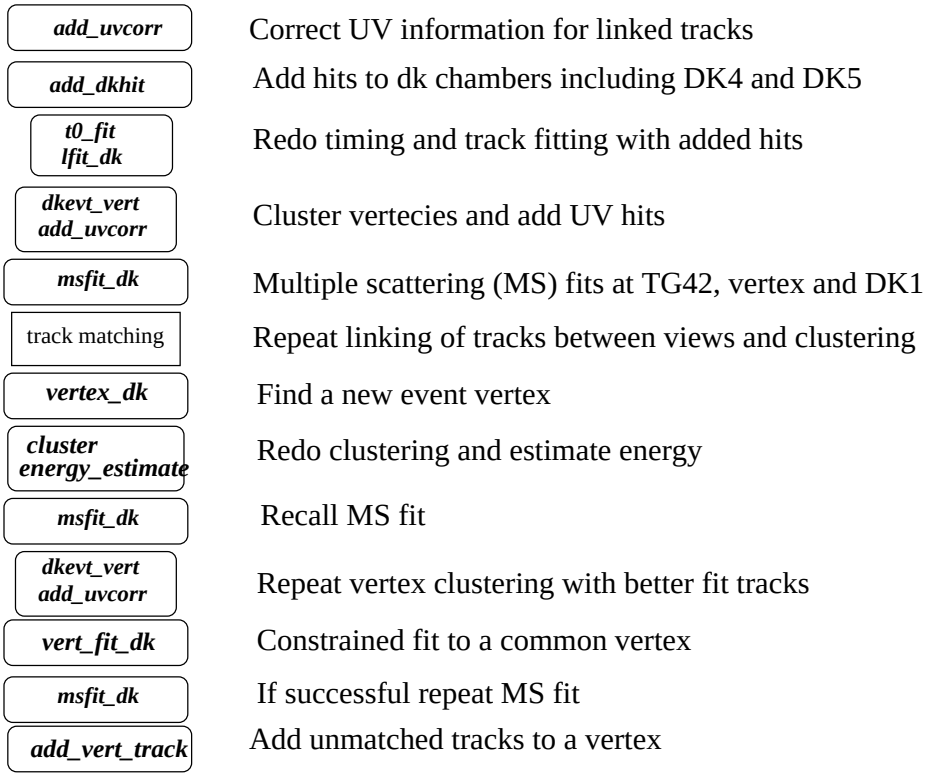

Figure 6.4: The structure of the final fit. The names of function and subroutines are shown in boxes with round corners.

- Did a final msfit to tracks and obtained the best slope and intercept estimates
- Recalled the linking and cluster routines with new fitted tracks
- Did a constrained fit to a common vertex for all tracks in the cluster

The initial tracking described in the previous section did not incorporate hits from the two most upstream chambers in the decay channel, DK4 and DK5, due to the large tracking errors, as was mentioned previously.

The scattering angle θ depended on the momentum of the scattered particle:

$$\theta = \frac{13.6(MeV)}{\beta cp}\sqrt{x/X_0}, \tag{6.4}$$

where p is the track momentum, X_0 is the radiation length of the material, and is the distance traveled in the material.

The initial tracking lacked the value for the momentum of the scattered track. Now, knowledge of the tracks energies made a multiple scattering fit possible. Final fitting included DK4 and DK5 into the "msfit" with weight

adjusted according to the multiple scattering (MS) effects. An error matrix was formed that included chamber resolution and multiple scattering effects with correlations between chambers. Due to the large lever arm for DK4 and DK5 multiple-scattering effects were large and their weights were respectively smaller than for the rest of the chambers.

The program looped over all decay channel drift chambers and tried to add more hits to the track, including UV chamber hits. In the initial tracking UV hits were not matched and the rotation into the UV frame was ambiguous. At this point, however, the code had three-dimensional tracks and the rotational transformation of the hits from the UV frame to the tracking (lab E) frame was trivial. After the rotation UV, hits were added into the tracking just like the rest of the decay channel hits. If the hit in the UV plane was within the allowed distance from the track, this hit was added to the track.

The two-parameter and three-parameter tracking fits were redone on the improved tracks with the added hits. The three fit parameters were the track slope, vertex and T_0, track timing. Slopes and intercepts were calculated at the position of the TG42 drift chamber which is closest to the clusters in the calorimeter. This minimized the error in the tracks-to-clusters linking. The tracks that did not satisfy the quality requirements were filtered out.

New tracks were linked to clusters by using the projected position of the track at the TG42 chamber. Energies of the clusters were reassigned to the tracks. The multiple scattering fit was done at the most probable position of the vertex, where the distance between tracks was smallest (distance of closest approach). The procedure was then repeated to allow it to find the best event vertex.

Finally, vertex constrained fit was done. All tracks were forced to converge to a common vertex. The fit itself was done by the CERN fitting package, Minuit [59]. The χ^2/DOF provided a measure of the quality as to whether the tracks came from a common vertex.

Figure 6.5 shows χ^2/DOF distribution for the Monte Carlo simulation of 1.15 GeV NHL decaying into $\mu\mu\nu$ mode. Track and vertex χ^2/DOF are peaked near 1 as expected, with the χ^2/DOF of the track in X-view mean value of 1.7, χ^2/DOF of the track in Y-view equals to 1.9 and the vertex χ^2/DOF is 1.16.

The reconstructed vertex distributions in the X,Y and Z-views are shown in the first column of the Figure 6.6. The gaps in the Z-vertex distribution are due to the fiducial cuts around the chamber. The second column shows the errors on the vertex distribution. The mean lateral errors in X and Y are found to be around 0.05 inches. The mean error on Z-vertex distribution is around 3.0 inches.

Figure 6.7 compares reconstructed vertex to the generated one. The high quality of reconstruction becomes obvious. X and Y- views have a RMS of the difference less than 0.1 inches, whereas difference in Z-distribution has a mean

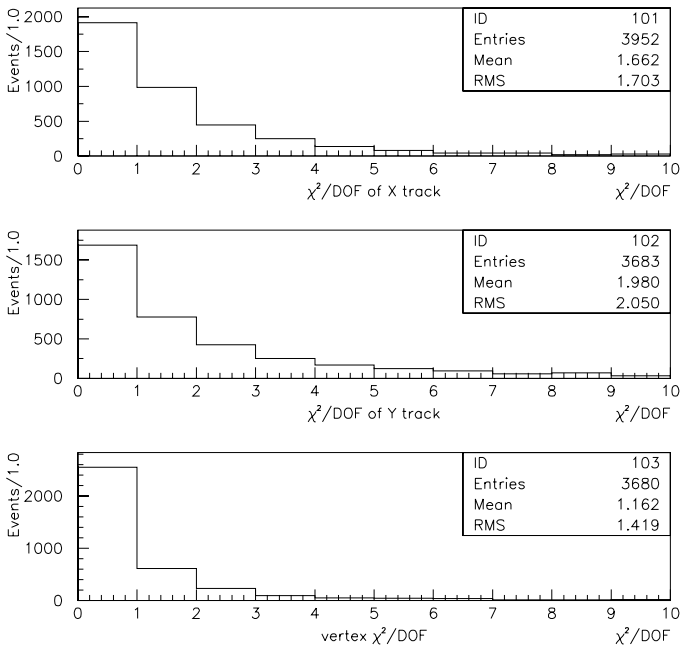

Figure 6.5: chi^2/DOF distribution of 1.15 GeV $\mu\mu$ Monte Carlo for X-view track (top), Y-view track (middle) and vertex(bottom).

of 0.25 inches, which indicates that we reconstruct the vertex slightly upstream of where it was generated. The RMS of the distribution is around 3 inches. The vertex resolution was well within 40 inches or $3 \times \sigma_{\text{vertex}}$ requirement fot the analysis.

The above distributions demonstrated the high quality of vertex reconstruction and it follows that cuts based on track and vertex reconstruction are reliable and highly conservative.

The information about found tracks, their energies, vertices and particle ids was summarized and stored into the final common block, "comlib/event_dk.com" in the NHL analysis code ("e815_analysis/nhldk" citecvs) . Event kinematic variables were calculated and stored as well. At this point the data can be used for the NHL decay search.

6.3 NHL analysis cuts/requirements

The NHL search cuts and requirements were subdivided into two categories: reconstruction and kinematic cuts. The cuts were developed with the intention of minimizing the background level without harming significantly the efficiency

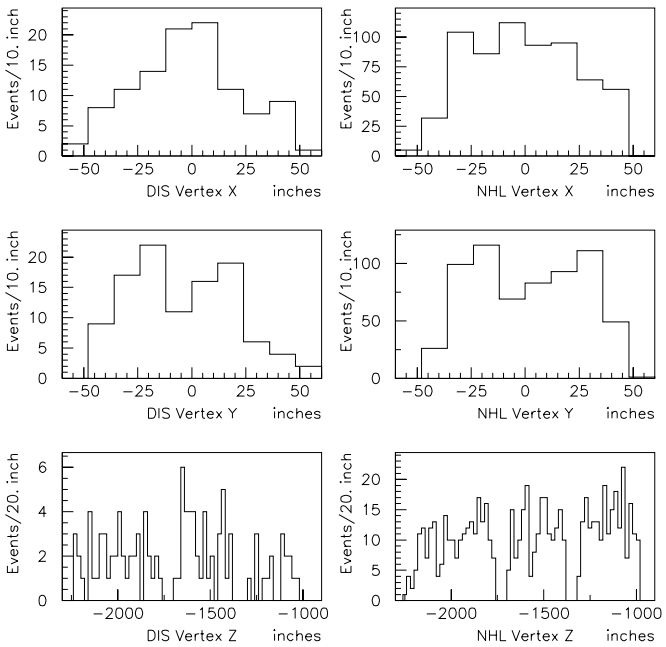

Figure 6.6: X,Y and Z-vertex distributions of 1.15 GeV $\mu\mu$ Monte Carlo left column) and the corresponding errors (right column). X and Y distributions are centered.

for signal detection. The expected background level was reduced to 0.57 events and the reconstruction efficiency remained around 25%, which was satisfactory for this analysis. The variable "topass" was formed that summarized all NHL cuts. The analysis was done using the condition that, $topass > 0$. The Fortran77 code for the NHL cuts is presented in Appendix B.

6.3.1 Reconstruction requirements

Reconstruction cuts isolated events with a two-track decay vertex within the decay channel fiducial volume and no charged particle identified in the upstream veto system. A description of the requirements is given below:

- Only 2 tracks connected to the common vertex
- There are no extra tracks unmatched to the common vertex
- Track projection satisfy a 50 inch box cut at face of calorimeter (both tracks project to 50" box;
  $-50'' < X < 50''$ and $-50'' < Y < 50''$)

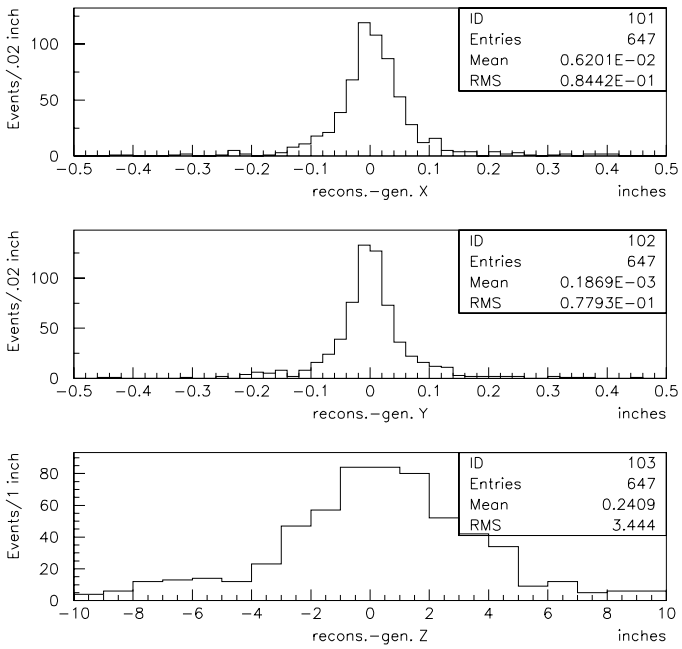

Figure 6.7: Difference of reconstruction and generated vertices. Z-vertex is reconstructed slightly upstream.

- Each track $\chi^2/DOF < 10$
- Each track slope less than 0.1 rad (cuts cosmic rays)
- Vertex $\chi^2/DOF < 10$
- Vertex within the fiducial volume:
  - 50 inch box cut ($-50'' < X < 50''$ and $-50'' < Y < 50''$)
  - 40 inches or $3\sigma_{\text{vertex}}$ away from chamber, whichever is larger
- No hits on the tracks from chambers upstream of the vertex.
- Particle identification is assigned to every track.
- Particle energies greater than:
  - 10 GeV for pions and electrons (to obtain differentiation between electromagnetic and hadronic showers)
  - 2.2 GeV (one cart) for muons (to differentiate from pion punch-through)

- No energy assignment problems (A flag indicating a single separated cluster is associated with each track)
- Good runs (runs when the NHL trigger was active; for runs 5583 and up; good DK Channel data, 10/15/96 and on)
- Tracks have good xy match (This flag required the match from the UV chamber only, the most reliable method of matching).
- Veto wall did not fire (LF bit code; see Ref. [57]).

The two tracks were required to be well-reconstructed, have an accompanying energy measurement, and form a common vertex. Large angle tracks arising from cosmic rays were removed by requiring tracks to form an angle of less than 0.1 radians with the beam direction. Exactly two tracks were required, both projecting to the calorimeter, with at least one of the two identified as a muon. To ensure good particle identification and energy measurement, muons were required to have an energy greater than 2.2 GeV; an energy greater than 10.0 GeV was required for electrons or hadrons. (The latter cut eliminated the low-energy pions associated with resonance production.) The reconstructed two-track decay vertex was required to be at least 40 inches (approximately 1m) from any material in the drift chambers.

6.3.2 Kinematic requirements

The kinematic cuts were designed to remove the remaining DIS and resonance backgrounds, since reconstruction cuts alone could not eliminate those events. Kinematic cuts were based on the calculated "effective" scaling variables usually used in the description of deep inelastic scattering.

The effective scaling variables $x_{\rm eff}$ and $W_{\rm eff}$ were calculated for each event under the following assumptions: 1) the event was a neutrino charged current interaction ($\nu N \rightarrow \mu N' X$); 2) the highest energy identified muon was the outgoing particle from the lepton vertex; and 3) the missing transverse momentum in the event was carried by an undetected final state nucleon. Specifically, $x_{\rm eff} \equiv \frac{Q^2_{\rm vis}}{2m_p\nu_{vis}}$ and $W_{\rm eff} \equiv \sqrt{m_p^2 + 2m_p\nu_{\rm vis} - Q^2_{\rm vis}}$, where $Q^2_{\rm vis}$ is the reconstructed momentum transfer squared, m_p is the mass of the proton, and $\nu_{\rm vis}$ is the reconstructed hadron energy. The momentum transfer squared $Q_{\rm vis}$ is defined as:

$$Q^2_{\rm vis} = -(k_\mu - k_\nu)^2 = \\ m_\mu^2 + 2E_\nu(E_\mu - p_\mu cos\theta_\mu),$$

where k_μ, p_μ, m_μ, and E_μ are 4-vector, momentum, mass and energy of a muon, k_ν, and E_ν are 4-vector and energy of the incident neutrino and θ_μ is

the angle of an outgoing muon. The energy transfered to the hadronic system, $\nu_{\rm vis}$, could be found as: $\nu_{\rm vis} = E_\nu - E_\mu = E_{\rm had}$.

The kinematic requirements were:

- $0.25 < m_T < 3.0$ GeV
- $x_{\rm eff} < 0.1$ GeV
- $W_{\rm eff} > 2$ GeV

Figures 6.8 and 6.9 show Monte Carlo DIS background and NHL signal distributions of m_T and $x_{\rm eff}$. The signal MC was done for a 1.15 GeV NHLs. One can see that requiring $x_{\rm eff} < 0.1$ and $m_T < 3.0$ GeV significantly reduced

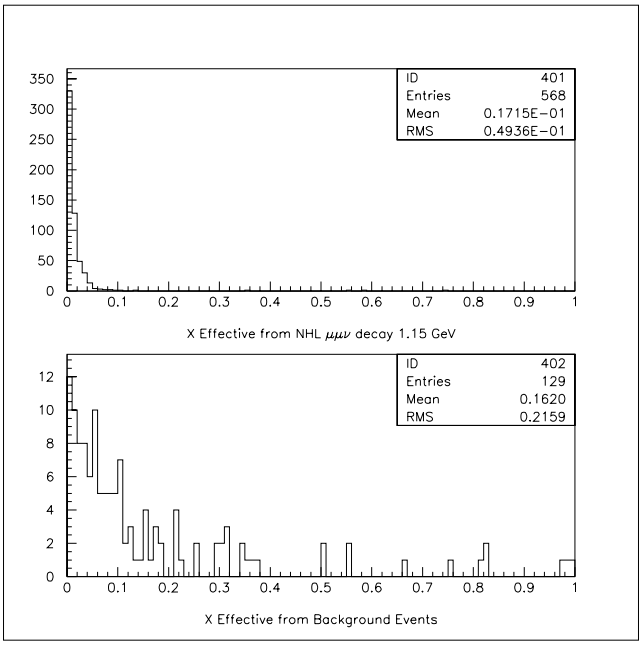

Figure 6.8: Top picture shows $x_{\rm eff}$ distribution from 1.15 GeV NHL decaying into $\mu\mu\nu$ mode. Below is $x_{\rm eff}$ for DIS background simulation.

the backgrounds from DIS and cut only a very small fraction of signal events. Requiring $W_{\rm eff} > 2.0$ GeV removed quasielastic and resonance backgrounds. Since we could not reconstruct the true mass of a NHL due to the missing neutrino, a cut was applied on the "transverse mass," $m_T \equiv |p_T| + \sqrt{p_T^2 + m_V^2}$. p_T is the component of the total visible momentum perpendicular to the beam direction, and m_V is the invariant mass for the two visible charged tracks. Requiring $m_T < 3.0$ GeV removed additional DIS background.

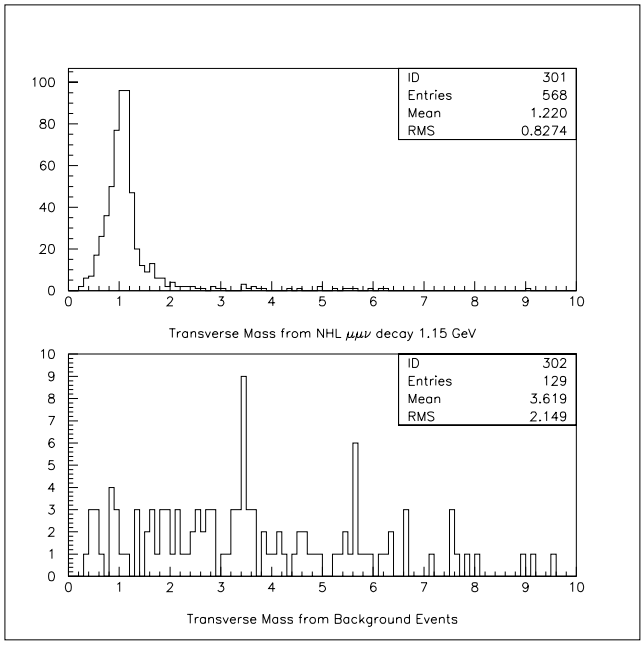

Figure 6.9: Comparison of m_T distribution from a Monte Carlo of 1.15 GeV NHL decaying into $\mu\mu\nu$ mode (top) with m_T distribution from DIS background simulation (bottom).

6.4 The neutrino event rate and Monte Carlo normalization

The prediction of DIS background depended on the correct Monte Carlo normalization. In the DIS Monte Carlo (Chapter 5), generated neutrinos were forced to interact for every event and every event had a weight of 1. The DIS Monte Carlo had to be absolutely normalized. The absolute normalization was based on a first-principles calculation of the neutrino event rate. Provided the number of neutrino interactions expected in the decay channel detector, $N_{\rm calc}^{DIS}$, the MC weight is calculated as the ratio of this calculated number to the number of generated events: $\frac{N_{\rm calc}^{DIS}}{N_{\rm gen}^{DIS}}$. Normalization factors are summarized at the end of this section in Table 6.3. The discrepancy between the number of neutrino events predicted by MC and observed in data were used as an estimate of the systematic error on the neutrino flux, as described in Chapter 8.

The number of neutrino interactions in the decay channel was calculated according to Eq. 6.5 by combining the neutrino flux and cross section with the value of the detector material density.

$$N_{\rm calc}^{DIS} = \int [\text{FLUX} \times \text{area} \times \sigma_{\rm tot}^{DIS}(E) \times \rho L N_A] dE \qquad (6.5)$$

where $\sigma_{\rm tot}^{DIS}$ is the total neutrino cross section, ρ is the material density in

(g/cm^3), L is the length of the detector and N_A is Avogadro's number. The FLUX in the above equation is defined as the number of ν's per area for the whole running. The neutrino cross section was calculated in the following three detector materials:

1. the decay channel helium,
2. drift chambers in the decay channel
3. the NuTeV calorimeter;

Neutrino cross section grows linear with the interaction energy. It could be conveniently redefined as $\sigma_{\rm tot}^{DIS} \equiv \frac{\sigma_{\rm tot}^{\nu N}}{E} \times E$, where $\frac{\sigma_{\rm tot}^{\nu N}}{E}$ could be approximated as a constant with the value of $0.676 \times 10^{-38} cm^2/GeV$ for the νN cross-section and $0.342 \times 10^{-38} cm^2/GeV$ for the $\bar{\nu}$. If we redefine flux as a number of incident neutrinos per unit area per energy bin multiplied by the average bin energy, $\Phi = \text{FLUX} \times E$, then Eq. 6.5 becomes:

$$N_{\rm calc}^{DIS} = \sum_i \Phi_i \times \left(\frac{\sigma_{\rm tot}^{\nu N}}{E} \right) \times \rho L N_A, \tag{6.6}$$

where Φ_i is the energy weighted flux in ith energy bin in GeV/cm^2.

In Eq. 6.6 integration over the energy energy was replaced by summation over the flux energy bins. The values in the flux bins were taken from the NuTeV neutrino beam flux files. The beam flux files were generated by the Turtle beam Monte Carlo [44]. Every bin contained the product of the number of incident neutrinos and the neutrino energy per unit area and per some fixed number of protons on target. Turtle flux files were generated assuming 10^6 protons on target, whereas the decay channel took 2.54×10^{18} protons. To account for the number of protons on target, The normalization was scaled by the factor of 2.54×10^{12}. The flux files were generated in the area of 66"×66", whereas fiducial volume was 50"×50". One can not just scale by the ratio of the area of a 50" box to the area of a 66" box, because the beam was not uniform. Instead, the beam profile histograms were used. Every energy bin had a corresponding beam profile histogram. To scale the energy bin value to the 50" box, beam profile histograms were integrated over the interval from -50" to 50", and the ratio of this integral to the integral over the whole histogram (or the number of entries) was formed for every energy bin. Every energy bin value was then scaled by the ratio of integrals. Adjusted bins then were summed over the energies varying from 15 GeV to 300 GeV.

The sum over all flux bins Φ_i in a 50"×50" box for neutrino mode was 60385.3 $GeV/10^6$ protons on target (POTs) and for antineutrino sample it was 19131.2 $GeV/10^6$ POTs. The numbers are summarized in Table 6.2

The product of flux, $\frac{\sigma_{\rm tot}^{\nu N}}{E}$ and Avogadro's number is shown in the last column of Table 6.2. By multiplying this number by square density of the

running mode	Flux GeV/10^6	POT 10^{18}	Flux 10^{12} GeV	$\sigma_{\rm tot}^{\nu N}/E$ $10^{-38} cm^2/GeV$	Flux$\times\sigma\times N_A$ cm^2/g
ν	60385.3	1.13	68235.4	0.676	277.77
$\bar{\nu}$	19131.2	1.41	26975.0	0.342	55.55

Table 6.2: The values of the flux in neutrino and antineutrino modes. The value in the left column is a sum over bins in the Turtle flux files, scaled to a 50" box cut. This value gets further scaled by the number of POTs in the second column. Last column is the flux multiplied by neutrino cross section and by Avogadro's number, this number multiplied by the square density, ρL, of the material yields the neutrino rate.

material, ρL, we get the number of expected ν interactions for the running with the decay channel on. Values of ρL for drift chambers and for the calorimeter subunits were taken from [60], where they were measured and quoted (see also Table 4.4). The calorimeter subunit consisted of two scintillation counters, one drift chamber and two steel plates, that were the biggest contribution to the density. [2] Fiducial length of the decay channel was 2848.127 cm. The area density of Helium in the decay channel was

$$\rho L = 1.67610^{-}4 g/cm^3 \times 2848.127 cm = 0.477 g/cm^2. \tag{6.7}$$

There were two drift chambers inside the decay channel and two chambers on the edges of the decay channel. The drift chamber sample consisted of events in four chambers: DK2, DK3, DK4 and DK5. The calorimeter fiducial volume contained 31 calorimeter subunits.

Table 6.3 shows calculations of the number of neutrino interactions in 3 detector materials, the decay channel helium ($\rho L = 0.477 g/cm^2$), drift chambers ($\rho L = 4 \times 2.87 g/cm^2$) and the NuTeV calorimeter($\rho L = 31 \times 178.17 g/cm^2$), for neutrino and antineutrino modes combined. The reconstruction efficiency was measured as a ratio of the number of reconstructed MC events, $N_{\rm MC}^{rec}$, to the number of generated events, $N_{\rm MC}^{gen}$. The calculated number of neutrino interactions was multiplied by the efficiency to get the Monte Carlo prediction for the number of events in the different materials. On top of that, the number of predicted events in the calorimeter was scaled by the ratio of the NuTeV calorimeter lifetime to the decay channel lifetime. Table 6.3 shows the agreement between MC and data within 20%.

Calculations yielded 797 ± 119 ν and 159 ± 24 $\bar{\nu}$ events expected per drift chamber in the decay channel, with the total of 956 ± 143 DIS ν interactions.

[2] The average area density of the drift chamber was 2.87 g/cm^2 and the density of the calorimeter subunit was 178.17 g/cm^2.

Detector material	Calculated event Num.	Measured MC efficiency in %	Observed Num. of data events	Predicted in MC Numb.
1 drift chambers	956 ± 143	51.7 ± 0.6	424 ± 20	494 ± 74
He volume	159 ± 24	48.0 ± 0.3	84 ± 9	70 ± 10
Calorimeter	31×5.9310^4	43.95± 0.04	1.0810^4	0.9210^4

Table 6.3: Number of ν events in 3 different detector volumes in ν and $\bar{\nu}$ modes combined. Data measurements (4th column) are quoted with statistical errors. The last column if the product of the calculated number of events(2nd column) and MC efficiency(3rd column). The predicted number for the calorimeter events was scaled by the ratio of lifetimes (decay channel was off during the beginning of the run.)

An efficiency predicted in the MC was 57.5%, thus we expected $956 \times .517 = 494$ neutrino interactions in a single decay channel chamber. We measured 424 ν events, thus MC overpredicted DIS events by 15%, as indicated in Table 6.3. A 15% error on the calculation was assumed based on the discrepancy of the predicted number of events with the observed number. In Helium, the number of expected ν events was less than the observed number by 15%. Helium MC underpredicted the number of DIS interactions. The calculation yielded 1.84 million CC interactions expected in the calorimeter, and the predicted number of CC events was less than the observed number by 16%.

In this analysis ν events were generated by the DIS MC in the fiducial volume of the decay channel (Helium) and in the drift chambers. There were 24207 MC events generated in four decay channel chambers, 6051 in each chamber and in each mode, ν and $\bar{\nu}$. [3] In the decay channel Helium, there were 24207 MC events in ν mode and 12294 in $\bar{\nu}$. After fiducial cuts there were 18155 ν and 9126 $\bar{\nu}$ Helium events left.

The MC is weighted by the ratio of the number of expected ν events over the number of generated events: $\frac{N_{\rm exp}^{DIS}}{N_{\rm gen}^{MC}}$. The normalization factors are summarized in Table 6.4:

Detector material	Neutrino			Antineutrino		
	$N_{\rm exp}^{DIS}$	$N_{\rm gen}^{\nu}$	norm.	$N_{\rm exp}^{DIS}$	$N_{\rm gen}^{\nu}$	norm.
1 drift chamber	797	6051	0.132±0.011	159	2995	0.053 ± 0.006
Helium	133	18155	$(7.32\pm1.10)10^{-}3$	26	9126	$(2.8\pm0.42)10^3$

Table 6.4: MC normalization of DIS samples generated in a drift chamber and in the decay channel Helium for neutrino and antineutrino running. Events in Helium are shown with 15% error, which is the amount of the disagreement between data and MC. Chamber events are shown without errors.

[3] 24207 is the number of noise events stored on disk. Events without noise were dropped.

6.5 Quasi-Elastic normalization

The Quasimodo (QE-RE, see section on "Quasimodo" in Chapter 5) Monte Carlo, which includes quasi-elastics and resonance production, forced an incident neutrino to interact every generated event in the similar fashion as DIS Monte Carlo. QE-RE Monte Carlo was reweighted after it has been generated on the basis of the neutrino flux and quasi-elastic and resonance cross section.

The neutrino flux files, the primary source of the flux information for my calculations, contained the number of incident neutrinos per unit area multiplied by the neutrino energy. This format accommodated the linear dependence of the neutrino total cross section with energy. However, the quasi-elastic and resonance cross section was constant with neutrino energy, thus the content of the bin in the flux file had to be divided by the energy to give just the number of incident neutrinos per unit area. If the content of the energy weighted flux bin is Φ_i, which is the number of ν's per area times energy, then the number of quasielastic/resonance interactions could be calculated similarly to Eq. 6.6:

$$N_{\rm calc}^{QE-RE} = \sum_i \frac{\Phi_i}{E_i} \times (\sigma_{qe} + \sigma_{\rm res}) \times \rho L N_A, \tag{6.8}$$

where $\sigma_{\rm qe}$ is the quasi-elastic neutrino cross section, $\sigma_{\rm res}$ is the resonance production cross section, ρ is the material density in $[g/cm^3]$, L is the length of the detector and N_A is Avogadro's number.

At this point however, the DIS Monte Carlo have been absolutely normalized. Using DIS normalization one can rewrite Eq. 6.8 as

$$N_{\rm calc}^{QE-RE} = \sum_{\rm i} N_i^{DIS} \times \left[\frac{\sigma_{qe} + \sigma_{\rm res}}{\left(\frac{\sigma_{\rm tot}^{\nu N}}{E_i}\right) E_i - \sigma_{qe} - \sigma_{\rm res}} \right], \tag{6.9}$$

where the number of deep-inelastic events, N_i^{DIS}, in the energy bin i is scaled by the ratio of quasielastic and resonance cross section to the deep inelastic cross-section.

The values of resonance, quasi-elastic and deep-inelastic cross sections ([29, 25]) are listed in Table 6.5.

cross section	$\sigma_{\rm QE}^{\nu}$	$\sigma_{\rm QE}^{\bar{\nu}}$	$\sigma_{\rm res}^{\nu}$	$\sigma_{\rm res}^{\bar{\nu}}$	$\sigma_{\rm tot}^{\nu N}$	$\sigma_{\rm tot}^{\bar{\nu} N}$
in $10^{-38} cm^2$	0.43	0.22	0.75	0.30	$0.676 \times E$ (GeV)	$0.342 \times E$ (GeV)

Table 6.5: Values of quasielastic cross section (constant with neutrino energy E) and deep-inelastic scattering cross section (linear with ν energy) for neutrino and antuneutrino modes.

In the comparisons between data and Monte Carlo, the quasielastic/resonance Monte Carlo was merged with DIS Monte Carlo. Quasimodo events were added

to DIS Monte Carlo events with the weight (w_{QE-RES}) proportional to the ratio of fluxes, similar to one used in Eq. 6.9.

$$w_{\rm QE} = \sum_i \frac{N_i^{DIS}}{N_i^{QE-RES}} \times \left[\frac{\sigma_{\rm qe} + \sigma_{\rm res}}{\left(\frac{\sigma_{\rm tot}^{\nu N}}{E_i}\right) E_i - \sigma_{\rm qe} - \sigma_{\rm res}} \right], \tag{6.10}$$

where N_i^{DIS} and N_i^{QE-RES} are the number of DIS and quasimodo events in the ith energy bin.

I generated 48414 quasielastic and resonance events in neutrino and antineutrino mode and with normalization expected 7 events in the helium which makes a 1.4×10^{-4} normalization factor.

6.6 Comparisons between data and Monte Carlo distributions

Deep Inelastic Scattering (DIS) events were the biggest background in this analysis and the determination of the background level used the Lund model implemented in a GEANT hit-level Monte Carlo. This section describes checks on the DIS Monte Carlo and proves that it accurately reflects the data.

• First, the comparisons of the number of events predicted in MC and observed in the data are shown;

Table 6.6 presents the number of neutrino events in the decay channel fiducial volume and drift chambers for neutrino and antineutrino modes and the corresponding efficiencies. Monte Carlo events are absolutely normalized. The agreement between data and Monte Carlo in the decay channel is within 20%.

The calculation based on the NuTeV ν flux and νN cross section predicted 956 neutrino events in one decay channel drift chamber when the decay channel was active. There were two drift chambers inside and two on the edges of the decay channel. In four drift chambers there were 1847 reconstructed data events out of $956 \times 4 = 3824$ neutrino interactions expected during the run. In the decay channel Helium, the calculation yielded 159 CC neutrino interactions, and in the NuTeV calorimeter 1.84 million CC interactions. Number of CC neutrino events was measured very precisely by the NuTeV detector, and it was $N_{\rm data}^{\rm CC} = 1084040 \pm 1041$. To compare the calculated number of CC events, $N_{\rm calc}^{\rm CC}$, with the above measurement, one has to multiply $N_{\rm calc}^{\rm CC}$ by the reconstruction efficiency and correct it by the lifetime ratio. The reconstruction efficiency of the NuTeV calorimeter was measured by the DIS MC, the value of the efficiency was 43.9%. This reconstruction efficiency was calculated as the ratio of MC events that passed CC analysis cuts (called "Structure Function cuts", see Ref. [61]) to the number of events generated in the fiducial volume of the

Location	Neutrino			Antineutrino		
	data	MC	MC eff.	data	MC	MC eff.
in DK3	440	518	65%	84	101	64%
in DK4	399	454	57%	72	84	53%
in DK5	289	279	35%	48	44	28%
in He $z < DK5$	18	12	32%	5	2	21%
DK5< z <DK4	30	23	61%	4	4	46%
DK4< z <DK3	20	26	69%	7	5	62%
the calorimeter	8.6×10^5	7.6×10^5	43.9%	2.2×10^5	1.5×10^5	43.9%

Table 6.6: Data vs Monte Carlo (MC) comparison of the number of reconstructed in the fiducial volume events in the different parts of the decay channel and in the NuTeV calorimeter with the decay channel operating (2.54×10^{18} protons on target). The only requirement applied was that the vertex will be reconstructed within the decay channel. The DK5< z <DK4 notation means events in Helium between DK5 and DK4 drift chambers. Fourth and seventh columns contain values of efficiency measured in Monte Carlo in %.

NuTeV calorimeter. The ratio of the calorimeter lifetime to the decay channel lifetime was 1.14 . Thus I would expect $N_{\rm MC} = 10 \times 0.439 \times 1.14 = 9.20710^5$, which was 16% smaller than the observed number of 1.08 million events.

Table 6.8 shows the result of applying the NHL cuts on the data and MC in the sample of neutrino events in DK4 drift chamber. As shown in the Table, the Monte Carlo and data chamber events behave similarly under the NHL analysis cuts.

• Second, absolutely normalized kinematic distributions of reconstructed Monte Carlo events were compared to the data.

Because the analysis box was closed, we could not use the NHL analysis data sample for the direct comparisons with Monte Carlo in the fiducial volume and within analysis cuts. We used 2 samples of DIS events in the decay channel drift chambers:

1. Multitrack events (> 2) in the decay channel drift chambers.

2. Two track neutrino events in the drift chambers that pass all NHL analysis cuts, except a fiducial cut.

Both those samples were orthogonal to the NHL analysis data sample.

6.6.1 Multitrack event sample in drift chambers

The multitrack neutrino event reconstructed in the DK4 chamber is shown in Figure 6.10. The multitrack sample consisted of DIS MC ν events reconstructed in the decay channel drift chambers with three or more tracks linked

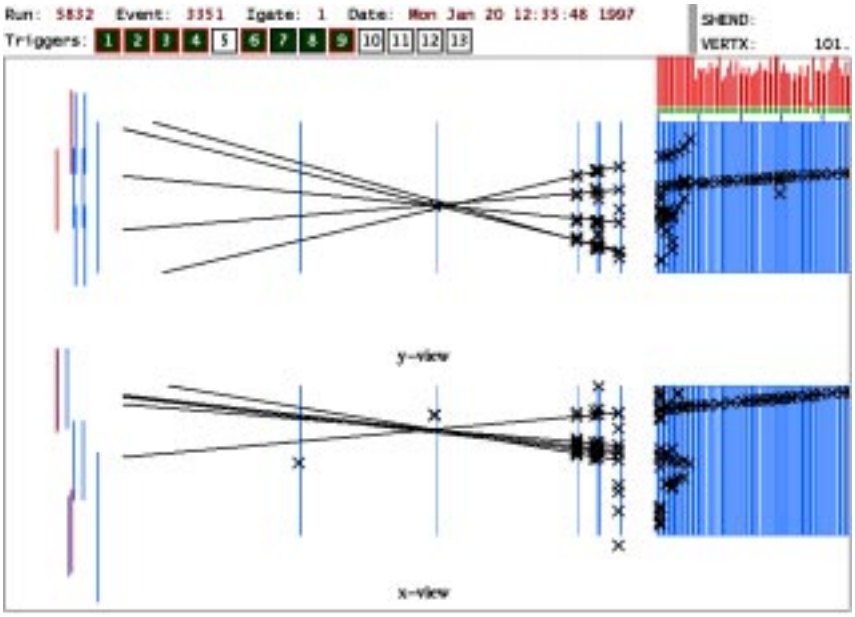

Figure 6.10: A multitrack event in the decay channel chamber DK4. The energy of the most energetic muon is about 70GeV. A X-plane of the chamber is more downstream than a Y-plane.

to the common vertex. It constituted around 40% of all reconstructed DIS events. The rest 60% belonged to the 2-track sample. This is explained by the fact that with the sparse number of chambers in the decay channel many tracks escape at large angles.

Kinematic variables were formed under the assumption that the event was a neutrino CC interaction with the missing transverse momentum in the event carried by an undetected nucleon. The data Monte Carlo comparison was based on the following variables:

- *inelasticity*, $y_{\text{eff}} \equiv \frac{E_{HAD}}{E}$
- *transverse mass*, $m_T \equiv \sqrt{m_p^2 + 2m_p\nu_{\text{vis}} - Q^2_{\text{vis}}}$
- *hadronic invariant mass*, $W_{\text{eff}} \equiv \sqrt{m_p^2 + 2m_p\nu_{\text{vis}} - Q^2_{\text{vis}}}$
- *momentum transfer sq.*, $Q^2_{eff} \equiv Q^2_{\text{vis}}$
- *Z-vertex*, Z-position of the vertex
- *bjorken X*, $x_{\text{eff}} \equiv \frac{Q^2_{\text{vis}}}{2m_p\nu_{vis}}$

where Q^2_{vis} is the reconstructed momentum transfer squared, m_p is the mass of the proton, and ν_{vis} is the reconstructed hadron energy. The suffix "*eff*" denotes that an undetected nucleon was assumed to balance the missing momentum.

Figures 6.16(y_{eff}), 6.17(m_T), 6.18(W_{eff}), 6.19(Q^2_{eff}), 6.20(Z-vertex) and 6.21(x_{eff}) compares the Monte Carlo sample of 215 multi track events with 193 data events in the two decay channel chambers DK 4 and DK5. The Kolmogorov-Smirnov probabilities that the Monte Carlo describes the data is presented in Table 6.7.

distribution	y_{eff}	m_T	W_{eff}	Q^2_{eff}	Z-vertex	x_{eff}
Prob.(KS)	94%	98%	42%	60%	38%	59.5%

Table 6.7: The probability that the Monte Carlo distribution describes the data correctly, calculated according to the Kolmogorov-Smirnov method.

6.6.2 2-track drift chamber event sample

An event display of a 2-track chamber ν event is shown in Figure 7.2. As a check on the two-track reconstruction efficiency, we have compared the fourteen two-track data events with vertices in the drift chambers to the Monte Carlo prediction of 15 $\pm$ 2 events. All NHL analysis cuts, but a fiducial cut and transverse mass cut, were applied to the neutrino event sample. The fiducial cut was modified to look for events in the chambers, rather than in the fiducial volume of the decay channel. Events with "transverse mass less than 5 GeV were allowed into the sample, as compared to the original transverse mass cut was $m_T < 3GeV$.

Figure 6.11 shows comparisons of distributions for the previously introduced DIS variables, x_{eff}, W_{eff}, Q^2_{eff} as well as m_T and $y_{\text{eff}} \equiv \frac{E_\nu - E_\mu}{E_\nu}$. Again, the agreement shows that Monte Carlo matches the data well. We expected around 24 times more events in four decay channel drift chambers than in Helium from the mass ratio of materials. By scaling 14 events observed in the drift chambers by the factor 24 we will get a rough estimate on the background of 0.6 DIS events in the decay channel helium. This is consistent with the predicted background of 0.56 events calculated in Chapter 7.

6.6.3 NHL Monte Carlo kinematic distributions

For comparison I present kinematic distributions similar to the presented above but for three NHL MC simulations: for 0.35 GeV NHL decaying to $\mu\mu\nu$, for 0.85 GeV NHL decaying to $\mu\pi$ and for 1.15 GeV NHL $\mu\pi$ mode. Presented distributions consist of events that pass all NHL cuts. The absolutely normalized distributions are presented in Figures 6.12, 6.13 and 6.14.

6.7 The Decay channel efficiency

The average reconstruction efficiency of the decay channel was 23% with the acceptance contributing to the 50% of rejected events. It was measured as the ratio of Monte Carlo events that passed NHL cuts to the number of events generated in the fiducial volume. The reconstruction efficiency is shown on the Figure 6.15.

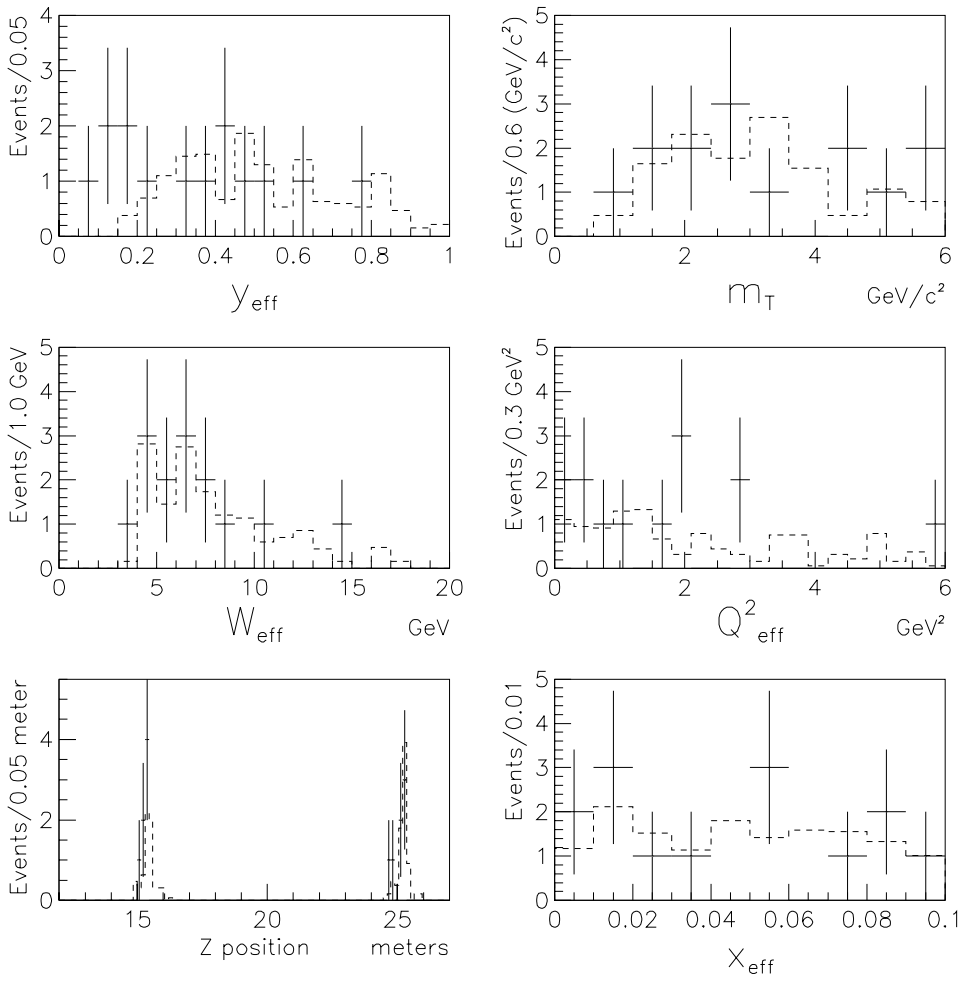

Figure 6.11: Kinematic distributions for data (crosses) and MC DIS background (dashed) events with two-track vertices reconstructed in the decay channel drift chambers. MC events are absolutely normalized to the number of protons on target. The DIS reconstructed variables $y_{\rm eff}$, $W_{\rm eff}$, $Q^2_{\rm eff}$, $x_{\rm eff}$ and m_T are defined in the text. Z positions are referenced to the veto array; spikes in the Z distribution correspond to the locations of the decay channel drift chambers.

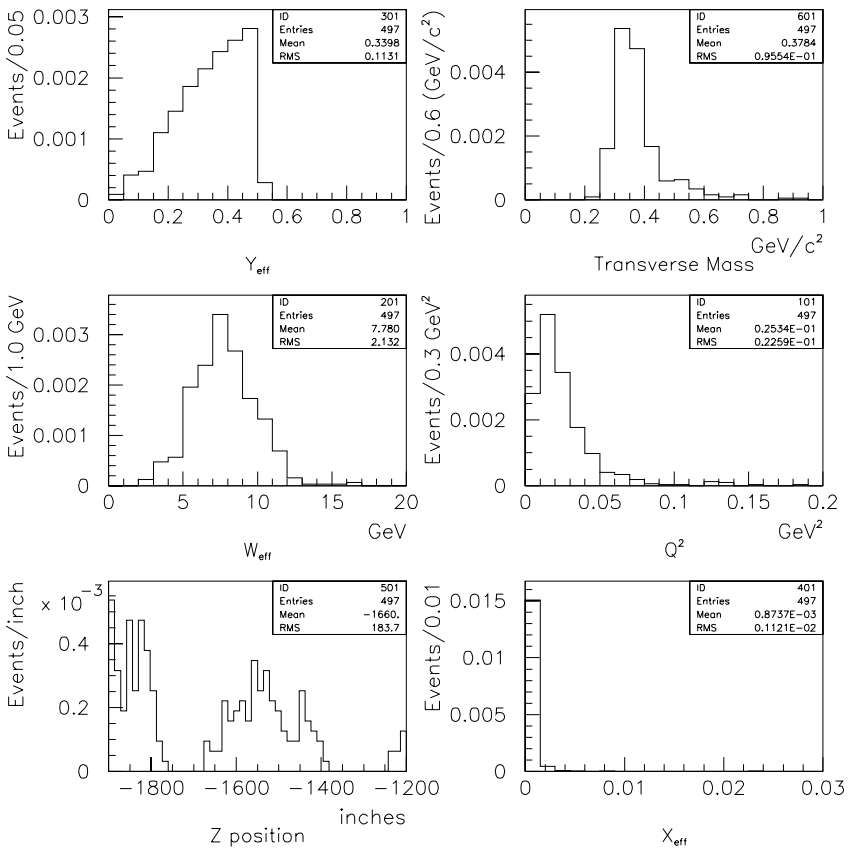

Figure 6.12: Kinematic distributions for NHL MC simulation of 0.35 GeV NHL decays in $\mu\mu$ mode. MC events are absolutely normalized. The DIS reconstructed variables $y_{\rm eff}$, $W_{\rm eff}$, $Q^2_{\rm eff}$, $x_{\rm eff}$ and m_T were defined in the text. Z positions are referenced to the veto array;

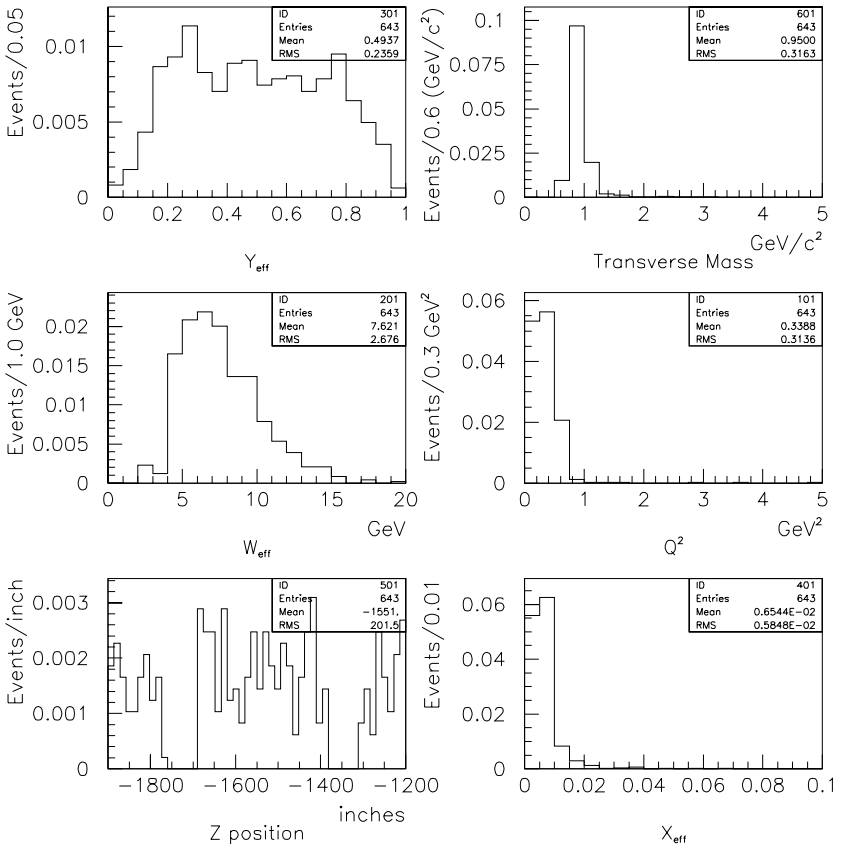

Figure 6.13: Kinematic distributions for NHL MC simulation of 0.85 GeV NHL decays in $\mu\pi$ mode.

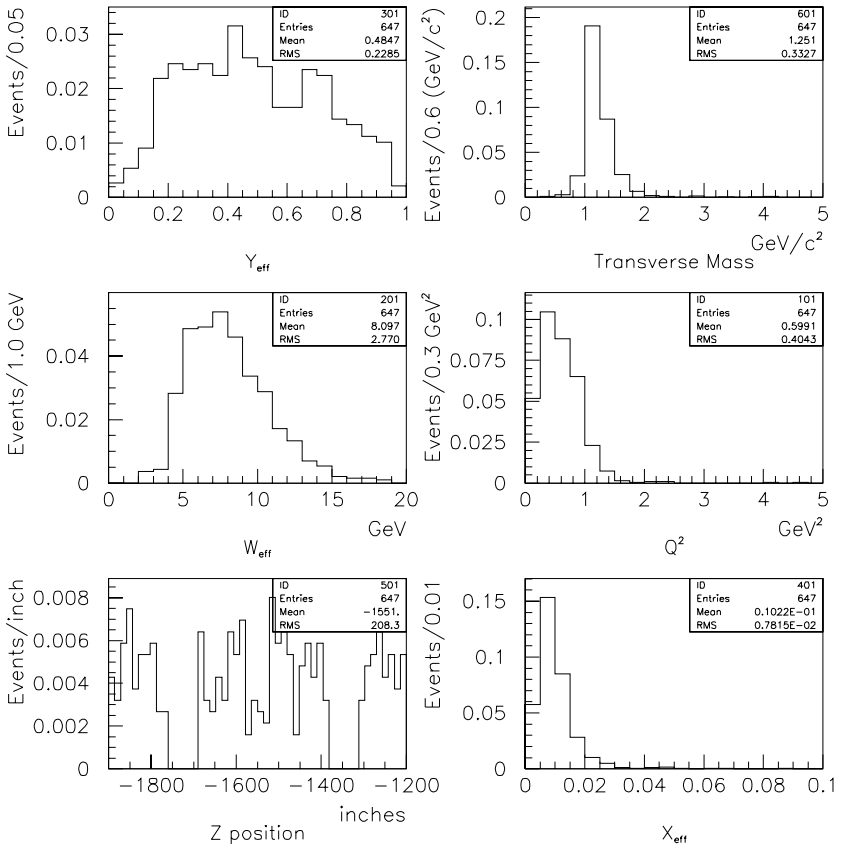

Figure 6.14: Kinematic distributions for NHL MC simulation of 1.15 GeV NHL decays in $\mu\pi$ mode.

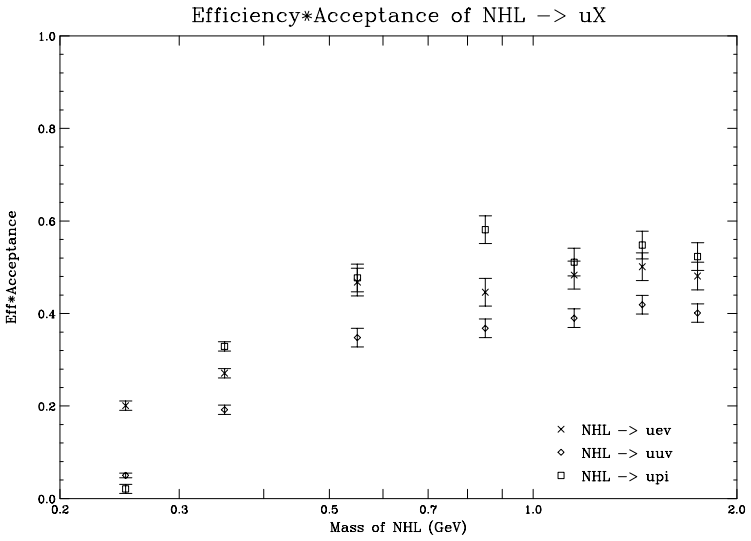

Figure 6.15: The NHL reconstruction effieciency plot without acceptance. The product of reconstruction cuts and acceptance formed the sensitivity.

cut number fiducial cuts	Lund MC ν in DC's	efficiency in %	data in DC's	efficiency in %
total	6051	-	2309	-
e(1) $\neq$ e(2)	3047	-	440	-
2 tracks	1738	57.0	269	61.1
no xtra	906	29.7	150	34.1
50"box	643	21.1	111	25.2
trk χ^2	422	13.8	83	18.9
slope	353	11.5	72	16.4
vertex χ^2	331	10.9	65	14.7
up vertex	317	10.4	55	12.5
PID	317	10.4	55	12.5
energy	317	10.4	55	12.5
rec.	203	6.7	31	7.0
m_T	131	4.2	25	5.6
x_{eff} 14	108	3.5	21	4.8
W_{eff}	108	3.5	21	4.8
bad run	108	3.5	20	4.5
beam on	108	3.5	20	4.5
XY match	108	3.5	20	4.5
no pair	93	3.0	19	4.3
LFbit	77	2.5	16	3.6

Table 6.8: The Monte Carlo and data samples of the events reconstructed in the DK4 drift chamber under the NHL analysis cuts. The third and the fifth columns show the efficiency of the particular cut as the ratio of the events passed this cut to events left after the previous cut. The table shows the discrepancy between MC and data within 20%.

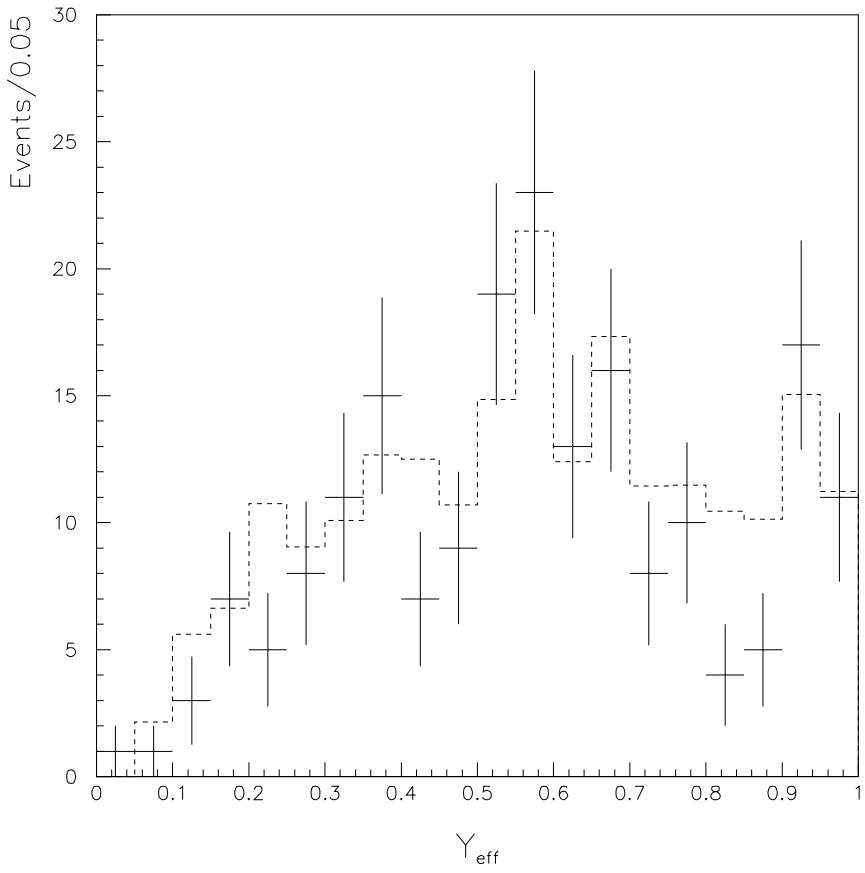

Figure 6.16: Inelasticity y_{eff} distribution for data (crosses) and MC DIS background (dashed) events with more than two (>2) vertices reconstructed in two decay channel drift chambers (DK4 and DK5).

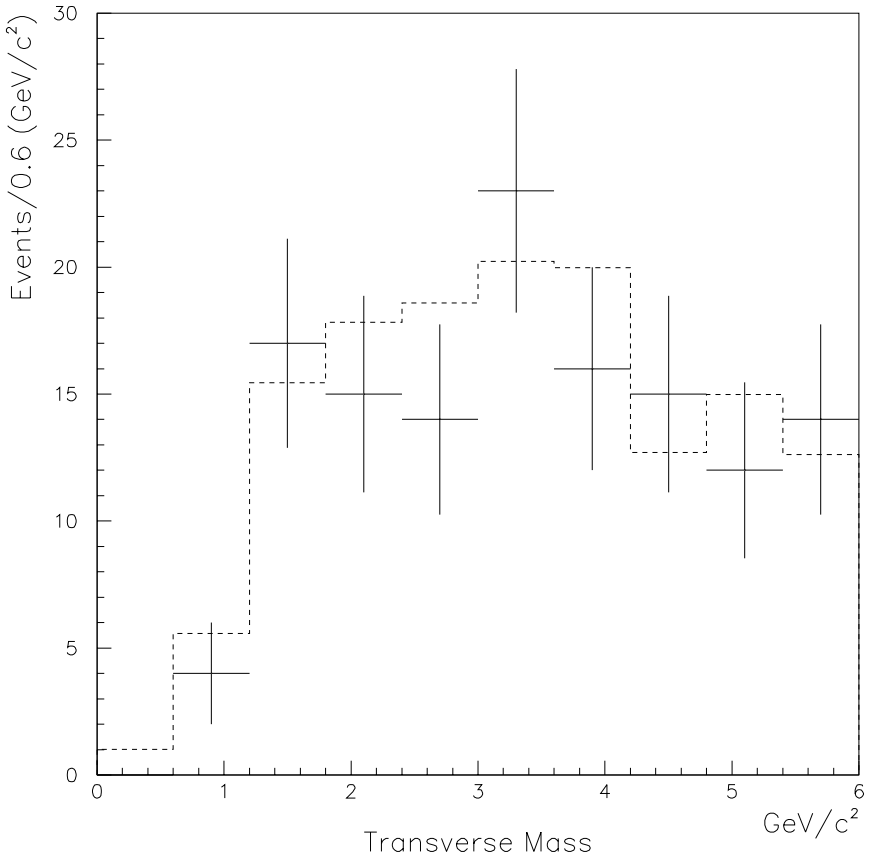

Figure 6.17: Transverse mass distribution of reconstructed data (crosses) and Monte Carlo events in DK4 and DK5.

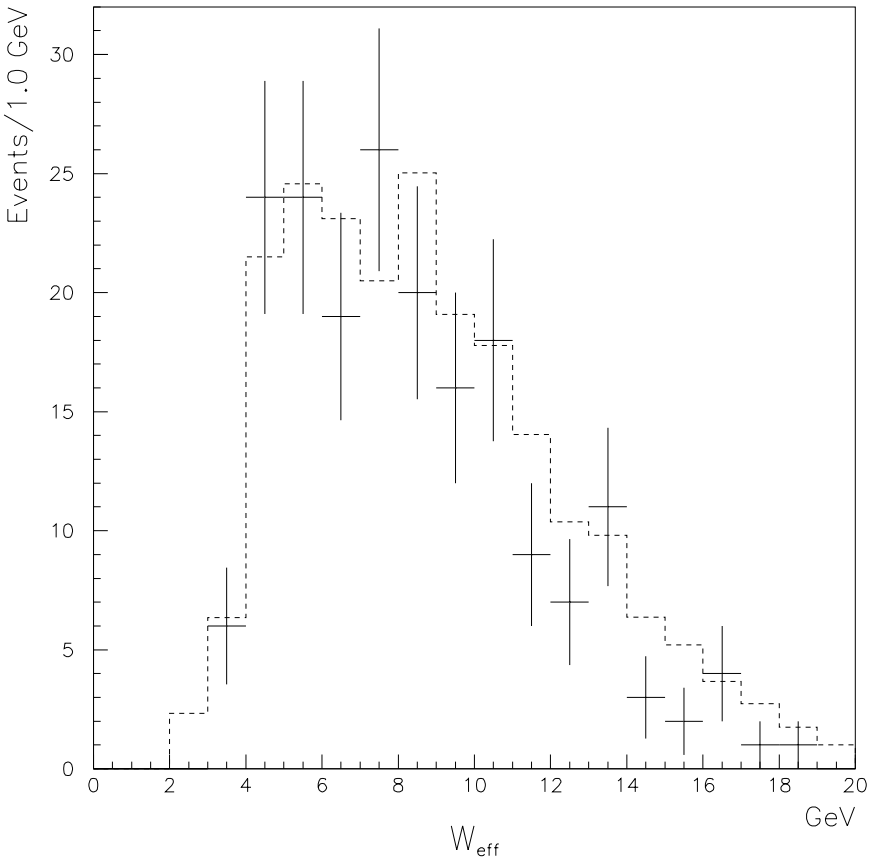

Figure 6.18: Reconstructed distribution of the invariant mass of hadronic system, $W_{\rm eff}$. Data is shown in crosses. Events reconstructed in DK4 and DK5.

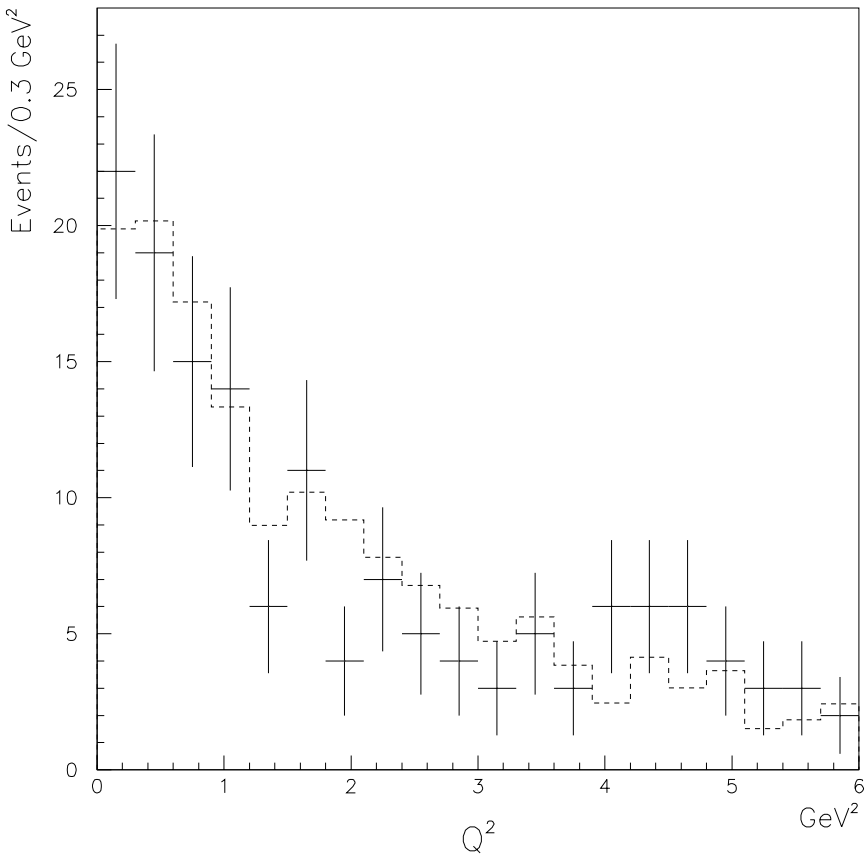

Figure 6.19: Distribution of the momentum transfer squared, $Q^2_{\rm eff}$, data (crosses) vs Monte Carlo. Events reconstructed by the NHL analysis software in DK4 and DK5 chambers.

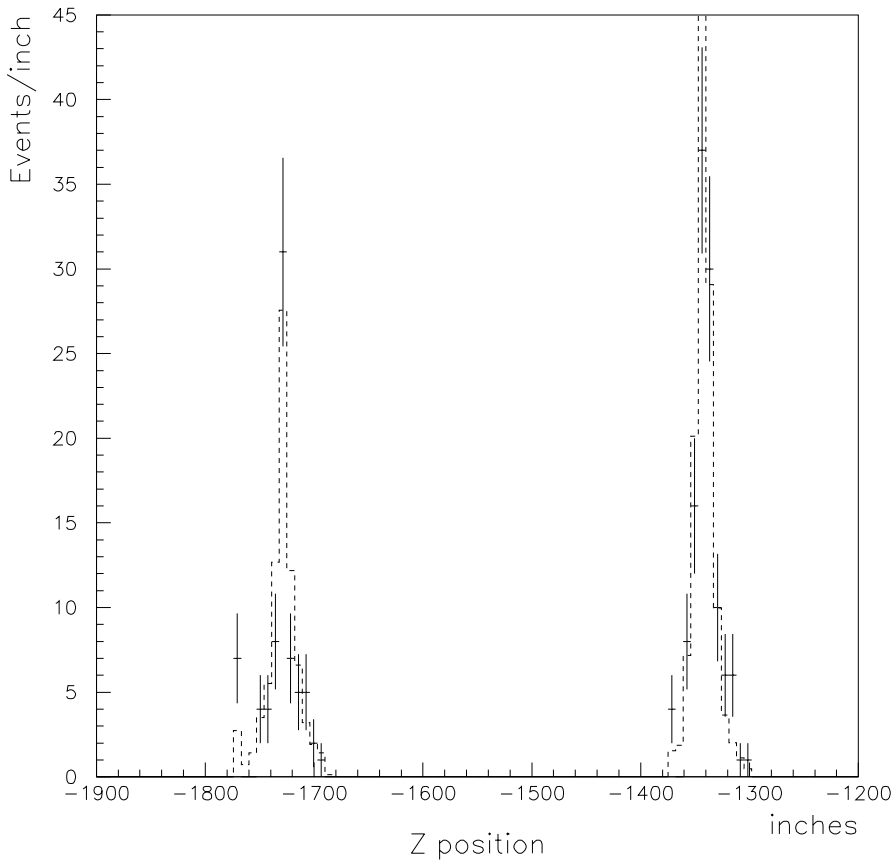

Figure 6.20: data (crosses) and Monte Carlo Z-vertex distributions. Events were reconstructed in the two chambers inside decay channel volume, in DK4 and DK5.

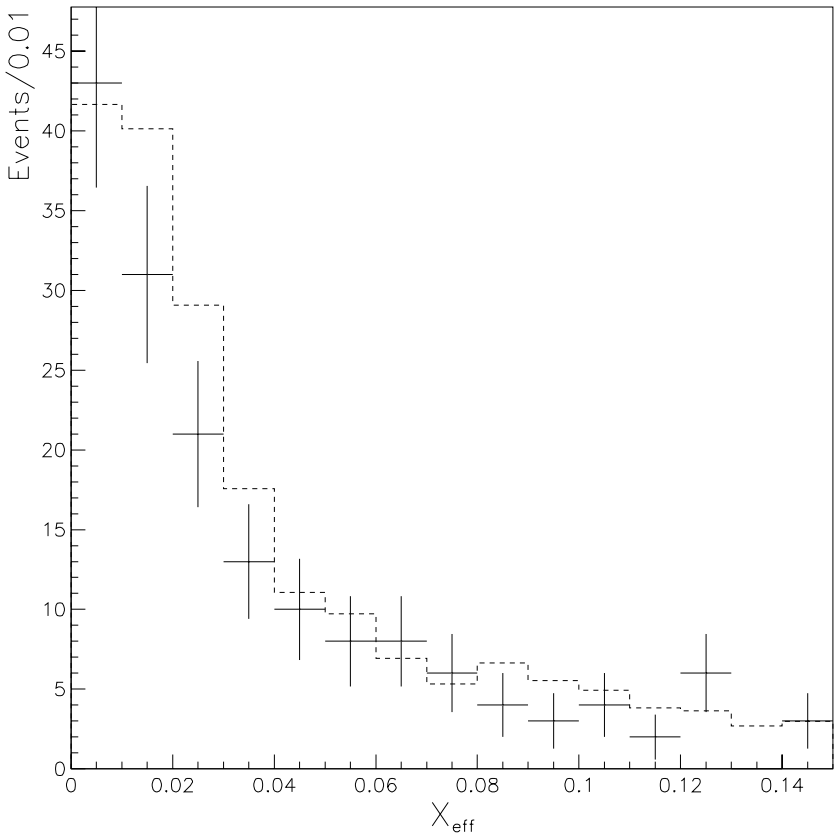

Figure 6.21: Reconstructed bjorken scaling variable, x_{eff}, data vs Monte Carlo distribution comparison.

Chapter 7

Backgrounds

Possible two-track background events, that could be mistaken as NHL signal events, occur from the following sources:

- Neutrino interactions in the helium
- K^0 punch-through from ν interactions in the berm
- Neutrino interactions in the material surrounding the decay channel
- Cosmic ray background

Each of the backgrounds is considered separately. The summary over all of the background event rates is at the end of this section.

The decay channel was designed to lower the background level. Large volume plastic bags were filled with helium, thus reducing the amount of material in the decay channel and the number of ν DIS interactions. Yet the DIS events were the most important background to this analysis. The level of DIS backgrounds was determined using LUND/GEANT DIS Monte Carlo [48, 47], which proved to accurately reflect the data (see section in Chapter 5 on data and MC comparisons).

In the end, the backgrounds were reduced to a level well below one event.

7.1 Neutrino interactions in Helium

The DIS Helium events were typically characterized by a high multiplicity. Requiring two-tracks linked to a vertex and no extra tracks cuts the majority of the DIS background. A potential source of two-track background events were quasielastic scatters and resonance production in the decay channel. Running on the sample of 48414 quasi-elastic and resonance events from the Quasimodo Monte Carlo also did not reveal any significant background. None of the generated events passed NHL cuts. As discussed in the Sec. 6.5, we expect 7

Table 7.1: Deep Inelastic Scattering background events in helium for the full run

Source	MC tot	$\mu\mu$	μe	$\mu\pi$	MC calc	expected	background
ν in Helium	24207	4	27	44	75	133	(0.47 ± 0.05)
$\bar{\nu}$	12294	37	5	7	14	26	(0.09 ± 0.01)

quasielastic and resonance events, which gives the normalization of $7/48414 = 1.4 \times 10^{-4}$. This makes the quasielastic and resonance background very small ($< 1.4 \times 10^{-4}$). Moreover, the two track event sample is highly suppressed by the kinematic cut, $W^2 > 2GeV$, according to the Ref.[27, 28]. Based on this, I assumed that quasielastic and resonance background in this analysis was negligible.

One could suppose that the remaining two-track events were multi-track events where the other tracks were lost due to the acceptance or it was a fluctuation in multiplicity of the event. The signature of the background event would vary depending on the NHL decay mode. Background in $\mu\pi$ mode could be from events with only one energetic pion and one scattered muon that hits the calorimeter. Background in μe mode could occur when a pion is misidentified as an electron, or when photons hit the NuTeV calorimeter. Backgrounds in $\mu\mu$ mode could be from the pion or charm decays to muons in a DIS event.

To give a scale, 159 DIS neutrino interactions were expected in the decay channel Helium for the run, with 133 events due to ν scatters and 26 due to $\bar{\nu}$ scatters. All of these events would be cut under the NHL analysis cuts. To make an accurate measurement of the DIS background, one has to run a large number of Monte Carlo events to form the ratio of the number of events that pass cuts to the number of generated events.

For the background estimate I generated 24207 neutrino and 12294 antineutrino DIS events. The number of MC events in Helium that passed the NHL cuts was 75 events in neutrino running and 26 events in antineutrino running. Table 7.1 summarizes the background level for the deep-inelastic neutrino events. The probability that a DIS event in the fiducial volume of the decay channel would pass the NHL cuts is $75/24207 = 3.1 \pm 0.3 \times 10^{-3}$. Plots of the vertex distributions for the helium DIS and NHL Monte Carlo events are shown in Figure 7.1. One can see that the two types of events have similar vertex distributions. From this study, the total DIS Helium background was (0.56 ± 0.15) events/run.

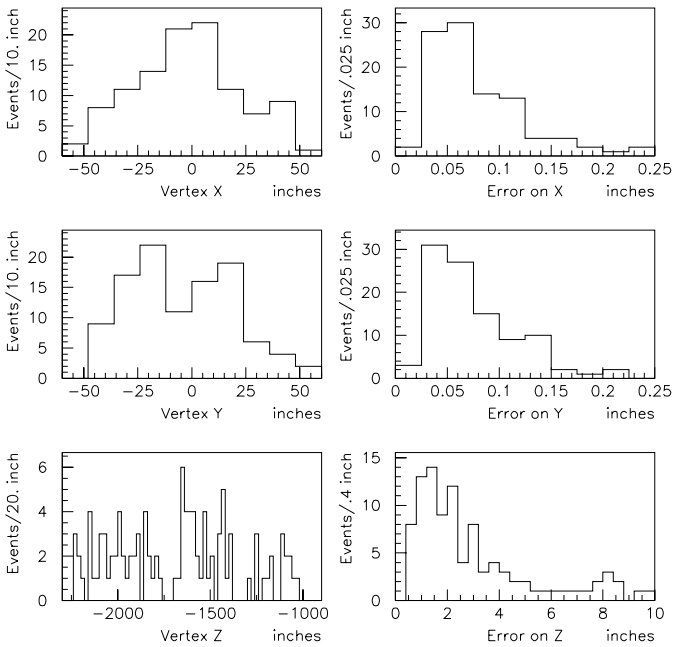

Figure 7.1: Vertex distributions of the helium DIS (left column) and NHL Monte Carlo (right column). Distributions are in inches.

7.2 K_L punch-through from the berm

This background comes from neutrino interactions in the berm that produce K_Ls, which punch-through the absorber, enter the decay channel and subsequently decay with a NHL decay topology. If these particles were not accompanied by charged partners they would not be vetoed, assuming that the veto wall is efficient. This assumption has been tested in the veto wall efficiency study, described in the analysis section in Chapter 6. From this study, the inefficiency of each individual section of the veto wall was $< 0.5\%$ and overall efficiency was more than 99%.

The K_L punch-through background was estimated using the berm MC (see "Neutral punch-through Monte Carlo" in Chapter 5). Berm MC simulated K_L and K_S mesons were allowed to enter the decay region and randomly decay. Two- and three-body decays of the kaons were simulated at random positions along the decay channel. The transverse vertex position was distributed according to the kaon beam flux modeled by the beam MC.

K_S mesons decayed too quickly to contribute to the neutral punch through background. We considered decays that result in muons, electrons and pions. The secondary pions decayed to muons.

- $K_L^0 \to \pi\mu\nu$,
- $K_L^0 \to \pi e\nu$,
- $K_L^0 \to \pi^+\pi^-\pi^0$,
- $K_L^0 \to \pi^+\pi^-$.

K_L mesons which enter the decay channel with a small transverse angle were cut by the transverse mass cut ($0.25 < m_T < 2.0$). Kaons that exit the berm at large angles were not reconstructed within the decay channel. In the data, we expect 620 K_L punch-throughs (according to Ref. [39]). Out of 891,000 MC generated events with K_L mesons, none of the events passed the NHL cuts. To get a more restrictive estimate, we imposed reduced requirements (listed below).

1. a decay within the decay channel volume
2. a reconstructed muon energy > 3 GeV.
3. a reconstructed hadron/electron energy > 10 GeV.
4. two tracks that hit NuTeV calorimeter

Total number of 7 events passed the NHL cuts, 1 event in $\mu\mu$ mode and 3 events in both $\mu\pi$ and μe modes. The background level then could be estimated as $< 7.0 \times 10^{-4}$ in $\mu\mu$ mode, and $< 2.0 \times 10^{-3}$ in both μe and $\mu\pi$ modes for the whole run. This gives a conservative estimate on the K_L punch-throughs of $(5.0 \pm 2.0) \times 10^{-3}$ events for the full run.

7.3 Neutrino interactions in the material surrounding the decay channel

This background had several sources defined by the different material encompassing the decay channel volume. Neutrino interactions that could mimic NHL decays could happen in the following places:

- Drift chambers
- Floor
- Tohoku steel plates, left over from a previous experiment

Each of the sources is investigated in more detail below.

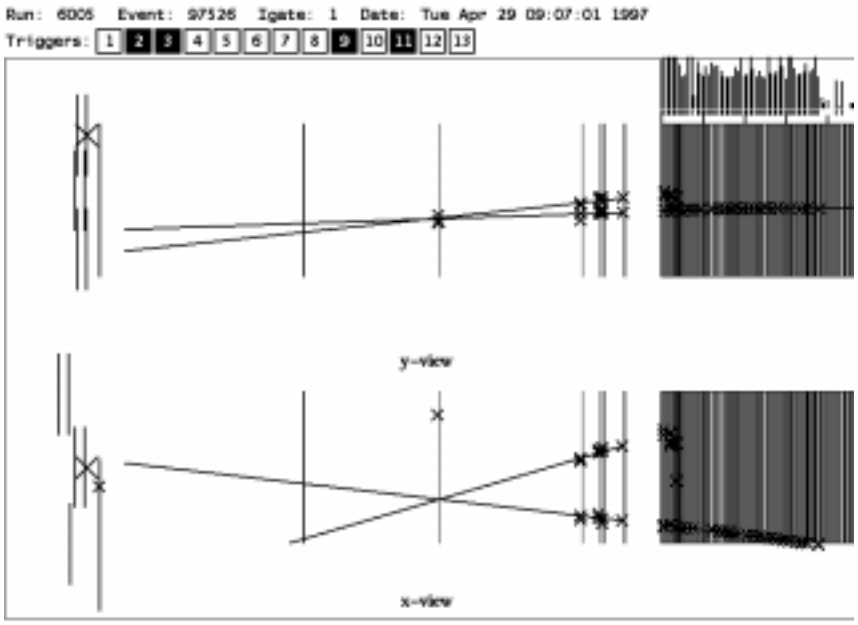

Figure 7.2: A neutrino event in the decay channel chamber DK4 that could be a background to the $\mu\pi$ NHL mode. Neutrino interaction produced a muon and a pion. A X-plane of the chamber is more downstream than a Y-plane.

7.3.1 Neutrino events in the chambers

The typical two-prong neutrino event in the chamber is shown in Figure 7.2. We expect 956 neutrino DIS events per drift chamber for the full run. To remove those events we required that any reconstructed vertex should be 40 inches (or $3\sigma_{\text{vertex}}$, whichever is bigger) away from a drift chamber. The error on the Z-vertex was sufficiently small (around 3 inches), so the 40 inch cut was reliable and conservative.

The chamber background to the NHL signal could come from events where the vertex was substantially mis-reconstructed. This could happen if the particle experienced a large multiple scattering or if it showered before the calorimeter, leading to excess hits which caused a mis-reconstructed vertex. The last case is the most probable due to the configuration of the decay channel, where the four chambers (DK1,DK2, DK3 and TG43) are grouped together and create a concentration of the material. In a $\mu\pi$ event, a π meson could decay and produce a muon track, which deviates and makes a mis-reconstructed vertex. If this happened a $\mu\pi$ event generated in a drift chamber would look like a $\mu\mu$ event reconstructed in the decay channel.

To estimate this background, 4×96828 MC events in the four decay channel chambers were generated. Each event was randomly placed at 10 different locations in the chamber, leading to 3.8 million chamber events. No events

passed the NHL cuts. Assuming 1±1 event, this set the background limit to $(1.0 \pm 1.0) \times 10^{-3}$.

7.3.2 DIS events in the floor

DIS neutrino interactions in the floor below the decay channel could be a background if:

- the Vertex was mis-reconstructed in the decay channel and
- the K_L escaped the floor and decayed producing a $\mu\pi$ vertex from the $K_L \to \pi_\mu \nu_\mu$ decay mode.

Both of these sources are modeled by the GEANT/LUND MC. To estimate this background DIS ν events were generated in the floor. The neutrino beam was lowered so that the center of the beam was at the floor level. This placed the highest intensity of the beam at the top of the floor in the center of the channel. The limit obtained via this MC is conservative because we are overestimating the rate of ν interactions in the floor.

The floor Monte Carlo was used to produce three sets of floor event samples with 24207 events each. Each event was randomly generated at 10 different positions in the floor (following the same technique as in the drift chamber background estimate) giving a total MC sample of $24207 \times 3 \times 10 = 726210$ events. None of the floor events passed the NHL cuts. Seeing zero events, we could assume the conservative estimate of 1±1 floor event mis-reconstructed in the decay channel for the above MC sample. The upper estimate on the probability of the misreconstruction is the $P_{\rm mis} = 1/726210 = (1.4 \pm 1.4) \times 10^{-6}$.

However we could get a more restrictive estimate on the floor DIS background if we use results from the previous studies of DIS events in the helium and in the NuTeV calorimeter. By scaling $N_{\rm CC}$, the number of neutrino charged current interactions observed in the NuTeV calorimeter, by the volume and density ratio we get the number of DIS ν events in the floor, $N_{\rm floor} = R_\rho \times R_V \times N_{\rm CC}$, where R_V is the ratio of the volume of the floor concrete where the MC events were generated to the volume of the calorimeter (1.0), and R_ρ is the ratio of the density of shielding concrete to iron (0.316).

The floor DIS background is the number of floor events that are mis-reconstructed in the decay channel and pass the NHL cuts:

$$N_{\rm floor}^{\rm bkg} = P_{\rm DIS} \times P_{\rm mis} \times N_{\rm floor}; \tag{7.1}$$

where $N_{\rm CC}$ is the number of charged current events in the calorimeter (2.47×10^6), $P_{\rm DIS}$ (3.1×10^{-3}) is the probability that DIS event in the decay channel would pass NHL cuts, $P_{\rm mis}$ (1.4×10^{-5}) is the probability that an event generated in the floor would be reconstructed in the decay channel. The probablility

$P_{\rm DIS}$ depended on the mode: for $\mu\pi$ mode it was 1.7×10^{-3}, 6.0×10^{-4} for μe and 8.0×10^{-4} for $\mu\mu$ mode. From this calculation, the limit on the floor DIS background comes to 0.0033 ± 0.0003 events, with 0.0018 ± 0.0002 events in $\mu\pi$ mode, $(6.0 \pm 1.0) \times 10^{-4}$ in μe and $(8.0 \pm 2.0) \times 10^{-4}$ in $\mu\mu$ mode.

7.3.3 DIS interactions in the Tohoku steel

The Tohoku steel was a remaining part of the steel magnet used in a previous experiment held in the same experimental hall, Lab F. It consisted of two steel pieces of the size of $182 \times 414 \times 584\ cm^3$. Steel parts associated with the Tohoku bubble chamber were situated about 10 feet from the beam center. Other parts that stick out in the beam direction were cut and removed before the NuTeV experiment began. Decay channel helium bags occupied the position in between those two pieces.

The background from neutrino interactions in the Tohoku steel was modeled in the Monte Carlo similarly to the ν floor background. The ν beam was shifted consequently to the left and to the right, placing the highest intensity near the decay channel border.

The calculation was done in the same manner. Each events was generated at 10 locations. The number of events in the calorimeter was multiplied by the probabilities of misreconstruction and ratios of volumes. Using the same formula as for the floor background: $N_{\rm floor} = P_{\rm DIS} \times P_{\rm mis} \times R_\rho \times R_V \times N_{\rm CC}$. The ratio of the volume of the Tohoku steel in which events were generated to the volume of the calorimeter was 0.37 and the ratio of density was 1. The calculation gives the Tohoku background estimate of 0.0038 ± 0.0003 events for the whole run, with 0.0021 ± 0.0002 events in $\mu\pi$ mode, $(8.0 \pm 1.0) \times 10^{-4}$ in μe and $(9.0 \pm 3.0) \times 10^{-4}$ in $\mu\mu$ mode.

7.4 Cosmic ray background

A typical cosmic ray entered the decay channel at large angles. Most of these events were then removed by requiring the angle < 0.1 rad. The events that entered at a small angle could have a hard bremsstrahlung or a delta ray, thus forming a false vertex. For the above reason, cosmic rays contributed to the background in this analysis.

An upper limit on the cosmic ray background could be obtained by looking at the sample of 3973 cosmic ray events with the NHL analysis cuts. The cosmic ray events were recorded during periods in between beam spills, when there was no accelerator beam present during "the cosmic ray gate". No cosmic ray events passed the NHL cuts. This allowed us to claim that the background from cosmics is less or equal to the ratio of the beam gate livetime to a cosmic

ray livetime:

$$\frac{\text{beam gate}}{\text{CR gate}} \simeq 1/2.5$$

To make a more restrictive estimate on the cosmic ray background, we assumed that the cosmic ray came in the decay channel at an angle < 0.1 rad and one of the following occurred:

- The muon scattered inelastically or
- A hard bremsstrahlung photon was produced (energy > 10 GeV) or
- A hard δ-ray was produced (energy > 10 GeV).

The number of events of this type was estimated using straight-through muons which interacted in the neutrino target-calorimeter. These events were required to reconstruct as muons with $\theta_{\text{beam}} < 0.01$, have at least 10 GeV deposited somewhere along the track, and occur within the cosmic gate (`IGATE=7`). In the 40% of the run which was examined, there were sixteen such events. The livetime of this sample was equal to the livetime for the NHL search. Scaling by the ratio of mass of the decay channel and calorimeter (1.1×10^{-3}), we found that we expected (0.035 ± 0.009) potential background events. This is before any reconstruction cuts are applied. It is a very conservative upper limit on cosmic ray background for the muonic decay mode search.

7.5 Summary of backgrounds

Table 7.2 shows the number of background events expected in $\mu\mu$, $\mu\pi$, $\mu\rho$ and μe modes for the decay channel run. Upper limits are indicated by the $<$ symbol. Total expected expected background is 0.57 ± 0.15 events.

Background Source	$\mu\mu$	μe	$\mu\pi$
DIS in the helium	0.05 ± 0.02	0.19 ± 0.03	0.32 ± 0.04
K^0 punch-through	$< (0.7 \pm 0.7) \times 10^{-4}$	$< (2.0 \pm 1.1) \times 10^{-3}$	$< (2.0 \pm 1.1) \times 10^{-3}$
DIS in the material	$(2.0 \pm 0.4) \times 10^{-3}$	$(2.7 \pm 0.4) \times 10^{-3}$	$(4.3 \pm 0.4) \times 10^{-3}$
cosmic rays	$< 0.1 \times 10^{-3}$	$< 0.1 \times 10^{-3}$	$< 0.1 \times 10^{-3}$

Table 7.2: Backgrounds to the NHL search.

Chapter 8

Systematic Uncertainties

In this search, no signal events were found and exclusion limits were set on the NHL mixing parameter and mass. Systematic uncertainties were composed from several sources listed below:

- D and D_s production cross section
- K meson production
- errors on drift chamber alignment
- resolution model
- reconstruction efficiency

Contribution of each individual source was calculated separately for the range of NHL masses (0.25-2.0 GeV/c^2) and then combined into an overall systematic error. The calculation was done by varying individual sources of errors and measuring the change in sensitivity. The summary of all systematics is presented in Table 8.1.

The result of the search is a 90% confidence level exclusion region in the 2-dimensional space of two parameters, the NHL mass and the mixing constant $|U|^2$. The NHL sensitivity was proportional to $|U|^4$ (one $|U|^2$ from NHL production and another $|U|^2$ from the NHL decay (see Eq. 2.40). To separate these two different components we first quote the systematic uncertainties on the sensitivity, $|U|^4$, and then we incorporate uncertainties into the overall error for the limit plot as described in the end of this chapter. Systematic uncertainties were in general small and for this analysis typically conservatively overestimated.

8.1 D and D_s production

The D and D_S cross section uncertainty was the biggest contribution to the NHL search systematics. They contributed in the allowed kinematic region of charm decaying into NHL with masses between 0.4 - 2.0 GeV/c^2. D production was modeled according to the heavy flavor cross section parameterization by *Frixione, et al* [55]. of the data from fixed-target experiments (E653 [53] , E769 [54]) and lower energy experiments (LEBC-EHS, LEBC-MPS, ACCMOR; see page 6 in Ref. [55]).

The experimental measurements for the $D\bar{D}$ production cross section in pN collisions at 800 GeV have a broad range, varying from the value of the $D\bar{D}$ pair cross section of $38\mu b$ measured by E653 [53] to the value of $8.8\mu b$ measured by E769 [54].

The systematic uncertainty was estimated by varying the D production cross section, $\sigma_{D\bar{D}}$, between $8.8\mu b$ and $38\mu b$ in the D-production MC and measuring the effect this change had on the NHL signal sensitivity. Systematic errors from D_s production and D production were estimated separately according to the empirical D-meson production parameterization [55]:

$$\frac{\sigma\left(D_s\right)}{\sigma\left(D^0+D^+\right)} \simeq 0.2; \tag{8.1}$$

The D_s cross section was varied from 1.8 μb to 7.6 μb [1].

The D production uncertainty effected the NHL sensitivity by $44.6 \pm 1\%$ and the D_S contribution was 5.6%. The overall systematic error of 50.2 % was consistent with the uncertainties in the *Frixione, et al* [55] parameterization uncertainties.

8.2 K production

Systematic uncertainty on K production contributed at the lower half of the NHL mass region (0.2-0.4 GeV/c^2). K production systematics came from the errors on the K flux model. The production of secondary kaons was modeled using the Turtle MC according to the production model from Ref. [43]. To get the good agreement with the data, the π production parameters of the model were varied. For instance, the ratio of K/pi was adjusted on the order of 2%.

The systematic error on the neutrino flux was based on the value of the discrepancy between the number of neutrino events predicted by MC and the number of ν events observed in data. As shown in Tables 6.4, 6.6 and 6.4, the disagreement between MC predictions and data were within 20%.

To get the systematic error on sensitivity, K production rates were varied by 20% in the NHL Monte Carlo. The change of 20.7% in the sensitivity was

[1] In Monte Carlo D mesons were simulated separately from D_s.

measured. Systematic errors on K and D production for different NHL masses are listed in Table 8.1

8.3 The alignment systematics

The systematic error associated with the chamber alignment was measured as the width of the residual distribution for each drift chamber. The residual is the difference between the hit position within the drift chamber cell and the projection of the track to the chamber. The residual distribution of a perfectly aligned chamber would show a very narrow peak at the origin.

There was a limit on how well we could align the drift chambers in the decay channel and tune the tracking. Alignment was limited by:

- The internal resolution of the chambers
- The chamber movements caused by the thermal expansion/contraction of helium bags.
- Multiple scattering in the chambers

Multiple scattering effects were small in the decay channel and included in the track reconstruction analysis. In principle, if not for the chamber movements during the run, the error on the alignment could have been comparable with the internal resolution of the chamber 11.5 mils or 0.029 cm. Chamber movements smeared the residuals as shown in Figure 8.1. On average the overall error was 1.5 times worse that the chamber resolution. The distribution was fit by a Gaussian distribution and the systematic error on the alignment was estimated as the sigma of this fit.

To get the value of the systematic uncertainty on the sensitivity ($|U|^4$ from Eq. 2.40) a GEANT MC was purposefully misaligned. The X_0 offset of the drift chamber cells was randomly smeared by a Gaussian with the mean value equal to X_0 and with the sigma of twice the alignment resolution $2 \times 15 = 30$ mils. The X_0 offset was stored in the chamber positions spec files, which were temporarily modified for this study. Files generated by the NHL MC were reconstructed with unmodified spec files and the change in the sensitivity was measured. The effect was small and depended on the mass of the generated NHL, varying from 0.02% at $m_{\rm NHL} = 1.15 GeV/c^2$ to 1.0% at 0.55 GeV/c^2. NHL events with the high transverse mass ($> 1 GeV/c^2$) were characterized by high energy tracks with large opening angle. As a result, the vertex reconstruction was excellent, because it was harder to confuse the tracking by misalignment. At low NHL mass, the misalignment effects were still small of order 1%. Alignment systematics is listed in the summary of this section.

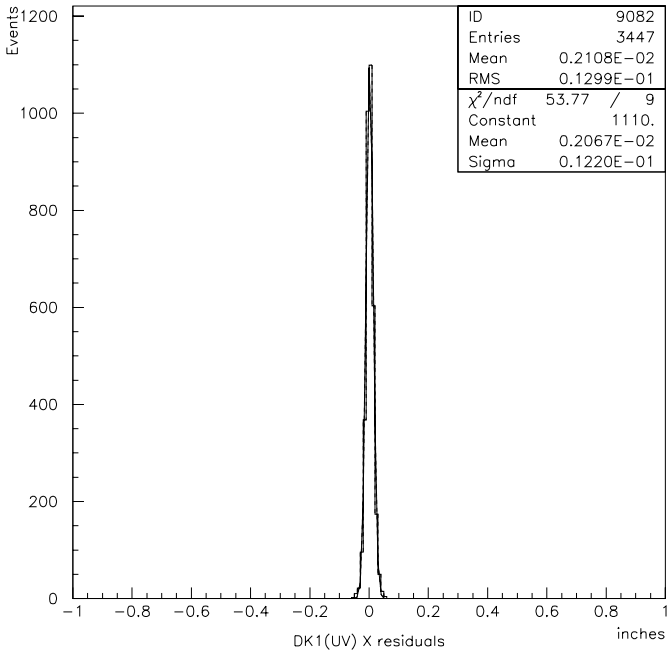

Figure 8.1: Residual distribution for the DK1(UV) drift chamber fitted with Gaussian.

8.4 Resolution Model Uncertainty

This uncertainty depended on how well we model the drift chamber resolution in our MC. The GEANT MC used 15.7 mils or 0.04 cm for the chamber resolution. The drift time of the chamber was smeared as

$$time = time + resol \times \frac{gauss(0,1)}{V_{\rm drift}},$$

where $V_{\rm drift} = 8.25$ mils/4ns (5.2×10^4 m/s) is the drift velocity, gauss(0,1) is the Gaussian distribution with the mean of 0 and sigma of 1 and $resol = 0.04cm$ is the resolution.

The systematic error was measured as the shift in the sensitivity when we varied the resolution from 0.02 cm (1/2 of its original value) to 0.08 cm. For the same reason as for the alignment, resolution systematics affect mostly the low NHL masses, where the opening angles are small and the vertexing error is larger. At large masses the resolution effects disappear. The numbers for the resolution uncertainty are given in Table 8.1 below.

8.5 Chamber Noise Modeling

The efficiency for NHL vertex reconstruction depended on the alignment, drift chamber resolution and the drift chamber noise modeling. Alignment and resolution effects were discussed above. Drift chamber noise includes electronic noise and extra hits from cosmic rays and out-of-time tracks. Chamber noise was determined from events triggered by the downstream end of Lab E neutrino target. These chamber noise events were written to noise files and merged with the files generated by signal or background MC simulations. The error on effects of noise in the reconstruction efficiency was determined by how well we modeled the drift chamber noise.

For the noise study, we took a very conservative approach. The error on the noise model was assumed to be equal to the total effect of adding the noise itself. We estimated the error on the reconstruction efficiency as the difference in sensitivity with and without noise. The change in sensitivity was measured to be about 17%. The reconstruction efficiency systematics has to vary depending on the NHL mass, however for transverse mass, m_T, from 0.2 to 2 GeV the systematics could not be larger than 17%. A 17% error independent of the transverse mass was assumed.

Table 8.1: Systematic uncertainties on the sensitivity of the NHL search.

	NHL mass (GeV/c^2)		
Source	0.38	0.85	1.45
D production	-	44.6%	44.0%
K production	20.7%	-	-
D_S production	-	5.6%	5.4%
alignment	1.0%	0.4%	0.02%
resolution model	9.3%	7.0%	0.8%
chamber noise	17.0%	19.1%	17.0%
TOTAL SYST.	28.4%	49.3%	47.5%

8.6 Summary of the systematics on the NHL sensitivity, and incorporating systematic uncertainties into the 90% confidence limit

Table 8.1 summarizes the final systematic uncertainty for the NHL search sensitivity. The systematic uncertainties were incorporated into the 90% confidence level limit by adding in quadrature a fractional term corresponding to the uncertainty for a given mass.

The 90% confidence level limit for a given mass for the null observation was calculated by finding the $|U|^2$ value for each mass such that $N_{\rm pass}(m_{\rm NHL}) = n_0$

events, where $n_0 = 2.3$ is the Poisson limit for 0 observed events in the absence of background, and $N_{\rm pass}(m_{\rm NHL})$ is the number of MC events that pass the NHL cuts; this number is a function of a NHL mass and mode. In this analysis, the NHL MC generated events with some fixed value of $|U_0|^2$ (5×10^{-8}). The value of $|U|^2$ was adjusted according to Eq. 8.2:

$$|U|^4 = |U_0|^4 \frac{n_0}{N^{MC}_{\rm pass}}. \tag{8.2}$$

This procedure will change when systematic errors are included. In Eq. 8.2, the value of denominator $N^{MC}_{\rm pass}$ would be different in the presence of systematic errors, and the Poisson limit of $n_0 = 2.3$ events would be modified by the addition of systematics, which could be estimated as

$$n_0' = n_0 \times \sqrt{1 + \left(\sum \frac{\delta a}{a}\right)^2}, \tag{8.3}$$

where $\sum \frac{\delta a}{a}$ is the sum of the fractional errors from all sources of systematic errors. However, the above equation is an approximation that works well only if a fractional systematic error in Eq. 8.3 is small. In this analysis the fractional errors on the NHL sensitivity were 49% for NHLs of mass 1.45 GeV/c^2 and 15% for NHLs of mass 0.35 GeV/c^2, which was not small.

A more precise way to incorporate systematic errors is through the the use of Monte Carlo simulations. We form a Poisson distribution with a mean of 1 to describe the event observation probability and then include the systematic uncertainties in deriving the $|U|^2$ limit. The value of $N^{MC}_{\rm pass}$ in Eq. 8.2 becomes a Gaussian distribution due to inclusion of systematic errors, and the 90% confidence limit is no longer $n_0 = 2.3$ events. To find the new value of n_0, we formed the ratio $\frac{P(1)}{gauss(1,\sigma)}$ for a number of MC generated events, where a value for the numerator is generated from the Poisson distribution and the value for the denominator is chosen from the Gaussian distribution. The ratios are stored in a histogram as shown on Fig. 8.2. The new value of n_0 that corresponds to 90% confidence level has to be such that the area in the ratio histogram to the left of n_0 equals to 0.9:

$$N(n_0)/N_{\rm tot} = 0.9, \tag{8.4}$$

where $N(n_0) = \int_{n<n_0} \frac{P(1)}{gauss(1,\sigma)}$, $N_{\rm tot} = \int_{tot} \frac{P(1)}{gauss(1,\sigma)}$, and σ is the systematic error, which depends on the NHL mass.

In the absence of systematic uncertainties, the $|U|^2$ limit would be simply related to the event limit through the $|U|^4$ scaling relation in Eq. 8.2. As systematic errors approach zero, Eq. 8.4 turns into a Poisson distribution and $n_0 \to 2.3$.

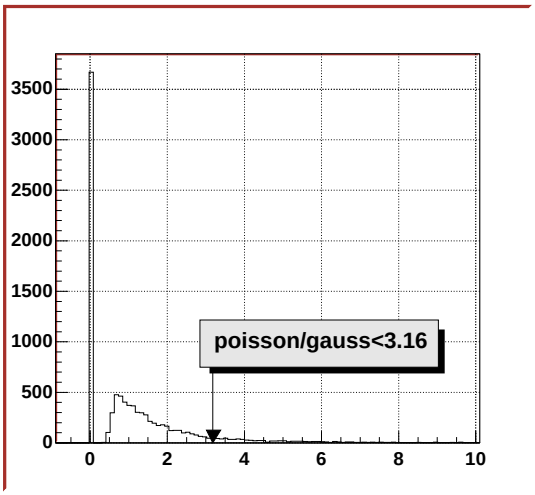

Figure 8.2: The Poisson distribution with mean of 1 convoluted with a Gaussian distribution with mean of 1.0 and sigma corresponding to the systematic error for a of 1.45 GeV/c^2 NHL produced via D-meson decays. For this mass, the fractional systematic error is 48%.

The calculated values of n_0 depended on the systematic errors, which varied greatly with mass. The systematic uncertainty on the number of produced NHLs of mass 1.45 GeV/c^2 was 49% and the corresponding n_0 was 3.16. For NHLs of mass 0.35 GeV/c^2 the uncertainty was 15% and n_0 was 2.42 . Adding the systematics uncertainties increased the $|U|^2$ limit by 4%(14%) at 0.35(1.45 GeV/c^2) GeV/c^2. The systematics was included into the final limit plot.

Chapter 9

NHL search results

In this search, we assumed a light muon neutrino mixing with a heavy isosinglet neutral heavy lepton and looked for heavy neutrino decays in the decay channel apparatus. Analyzed events were identified as NHL decays if they passed the analysis cuts described in Chapter 6. Events were required to have two outgoing tracks with a common vertex in the decay channel fiducial volume, with one track identified as a muon. In the full NuTeV data sample, no events passed NHL cuts. This is consistent with the expected background of 0.57 ± 0.15 events.

We have set 90% confidence limits on the NHL decays from this null result. The number of observed heavy leptons depends on mixing $|U|^2$ and NHL mass in Eq. 2.40. The mass and mixing limits were calculated using the method described by Gronau, Leung and Rosner (GLR) [42]. Using the NHL MC code we predicted the value of $N_{\rm pred}(m_{\rm NHL}, |U|^2)$, the number of NHL events expected in the decay channel, as a function of $m_{\rm NHL}$ mass and $|U|^2$. NHL Monte Carlo samples were generated for eleven values of $m_{\rm NHL}$ (in GeV):

$$0.15, 0.25, 0.35, 0.38, 0.55, 0.85, 1.15, 1.45, 1.75, 1.85, 1.87;$$

Each generated NHL event was assigned a weight corresponding to the probability of NHL production and decay in the decay channel. The NHL weight was normalized to the number of protons received on target during the 1996-1997 run in the positive or negative focusing. Initially, the $|U_0|^2$ value was set to the 5×10^{-8}. The 90% confidence level limit at a given mass was calculated for the null observation by finding the $|U|^2$ value for each mass such that $N_{\rm pass}(m_{\rm NHL}, |U|^2) = n_0$ events, where n_0 corresponds to the 90% limit for Poisson distribution, that is zero could fluctuate to n_0 with 10% probablility. In the absence of systematic errors, $n_0 = 2.3$. However in this analysis, the systematic errors were included and the value of $n_0 > 2.3$ was calculated from the MC simulation of the Poisson distribution convoluted with Gaussian (see Sec. 8.6).

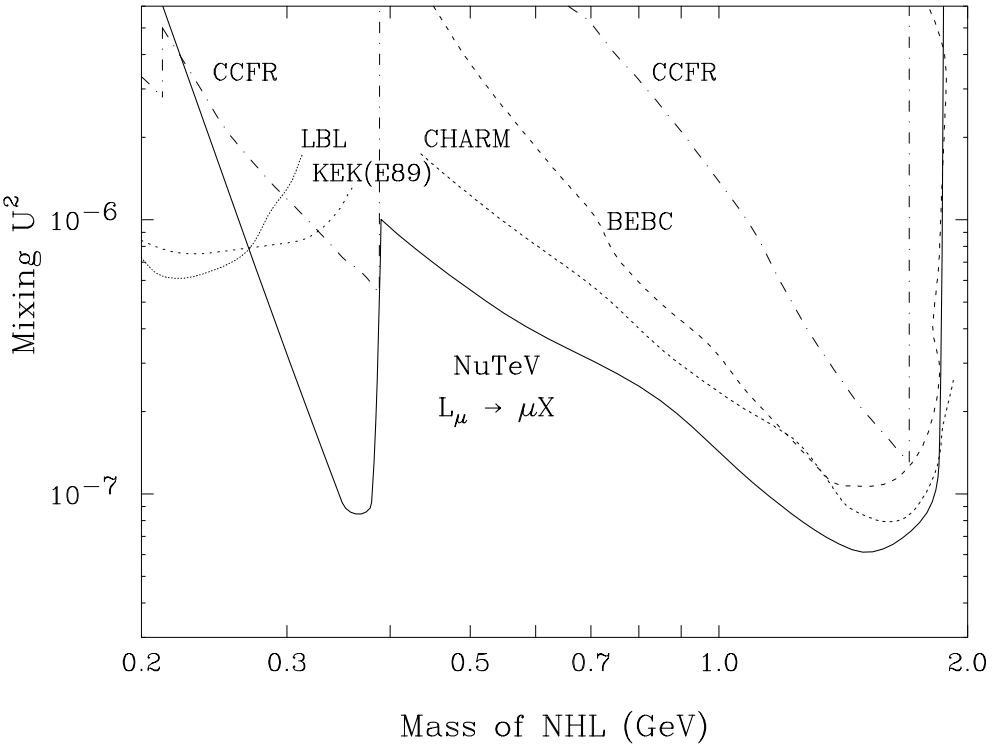

Figure 9.1: NuTeV 90% confidence limit on U_μ^2, the mixing of NHLs to Standard Model left-handed muon neutrinos, as a function of NHL mass. The solid line in the figure corresponds to the limit with systematic errors included.

Given $N_{\rm pass}^{MC}$ Monte Carlo events that pass NHL cuts, $|U|^2$ was adjusted according to:

$$|U|^2 = |U_0|^2 \sqrt{\frac{2.3}{N_{\rm pass}^{MC}}},$$

where$|U_0|^2 = 5 \times 10^{-8}$. There were eleven values of $|U|^2$ corresponding to the 90% confidence limit for each of the eleven generated NHL masses. The exclusion plot was obtained by drawing a smooth curve in the $|U|^2$ and $m_{\rm NHL}$ two-parameter space through these eleven points. The 90% confidence limit is shown in Figure. 9.1 along with the previous limits described in Chapter 1.

9.1 Summary and Conclusions

We have performed a search for NHLs that mix with muon neutrinos with transverse mass ranging from 0.25 to 2.0 GeV. No evidence for NHLs was observed. The limits that have been set are as much as an order of magnitude better than previous searches in the lower mass range, and are the strictest

limits on the NHL mixing parameter yet. The limits are presented in Figure 9.1.

The NHL mass range reported in this thesis will be extended in the future by the NuTeV collaboration to NHLs with masses above 2.0 GeV and below 0.25 GeV. The search in the lower NHL mass region is in the range of the KARMEN timing anomaly [23] (33.9MeV). This search has found no NHLs in this mass region and excluded part of the KARMEN allowed region [62]. The high transverse mass analysis is also under way. High mass NHLs might be produced in B decays or from neutrino interactions in the shielding upstream of the decay channel/veto wall ("berm"). Preliminary calculations indicate that none of these sources could produce a NHL that we would have sensitivity to detect. Another possibility is that the events with high transverse mass could be Super Symmetry neutralinos. There may be some regions of SUSY parameter-space that are not ruled out by collider experiments and that could be probed by the NuTeV experiment.

A new neutrino oscillation experiment, BooNE (E898), has been approved as a part of the Fermilab neutrino program after the year 2000. Besides the primary goals, such as confirming or denying the LSND signal [4], BooNE could also detect NHL decays. Because of the relatively low energies involved, the NHLs would be produced primarily from pions and the new search will be sensitive to low-mass NHL production.

Appendix A

The alignment and performance of the detector.

The quality of this analysis greatly depended on how well the decay channel detector and veto wall performed. The outline of this chapter is as follows:

- The alignment
- The veto wall efficiency
- The drift chamber efficiency

A.1 The alignment

The alignment is a procedure for tuning the tracking system's ability to reconstruct straight lines. More precisely, the alignment is a procedure for measurement and correction of wire positions, timing offsets and electron drift velocity of the particular drift chambers.

After alignment, the resolution, average over the decay channel chambers was 15 mils (1/1000 of an inch). It was 3-4 times better than resolution in the calorimeter chambers, which had a much larger contribution from multiple scattering.

A.1.1 The selection of muon candidates

The alignment was done on the sample of "trigger 6" single high energy muons. The muon path was approximated as a straight line assuming that there were no significant magnetic fields in the decay channel. The "trigger" muons came with the neutrino beam and illuminated all 24 cells of the decay channel chambers more or less uniformly. Muons having energies greater than 50 GeV as measured in the toroid spectrometer were selected for the alignment.

The tracks used in the decay channel alignment were found by the decay channel tracking. To align the decay channel to the NuTeV calorimeter, the tracks found by the calorimeter tracking were used. The requirements used in the selection of muon candidates for the alignment were:

- The neutrino (fast) gate is on
- Trigger 6 or 1 or 3
- There is only one track in each view in the calorimeter
- There is only one track in each view in the decay channel
- The energy E_μ of the muon is measured and $50 < E_\mu < 300$ GeV

A.1.2 The alignment algorithm and residual histograms

The alignment algorithms used "residual" histograms. The "residual" (defined in Eq. A.2) of a drift chamber is the difference between the position of the hit measured by a particular drift chamber and the projection of the track averaged over all cells in this drift chamber. The bigger this difference, the bigger the misalignment of the chamber. In the alignment procedure, the residuals were stored in "residual histograms". The alignment procedure adjusted the chamber parameters in order to minimize the residuals.

Drift chambers measured the drift time of the ionization from the particles. To reconstruct the position of the hit one had to know an average drift velocity of electrons and two more parameters: time offset and position of the wire. The position of the hit X is

$$X = X_0 \pm V_0 \times (T - T_0), \tag{A.1}$$

where T is a measured time, T_0 is the time offset, V_0 is the drift velocity, X_0 is the position of the wire, and plus or minus in the above equation depends on the side of the cell a particle traversed and left a hit. In case of the hit was on the positive side, Eq. A.1 a has plus sign, and it's the sum of X_0 and V_0. In case of the negative sign, it is other way around. In the reconstruction code, the notation $X0, T0, V0$ was used instead of X_0, T_0, V_0.

Drift chambers were staggered and the position of the first wire, X_0, was slightly different for every chamber. X_0 was measured by an optical survey. The time offset T_0 depended on the length of the signal cables and was also different for every chamber.

Let's introduce misalignment into Eq. A.1. The new misaligned hit will be $\tilde{X}$. X is the real position of the hit, which would be measured by a perfectly aligned chamber with perfect resolution. We approximated the perfectly aligned X by projecting the track onto the chamber being aligned. Even

though the projection may not coincide with the real position X due to misalignment and resolution, it is our best guess, and in an iterative process, it eventually converges to X. The residual, which is the difference between the hit and the track projection is

$$X - \tilde{X} = X_0 \pm V_0 \times (T - T_0) - (\tilde{X}_0 \pm \tilde{V}_0 \times (\tilde{T} - \tilde{T}_0), \tag{A.2}$$

where $\tilde{X}$ is the measured position of the hit and X is the track projection. Again, plus or minux in the above equation depended on the side of the cell a passing particle traversed.

The residual histogram for the perfectly aligned chamber should resemble a narrow peak at the origin. As the alignment of the chamber gets worse, the residual peak turns into a Gaussian-like distribution. The wider distribution, the worse the alignment. Resulting residual distributions for aligned decay channel drift chambers are shown in Figure A.1

Plain residual histograms contained information only about the difference $X - \tilde{X}$, whereas in order to do the alignment one needs to tune X_0, T_0 and V_0 parameters. We used two-dimensional profilehistograms called "residuals across the cell" to fit for the values of three alignment constants. The histograms of "residuals across the cell" were made by averaging the residuals in all cells of a drift chamber in a single view and plotting against the position inside the cell. The histogram of residuals across the cell of a perfectly aligned chamber would look like a horizontal line going through the origin. Misalignment in X_0 would shift the line vertically up or down, in V_0 would introduce a slope, and in T_0 would split the line in two. This behavior follows Eq. A.2. A typical residual histogram is shown in Figure A.2. The residual distribution was fit to one line on the positive and another line on the negative side of the cell. The two lines were constrained to have the same slope and different offsets. The fit had three parameters: the slope, positive offset, and negative offset. The fit results were used to calculate new alignment parameters for the chambers, minimizing the residuals.

The values of X_0, T_0 and V_0 depended on the three parameters of the fit: the slope, overall offset above the horizontal axis, and the difference in offsets between positive and negative sides of the cell. Using a new set of parameters one could recalculate a new position of the hit X by finding the minimum of the residual, $X - \tilde{X}$. The alignment procedure is iterative:

1. fit a line through a single muon track
2. fill the residual histograms for every chamber
3. calculate a set of alignment constants which minimizes the residual
4. repeat

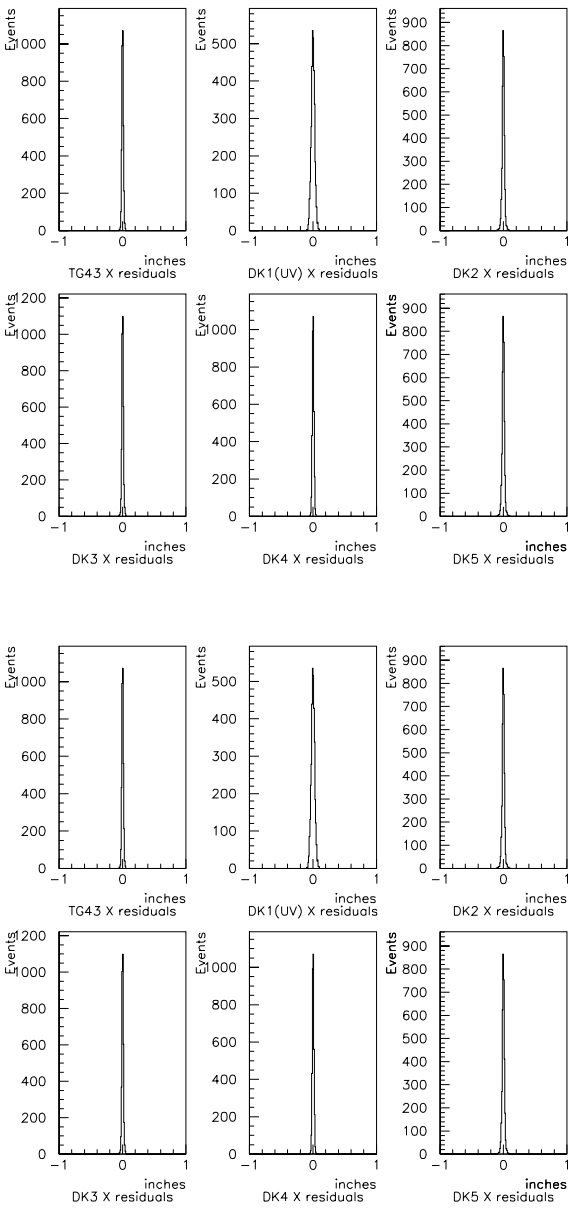

Figure A.1: Plain residual histograms of decay channel chambers.

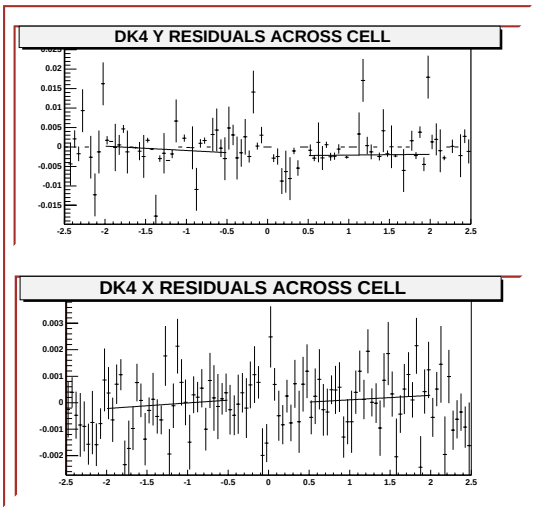

Figure A.2: Residual histogram across the cell of the decay channel chamber. The slope, difference in offsets and overall offset provided information about the alignment constants X_0, T_0 and V_0.

Table A.1: The alignment periods marked the movements of the chamber TG43 (DOC) during the run.

Run Periods	Doc centered	moved 18" east	9" east	Centered
run number	0 – 5652	5653 – 5707	5708 –5947	5948 – end
tape numb.	0 – 319	320 – 338	339 – 475	476 – end

The alignment code can be found in the NHL analysis software package in the subdirectory "*alignment*": "*e815_analysis/nhldk/alignment*" [63].

A.1.3 Alignment results

Running on 130 000 "trigger 6" muons over six time periods, which marked the major changes in the hardware of the detector (mainly due to the movements of chamber TG43), produces alignment constants for the periods shown in Table A.1. During the alignment we found a hardware mishap with chamber TG43 and modified the software procedure to correct for the problem. Chamber TG43 had signal cables of significantly different lengths which caused an unexpected offset of the signal propagation time. As a result, chamber TG43 could not be aligned with the standard alignment algorithm. This was fixed in the software. The fact that we saw the error in the hardware and were able to correct it in the software gives confidence to the alignment procedure. An

average over all 6 DK channel chambers sigma of a Gaussian fit to a plain residual histogram was of order 0.038 cm or 15 ± 3 mils, where mil is $\frac{1}{1000}$ of an inch.

The above number was much less than the average residual of the calorimeter, where the multiple scattering effects in the calorimeter iron were significantly larger.

After the internal alignment of the decay channel drift chambers we checked the alignment of the decay channel to the NuTeV calorimeter as a whole. The alignment of the decay channel to the calorimeter is shown in Figure A.3 The

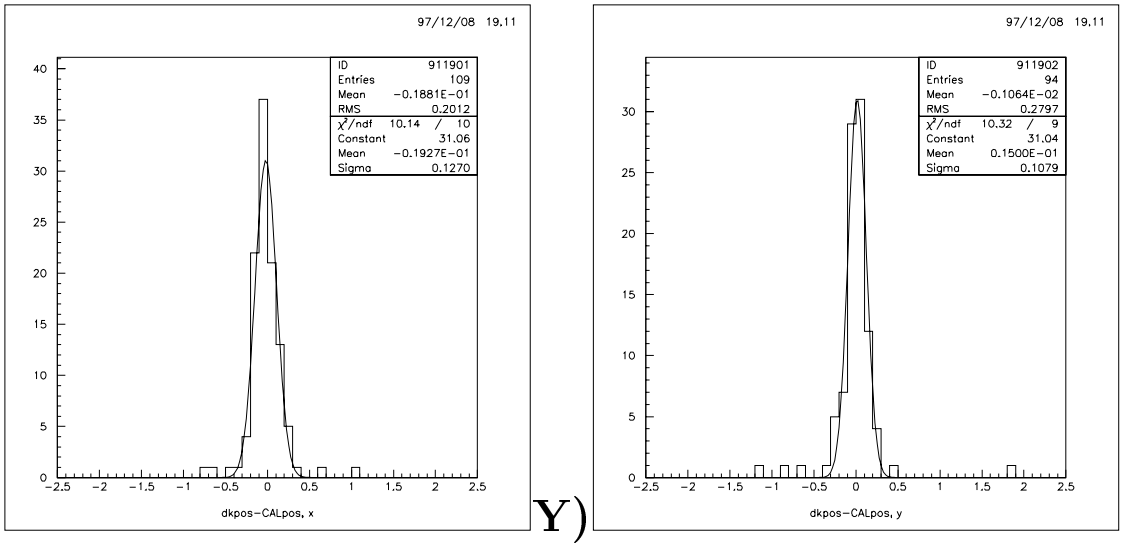

Figure A.3: Difference between the track projected from the calorimeter and the track from the decay channel in **X**) and **Y**) views.

difference between projections was of order of .12 inches. It was mainly due to an error in the calorimeter alignment which was large because of the multiple scattering in the calorimeter steel. This multiple scattering was about 10 times bigger than the DK channel internal resolution and was taken as the maximum distance to seek the hit on the track $DIFMIN$ (see Chapter6).

Residuals for every chamber were fit to a Gaussian distribution, with the average χ^2/DOF in the range 1-2. The alignment resolution was taken as a sigma in the Gaussian fit. The residual means and alignment resolutions (residual sigmas) after the last iteration are presented in Figure A.4 for all 4 alignment periods.

The alignment resolutions were averaged over the 4 alignment periods and presented in Table A.2

The resolutions averaged over all chambers were 14.6 mils in X view and 15.4 mils in Y view. Alignment resolution had contributions from multiple scattering and from the internal resolution of the drift chamber. To estimate

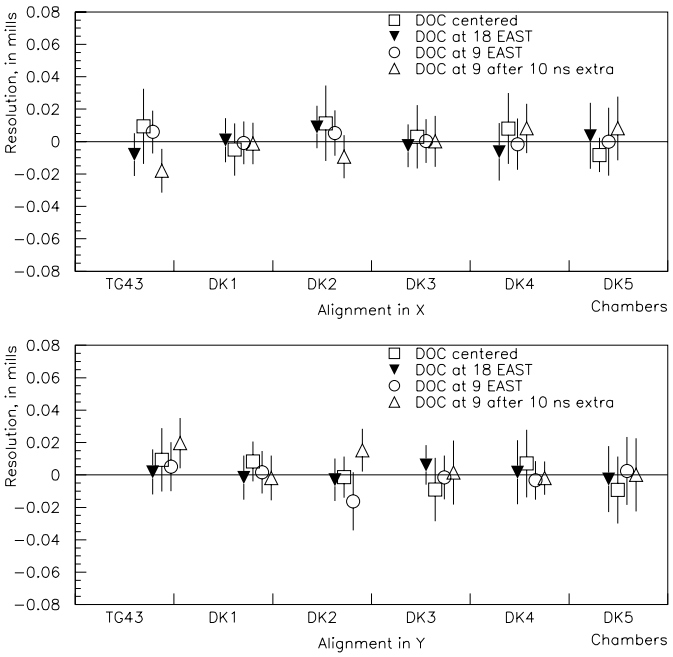

Figure A.4: Residual means and resolutions are presented for 4 alignment periods. The means and resolutions are shown in mils (1/1000 of an inch).

the internal resolution of a drift chamber, we did a weighted fit to the reconstructed straight line. Due to the multiple scattering, weights in the drift chamber were assigned to every hit. A free parameter was used for the internal resolution of the chambers. Results of this fit indicate that the internal resolution of the decay channel drift chamber is 11.5 mils.

Alignment constants were incorporated into the NuTeV analysis spec files [63].

A.2 Drift chamber efficiencies measurements.

During the run some of the cells in the decay channel drift chambers were partially or fully inefficient for some period of time. The chamber cells were called "dead" if they were totally inefficient or turned off. Dead or partially efficient cells were fixed and drift chambers replaced as soon as possible.

One of the causes for the inefficiency was that during the run drift chambers were exposed to mechanical deformations. This was especially true for chambers in the decay channel placed between the helium bags. The pressure exerted on the chamber by the helium bag could change drastically due to changes in the atmospheric temperature. The helium gas flow was controlled

Chamber	X	Y
TG43	11.9	13.8
DK1	11.6	13.6
DK2	11.9	13.9
DK3	12.9	13.1
DK4	15.4	15.1
DK5	23.6	23.1

Table A.2: Individual resolutions of drift chambers in X (2nd column) and Y (3rd column) planes in mils (1/1000 of an inch).

and monitored, but rapid changes in temperature could not be controlled due to the vast volume of Helium in the plastic bags. The significant change in temperature (by more than 20 degrees in F.) could cause the chambers to have high voltage trips. The chamber had to be brought back on, but this procedure could result in disconnected or dead cells, thus increasing the inefficiency of the chamber. This inefficiency had to be studied and modeled in the Monte Carlo.

The signal from each cell of every drift chamber was recorded in the course of the run into a set of occupancy histograms. There were two occupancy histograms per chamber, one for each view. Each occupancy histogram had 24 bins corresponding to 24 drift chamber cells. Figure A.5 shows the occupancy of the calorimeter chambers versus decay channel chambers. The histogram on the lower half of the figure has an inefficient cell.

By storing integrated occupancies for the whole run period one could notice inefficient cells as dips in the distribution. The relative level of inefficiencies for the cell k_i in the particular drift chamber was determined by taking the ratio of the content in the bin i in the occupancy histogram to the content of fully efficient cell i: $k_i = \frac{N_i^{data}}{N_i^{eff}}$. The content of the fully efficient cell was determined from the parameterization of the histogram by a polynomial of the 4th order. A polynomial as a fit parameterization yielded smaller χ^2 values than other functions (Gaussian, exponent etc.). The χ^2/DOF of the fit with polynomials of 3rd and 5th order was larger than the χ^2/DOF of the 4th order polynomial, still being large chi^2/DOF ≈ 8. Thus one can determine the relative level of inefficiency. If the whole chamber was turned off it would not be reflected in the occupancy histograms. The absolute level of inefficiency was determined by comparing the occupancy histograms to a chamber that was fully efficient during the run, DK1. There was no significant down time that would make the number of entries in occupancy histograms significantly different from DK1. Also written records from the drift chamber log book [38] were used. Note

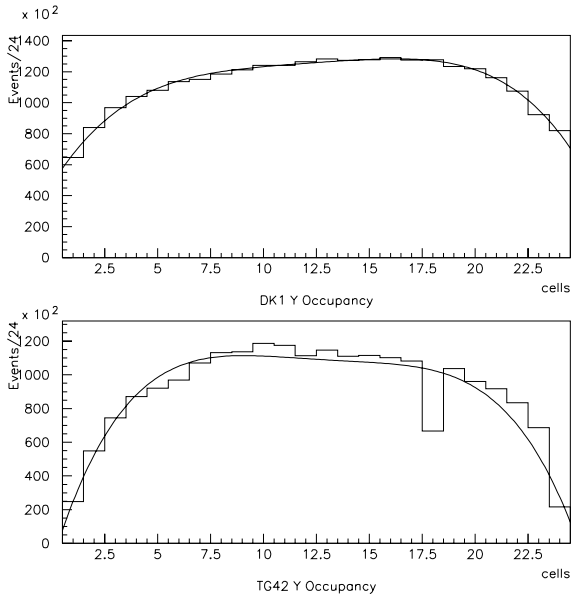

Figure A.5: Example of the occupancy histograms parameterized with the 4th order polynomial. The histogram below had a cell 18 inefficient, which shows as a dip in the occupancy distribution. The level of inefficiency was determined as the ratio of the content of 18th bin to the value of the polynomial at this bin.

that a more common procedure of using tracking to find the efficiency was not possible due to the small number of the drift chambers in the decay channel. Also this procedure is not affected by the tracking efficiency.

The described above procedure worked in the absence of noisy cells. If for some period of time a cell was inefficient and for some other period it was noisy, the two effects could cancel each other. The only way to separate two effects was to divide the run into the smaller portions and measure inefficiencies for every portion separately and combine them later. I formed occupancy histograms by running on the sample of trigger 6s, straight-through muons that illuminated all 24 cells of the drift chambers. There were 7 files of approximately the same size. The measured efficiencies were weighted, with weights proportional to the number of events in the sample and combined together $k_{tot} = \frac{\sum(k_j * N_j)}{N}$, where k_j is the efficiency for the part of the run j, N is the total number of events and N_j is the number of events in the jth part of the run.

Inefficient cells were simulated in the signal/background Monte Carlo. The routine in the DIS Monte Carlo ("*McNuTeV/deadcell.f*") called an analysis routine hot_dead.c in the "*e815_analysis/nhldk/hot_dead.c*" [63], which read

a data file with the list of the inefficient cells. The inefficient cell in the MC simulation randomly produced a hit with the probability equal to its efficiency. If the efficiency is 0 it is the dead cell. There was no simulation of the correlated cells, for example cells that were off simultaneously when the portion of the chamber was off.

Figure A.6 represents drift chamber cells inefficiencies for X- and Y-views.

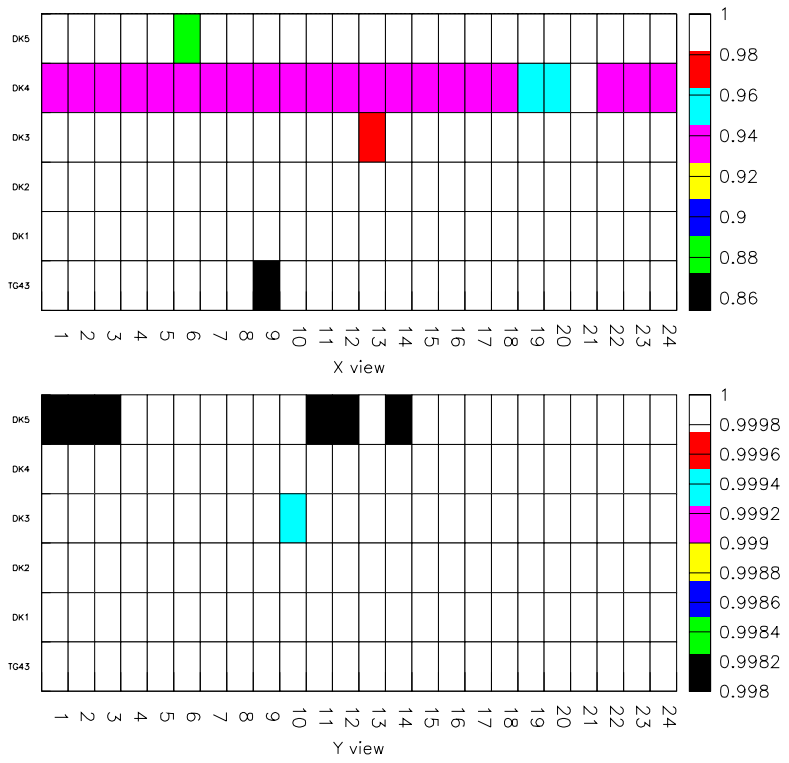

Figure A.6: Drift chamber inefficiencies. Drift chambers are on the Y-axis, cell number is on the X-axis. Inefficiencies are shown in the darker color.

The overall decay channel inefficiency due to the dead and inefficient cells was $3.3 \pm 0.1\%$. One decay channel chamber, DK1, was efficient and did not have any dead cells, according to the occupancy histograms. However there was an additional overall inefficiency of 2% due to the structure of the drift chambers, which has a dead region near the aluminum I-beams.

A.3 Lab F veto wall efficiency measurements

The efficiency of the veto wall scintillator was measured before and after the 1996-97 fixed-target run.

Before the run two scintillation counters were randomly selected among 19 veto wall counters. Each of the two counters have been placed horizontally on the test setup table. They were connected to the test readout electronics. Two small scintillator paddles were placed just above and below the central region of the counter and leveled. Cosmic rays induced the light in the scintillator in the paddles. The signal from the scintillators was read out by LeCroy logical fan-in modules and put into coincidence. The measurements of the counter efficiency were based on the rate of coincidences. The efficiency f_i of the chosen counter i was the ratio of the number of times the given scintillating counter fired in coincidence with paddles, N_i^{scint}, to the number of coincident signals from the paddles, $N^{coinsid}$: $f_i = \frac{N_i^{scint}}{N^{coinsid}}$. The measurement gave 99.96% efficiency as an average of all the counters.

After the run the counter efficiencies were measured in the offline analysis. Measurements were based on the sample of trigger 6s collected throughout the run. Trigger 6s were straight through muons produced in the neutrino interactions in the berm upstream of the detector. The trigger required a veto signal and the muon penetrating the calorimeter. Berm muons came in a wide beam illuminating every counter in veto wall with the beam centered on the counters 9 and 10 in the middle of LabF veto wall. It was called the veto wall X-ray.

X-ray muons left hits in the downstream decay channel drift chambers. The tracking software reconstructed decay channel tracks. Those tracks were projected back to the veto wall counters and used in the veto wall efficiency measurements. If the track projection was within the counter boundaries, the scintillator in the counter should fire. The positions of all counters were measured. The positions of counters 5, 7, 9, 13 and 15 have been measured by the Fermilab optical survey team. The efficiency of a scintillation counter was measured as the ratio of events, when the scintillator fired and track projected to it, to events with the decay channel track projected into the scintillation counter, $f_i = \frac{N_i^{fired}}{N_i^{proj}}$.

Multiple scattering in the drift chambers would smear the projection of the muon track and would smear edges of the X-ray image of the counter. To take into account edge effects the track was projected only to the central part 10" away from the edge of the counter. This are was called active area. The assumption was that the efficiency of the veto wall is close to the efficiency of the scintillator. The measured counter efficiencies are shown in the Table A.3 below:

Errors on the efficiencies were calculated statistically. The number of events

counters	efficiency in %	error in %
1	99.39	± 0.0060
2	99.39	± 0.0061
3	> 99.78	± 0.0022
4	> 99.77	± 0.0023
5	> 99.67	± 0.0033
6	> 99.67	± 0.0033
7	99.85	± 0.0009
8	99.90	± 0.0007
9	99.90	± 0.0005
10	99.88	± 0.0005
11	99.91	± 0.0006
12	99.91	± 0.0006
13	> 99.37	± 0.0063
14	> 99.38	± 0.0063
15	> 99.76	± 0.0024
16	> 99.76	± 0.0024
17 18 19	> 99.83	± 0.0017

Table A.3: Efficiencies of the Lab F Veto Wall scintillator measured on the sample of straight-through muons. Errors were calculated assuming Gaussian distribution of the events that went into the sample. Lower limits are indicated by the < symbol (counter 3-4 and 13-19).

that failed to fire a scintillation counter was small and we assumed Poisson distribution. For some of the counters only the lower limit on the efficiency was measured. In this case the error quoted on the limit was the variance of the Poisson distribution with mean 1. The statistical errors of the ratios are presented in Table A.3.

The overall efficiency of the veto wall was measured separately. Decay channel tracks were projected into the area of the whole veto wall array, rather than to individual counters. Efficiency of the LabF veto wall was (99.94 ± 0.01)%.

A.4 Study of the Lab F veto wall noise.

The noise in the veto wall was studied and cuts were developed that significantly reduced the noise. This section reports on this study (details are in Ref. [57]). One of the NHL analysis cuts, the LFBIT cut, was based on the veto wall rejection of charged particles. Efficiency of this cut depended on the

veto wall performance. In principal, the noise in the veto wall counters could fire the veto wall without an actual veto caused by a charged particle, thus unnecessarily rejecting a potentially interesting event. We would call the rate of veto wall misfiring an "overkill". The study of the relative cut efficiencies for the NHL data indicated that the veto wall cut was eliminating up to 15% of the data sample. It was desirable to refine the veto wall cut with the goal of increasing the size of the data sample.

For the purpose of this study, a sample of events containing only noise in the veto wall was extracted under the assumption that, none of the noise events had any real veto wall hits. A data file was produced from a set of neutral current events (Trigger 2), for which the hadron shower occurred in either the last, or next–to–last downstream cart of the NuTeV detector. In this way, any signals associated with the Lab F veto wall may be interpreted as noise in the counters. This noise data were then overlayed on a sample of McNuTeV events having a short muon track with a hit near $x = 0$ and a large y–slope. This noise file contained 24207 events. During the study three characteristics were recorded: the number of hits recorded during each event, the starting time of each TDC pulse, and the width of the pulse.

Based on this sample of the noise events the rate of the veto overkill was measured to be around 15%. It was too high, and one of the purposes of this study was to find a cut that would improve the performance of the veto wall and reduce the veto overkill rate.

One of the characteristics of the electronic noise in the counter is the unusual width of the TDC pulses. For the purpose of noise studies widths of TDC pulses for each counter (LFBIT) were recorded and compared. The recorded TDC pulse widths are shown in Figures A.7

This study revealed that counter 3, corresponding to LFBIT 3, was markedly different from the other counters. The timing width of the counter 3 was very short ($0 - 10$ TDC units) compared to the typical values of 110 TDC units. This was an indication of the noise in the counter. By requiring the TDC pulse width to be greater than 10 TDC units the total number of counter 3 hits was reduced by 21%, with very little change (0.1%) in the veto wall cut. However the cut on the width of the timing pulse did not reduce the veto overkill rate to the satisfactory level. Instead, the requirement of the starting time for each TDC pulse to occur during the active part of the trigger (beam) cycle was introduced. Both data with straight–through muons (Trig. 6) and the testbeam data were used to established a new timing cut. Based on a 5-σ deviation from the mean, a starting time ranging from 210 to 300 TDC counts was selected and incorporated into the veto wall cut, called "cut_lf". Running the code on the noise file under these new conditions produced the results shown in Table A.4.

In a totally efficient veto wall with no overkill, all noise events and no

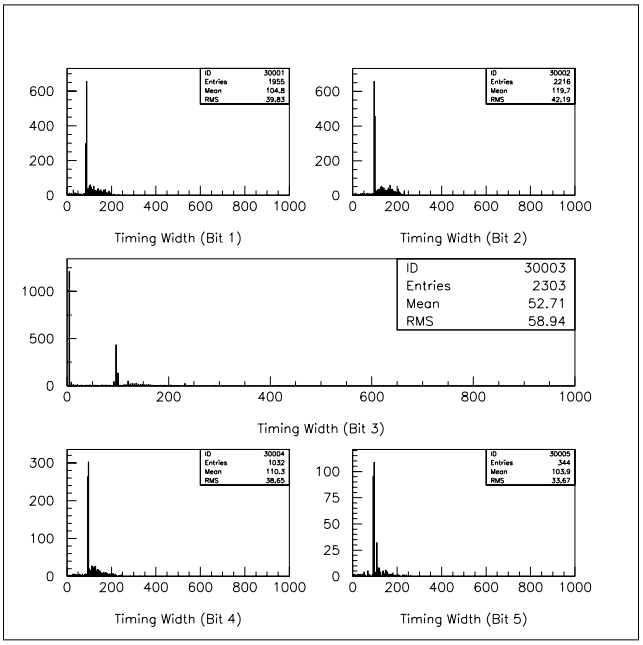

Figure A.7: The width of the TDC pulse from the veto wall counters. The plot in the middle indicates that counter 3 of the veto wall was noisy during the run.

charged particles should pass the veto wall cut. Table A.4 shows the number of noise events, straight-through muons and testbeam charged particles (hadrons) that passed this cut. The overkill rate is calculated as $1 - \frac{N_{\rm pass}}{N_{\rm tot}}$, where $N_{\rm pass}$ is the number of events that passed the veto wall cut and $N_{\rm tot}$ is the total number.

As one can see from the Table A.4, the level of the veto wall overkill was reduced from 14.2% to 0.8%.

Source	$N_{\rm tot}$	$N_{\rm pass}$	veto overkill $1 - \frac{N_{\rm pass}}{N_{\rm tot}}$
noise file with original cut	24207	20769	14.2%
noise with timing cut	24207	24187	0.82%

Table A.4: Number of noise events that pass the veto wall cut. Ideally, the noise events should not fire veto wall and should not be rejected. The last column is calculated as the 1 minus the ratio of 4th($N_{\rm pass}$) and 2nd ($N_{\rm tot}$) columns. The rate of rejection in the 1st row ("noise file") is the rate of the veto wall overkill.

A.5 Shower leakage effects on the NHL analysis

This study was relevant for the 50" box fiducial cut. We required two tracks from the vertex in the decay channel to project onto the front face of the calorimeter with projected coordinates X and Y such that, $-50'' < X < 50''$ and $-50'' < Y < 50''$. If any of the 2 tracks were a hadron, then there would be a hadron shower developed in the calorimeter. The hadron energy measurements could be different depending if the shower have been contained in the calorimeter or if it leaked through the edges. This study proved that with the 50" cut the shower leakage was less than 15%.

In the calorimeter shower studies it was determined that hadron shower leakage does not begin to effect the energy reconstruction until the shower starts at 25 cm from the calorimeter edge (see Ref. [37]). At 5" from the edge (12.7 cm) shower will leak 7.5% of its energy. This assumes that the hadron track has a small angle, which was not true in general for the decay channel. Hadrons from interactions in the downstream part of the decay channel, say in the DK 2 drift chamber, could come at the angles as large as 0.27 radians. I assumed the worse case of a 0.27 rad incident angle and approximated the shower as a cylinder with an average radius and length of the hadronic shower. The 50 GeV hadron shower had an average width of 6" and an average length of 4 counters (34.1 "). If we assume that the shower started 10" from the calorimeter edge at a 0.27 angle, then 89% of the cylinder will be outside of the calorimeter. Thus less than 11% of the shower will leak out the edge. This approximation is an overestimate of the leakage and still shows that 50" box was the appropriate choice.

Appendix B

The computer code with the NHL analysis cuts

```
      subroutine nhl_candidate(topass)

      Implicit none

C
C *-------------------------------------------------*
C |  Purpose:  select and filter NHL candidate events |
C |                                                   |
C |  INPUT:                                           |
C |  ------                                           |
C |      uses the common blocks that contain the e815 |
C |      raw data, see include                        |
C |      statements below                             |
C |                                                   |
C | OUTPUT:                                           |
C | -------                                           |
C |     variable pass                                 |
C |                                                   |
C | Author:                                           |
C | -------                                           |
C |   Arturas Vaitaitis                               |
C |   (arturv@miranda.fnal.gov), Apr 14  1998         |
C |                                                   |
C | Modified:                                         |
C | ---------                                         |
C |   Joseph Formaggio                                |
C | (josephf@beatrice.fnal.gov), Jun 3 1998           |
```

```
C | (arturv@miranda.fnal.gov), Apr 1   1999           |
C |                                                   |
C *---------------------------------------------------*

#include <dkanacuts.com>
#include <event_dk.com>
#include <record.com>
#include <comgen.com>
#include <beamline.inc>

*   output variable

      integer topass

*   local stuff

      double precision limit_vert,slope
      double precision p1,p2,op_ang,E
      double precision xvert,yvert,zvert
      double precision x_max,y_max,z_max
      double precision ch_begin,ch_end,ch_pos(2)
      double precision max_slope

      parameter (max_slope = 0.1)

      real Ratio_Energy

      parameter (Ratio_energy=0.7)

      integer i,view,idn,j,idpass,ixy

      logical icut(ncuts)
      logical cut_switch(ncuts)
      logical first, bad_signal, strip_pass

      data ch_begin/ -2280.6/
      data ch_end/   -939.7 /
      data ch_pos/  -1343.61, -1729.32/

      data first/.true./
      save first
```

```
      data cut_switch /
     $    .false.,  ! ( 1)  Strip cuts
     $    .true.,   ! ( 2)  Only two tracks
     $    .true.,   ! ( 3)  No extra tracks
     $    .true.,   ! ( 4)  Hits must be in calorimeter
     $    .true.,   ! ( 5)  Chi square on tracks
     $    .true.,   ! ( 6)  Slope cuts
     $    .true.,   ! ( 7)  Chi square on vertex
     $    .true.,   ! ( 8)  Vertex outside detector
     $    .true.,   ! ( 9)  Track flag check
     $    .true.,   ! (10)  Pid flag check
     $    .true.,   ! (11)  Energy flag check
     $    .true.,   ! (12)  ID and energy cuts
     $    .true.,   ! (13)  Transverse mass cut
     $    .true.,   ! (14)  Effective x cut
     $    .true.,   ! (15)  Effective W cut
     $    .true.,   ! (16)  Run number cut
     $    .true.,   ! (17)  Beam on cut
     $    .true.,   ! (18)  Match views valid cut
     $    .true.,   ! (19)  No pair
     $    .true./   ! (20)  LF bits cut

c-- initialise
**********************
      topass=0

      limit_vert  = 10.*(vert_ndof)

      dkcutevt = 0
      do i = 1, ncuts
        icut(i) = .false.
        dkncut(i) = 0
      enddo

**********************

      if (first) then
        first=.false.
        do i=1,ncuts
          dkncut(i)=0
        enddo
        dkntot = 0
```

```
        dkcutevt = 0
      endif

C=================================================
      dkntot=dkntot+1
c--------------------------
c-- strip cuts; Turn this on only for Monte Carlo
c-- also have to remove  any trigger
c-- requirements from strip_exotic

      if (cut_switch(1)) then
        call strip_exotic(strip_pass)
        if(.not.strip_pass) then
          dkcutevt=1
          icut(1) = .true.
        endif
      endif

c-------------------------------------
c-- require only 2 tracks in dk channel
c

      if (cut_switch(2)) then
        if (npart.ne.2) then
          dkcutevt=2
          icut(2) = .true.
        endif
      endif

c--------------------------
c-- no excess tracks

      if (cut_switch(3)) then
        if ((nx_extra.ne.0).or.(ny_extra.ne.0)) then
          dkcutevt=3
          icut(3) = .true.
        endif
      endif

c--------------------------
c-- Make sure hits not outside box
```

```
      if (cut_switch(4)) then
        bad_signal=.false.
        do view = 1,2
         do i=1,npart
          if(abs(cal_pos(view,i)).gt.50.) bad_signal=.true.
         enddo
        enddo
        if (bad_signal) then
          dkcutevt=4
          icut(4) = .true.
        endif
      endif

c---------------------------
c-- Make chi-squared cut on each track

      if(cut_switch(5)) then
        bad_signal = .false.
        do view = 1,2
          do i = 1,npart
           if (track_chi2(view,i).gt.
     +      (10.*(track_nhits(view,i)-2))) bad_signal=.true.
          enddo
        enddo
        if (bad_signal) then
          dkcutevt=5
          icut(5) = .true.
        endif
      endif

c--------------------------
c-- cut CR they have too big slope,
c-- NHL of maximum mass that we are
c-- sensitive (2GeV) with the minimum
c-- energy 10GeV will decay at maxim
c-- angle  0.06729 rads we'll take 10x0.06729
c

      if (cut_switch(6)) then
        bad_signal = .false.
        do i = 1,npart
          do ixy = 1,2
```

```
            slope = abs(p_event(ixy,i)/p_event(3,i))
            if(slope.ge.max_slope) bad_signal=.true.
          enddo
        enddo
        if (bad_signal) then
          dkcutevt = 6
          icut(6) = .true.
        endif
      endif

c-------------------------
c-- Cut on vertex chi2

      if (cut_switch(7)) then
        if(vert_chi2.gt.limit_vert) then
          dkcutevt = 7
          icut(7)=.true.
        endif
      endif

c-----------------------------------
c-- vertex outside of the detector
c
c-- cut 40 inches around DK4
c-- cut 40 inches around DK5
c-- outside the DK channel

      if (cut_switch(8)) then

        bad_signal = .false.
        xvert = vert_event(1)
        yvert = vert_event(2)
        zvert = vert_event(3)
        x_max = abs(xvert) + abs(3.0*evert_event(1))
        y_max = abs(yvert) + abs(3.0*evert_event(2))
        z_max = abs(max(40.0, 3.0*evert_event(3)))

        if (x_max.gt.50.0) bad_signal=.true.
        if (y_max.gt.50.0) bad_signal=.true.
        if (zvert.lt.(ch_begin+z_max))
     +      bad_signal=.true.
        if (zvert.gt.(ch_end  -z_max))
```

```
     +       bad_signal=.true.
          do i = 1,2
            if (abs(zvert - ch_pos(i)).lt.z_max)
     +         bad_signal=.true.
          enddo

          if (bad_signal) then
            dkcutevt=8
            icut(8) = .true.
          endif
        endif

c--------------------------------
c-- Cut on flags

        if (cut_switch(9)) then
          bad_signal = .false.
          do i = 1,npart
            if (good_track(i).ne.0) bad_signal=.true.
          enddo
          if (bad_signal) then
            dkcutevt=9
            icut(9) = .true.
          endif
        endif

c--------------------------------
c-- Cut on flags

        if (cut_switch(10)) then
          bad_signal = .false.
          do i = 1,npart
            if (good_pid(i).ne.0) bad_signal=.true.
          enddo
          if (bad_signal) then
            dkcutevt=10
            icut(10) = .true.
          endif
        endif

c--------------------------------
c-- Cut on flags
```

```
       if (cut_switch(11)) then
         bad_signal = .false.
         do i = 1,npart
           if (good_e(i).ne.0) bad_signal=.true.
         enddo
         if (bad_signal) then
           dkcutevt=11
           icut(11)=.true.
         endif
       endif

c-------------------------------
c-- Place id and energy cuts

       if (cut_switch(12)) then
         bad_signal = .false.

         do i = 1,npart
           idn = 0
           if ((pid_event(i).gt.0).
     +          and.(pid_event(i).lt.10)) idn=1
           if ((pid_event(i).gt.9).and.
     +          (pid_event(i).lt.20)) idn=2
           if ((pid_event(i).gt.19).and.
     +           (pid_event(i).lt.30)) idn=3
           E = p_event(4,i)
           if (idn.gt.0) then
             if ((idn.eq.1).and.(E.lt.2.2))
     +           bad_signal = .true.
             if ((idn.gt.1).and.(E.lt.10.0))
     +           bad_signal = .true.
           endif
         enddo

         if (bad_signal) then
           dkcutevt=12
           icut(12) = .true.
         endif

       endif
```

```
      if (cut_switch(13)) then
        if (trans_mass.gt.3.) then
          dkcutevt = 13
          icut(13) = .true.
        endif
      endif

      if (cut_switch(14)) then
        if (eff_x.gt.0.1) then
          dkcutevt = 14
          icut(14) = .true.
        endif
      endif

      if (cut_switch(15)) then
        if (eff_W.lt.2.) then
          dkcutevt = 15
          icut(15) = .true.
        endif
      endif

      if (idatim.ge.790000000) then
c
c       These are cuts specific to data and
c       are not applied to MC
c       ========================================
        if (cut_switch(16)) then
          if (run.lt.5583) then
            dkcutevt = 16
            icut(16) = .true.
          endif
        endif

        if (cut_switch(17)) then
          call fill_beamline(run,event,igate,cycle)
          if (pot_spill.le.5.0E11) then
            dkcutevt = 17
            icut(17) = .true.
          endif
        endif

      endif ! Not MC Data
```

```
      if (cut_switch(18)) then
        if (good_matching.ne.0) then
          dkcutevt = 18
          icut(18) = .true.
        endif
      endif

      if (cut_switch(19)) then
        if (no_pairs.ne.0) then
          dkcutevt = 19
          icut(19) = .true.
        endif
      endif

      if (cut_switch(20)) then
        if (good_lf.ne.0) then
          dkcutevt = 20
          icut(20) = .true.
        endif
      endif

c   Done with cuts.  Now check which events pass.

      if (dkcutevt.gt.0) then   ! Event fails
        do i = 1,ncuts
          if (icut(i)) dkncut(i) = 1
        enddo
        return
      endif

c-----------------------------------------
c-- Now all cuts have been passed.
c-- Assign topass
c-- TOPASS = 6 (two pions)
c-- TOPASS = 5 (two electrons)
c-- TOPASS = 4 (one pion, one electron)
c-- TOPASS = 3 (one muon, one electron)
c-- TOPASS = 2 (one muon, one pion)
c-- TOPASS = 1 (two muons)
c-----------------------------------------
```

```
 topass = 0
 idpass = 0

 do i = 1, 2
   if ((pid_event(i).gt.0).and.
+  (pid_event(i).lt.10)) then
     idpass = idpass + 1
   elseif ((pid_event(i).gt.9).and.
+    (pid_event(i).lt.20)) then
     idpass = idpass + 10
   elseif ((pid_event(i).gt.19).and.
+    (pid_event(i).lt.30)) then
     idpass = idpass + 100
   endif
 enddo

 if (idpass.eq.2  ) topass = 1       ! MUON + MUON
 if (idpass.eq.11 ) topass = 2       ! MUON + PION
 if (idpass.eq.101) topass = 3       ! MUON + ELECTRON
 if (idpass.eq.110) topass = 4       ! PION + ELECTRON
 if (idpass.eq.200) topass = 5       ! ELECTRON + ELECTRON
 if (idpass.eq.20 ) topass = 6       ! PION + PION


 if (idatim.ge.790000000) then   !i.e. Not MC data
   print*,'Event #',dkntot,' passed. Run,
+     event = ',run,event
 endif

 return
 end
```

Appendix C

The article published in Phys.Rev.Lett. [26]

Search for Neutral Heavy Leptons in a High-Energy Neutrino Beam

A. Vaitaitis,[2] R. B. Drucker,[6] J. Formaggio,[2] S. Koutsoliotas,[2] T. Adams,[4] A. Alton,[4] S. Avvakumov,[7] L. de Barbaro,[5] P. de Barbaro,[7] R. H. Bernstein,[3] A. Bodek,[7] T. Bolton,[4] J. Brau,[6] D. Buchholz,[5] H. Budd,[7] L. Bugel,[3] J. Conrad,[2] B. T. Fleming,[2] R. Frey,[6] J. Goldman,[4] M. Goncharov,[4] D. A. Harris,[7] R. A. Johnson,[1] J. H. Kim,[2] M. J. Lamm,[3] W. Marsh,[3] D. Mason,[6] K. S. McFarland,[3,7] C. McNulty,[2] J. Monroe,[2] D. Naples,[4] P. Nienaber,[3] A. Romosan,[2] W. K. Sakumoto,[7] H. Schellman,[5] M. H. Shaevitz,[2] P. Spentzouris,[2] E. G. Stern,[2] M. Vakili,[1] V. Wu,[1] U. K. Yang,[7] J. Yu,[3] G. P. Zeller,[5] and E. D. Zimmerman[2]

[1]*University of Cincinnati, Cincinnati, Ohio 45221*
[2]*Columbia University, New York, New York 10027*
[3]*Fermi National Accelerator Laboratory, Batavia, Illinois 60510*
[4]*Kansas State University, Manhattan, Kansas 66506*
[5]*Northwestern University, Evanston, Illinois 60208*
[6]*University of Oregon, Eugene, Oregon 97403*
[7]*University of Rochester, Rochester, New York 14627*

(Received 4 August 1999)

A search for neutral heavy leptons (NHLs) has been performed using an instrumented decay channel at the NuTeV (E-815) experiment at Fermilab. The data were examined for NHLs decaying into muonic final states ($\mu\mu\nu$, $\mu e\nu$, $\mu\pi$, and $\mu\rho$); no evidence has been found for NHLs in the 0.25–2.0 GeV mass range. This analysis places limits on the mixing of NHLs with standard light neutrinos at a level up to an order of magnitude more restrictive than previous search limits in this mass range.

PACS numbers: 13.15.+g, 13.35.Hb, 14.60.Pq, 14.80.–j

Various extensions [1,2] to the standard model, including most grand unified theories, predict neutral heavy leptons (NHLs, or "heavy neutrinos") which can mix with the standard light neutrinos. In these extensions, the NHLs are weak isosinglets which do not couple directly to the Z and W bosons, but can be produced and decay via mixing with the standard model neutrinos. Figure 1 shows one possible set of tree-level diagrams for NHL production and decay.

NHLs are expected to decay (e.g., Fig. 1b) as heavy neutrinos into a light neutrino and two charged leptons, into a lepton and two quarks, or into three neutrinos. The NHL decay width is proportional to the phase space available for the decay, as well as the mixing parameter $|U|^2$ [1]. In general, there may be three different mixing parameters (U_e, U_μ, U_τ) which describe mixing of the heavy NHL state with the three weak neutrino flavor eigenstates.

The E815 (NuTeV) neutrino experiment at Fermilab has performed a search for these NHLs by combining the capabilities of a high-intensity neutrino source with an instrumented decay region. NHLs may be created in the NuTeV beam line by the decays of secondary mesons produced by the Tevatron proton beam. During the 1996–1997 fixed-target run at Fermilab, NuTeV received 2.54×10^{18} 800 GeV protons on a BeO target with the detector configured for this search. A sign-selected quadrupole train focused secondary π and K mesons down a beam line 7.8 mrad from the primary proton beam direction. 1.13×10^{18} protons were received with the magnets set to focus positive mesons, and 1.41×10^{18} protons with negative meson focusing. The mesons could decay into NHLs as shown in Fig. 1a. The production of secondary pions and kaons was simulated using the parametrization in Ref. [3]; the Decay Turtle program [4] simulated the propagation of charged particles through the beam line.

NHLs may also be produced by prompt decays of charmed mesons produced by incident protons on the BeO target and proton dumps. These processes were simulated using a Monte Carlo (MC) program based on measured production cross sections [5]. The effects of decay phase space, NHL polarization, and helicity

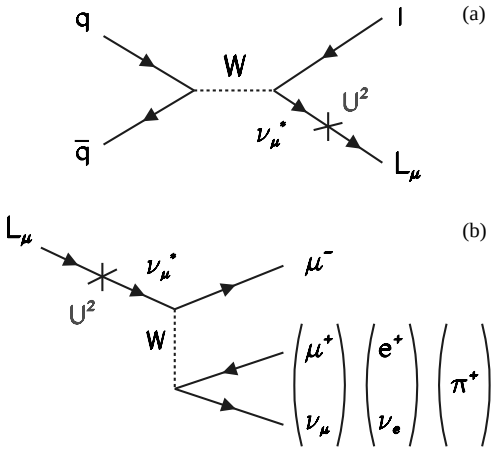

FIG. 1. Feynman diagrams for the (a) production and (b) decay of neutral heavy leptons (L_μ). $|U|^2$ is the mixing between the muon neutrino and the NHL. (The alternative allowed decay via a Z boson is not shown.)

0031-9007/99/83(24)/4943(4)$15.00

suppression [6] were included in the simulation of the production and decays. For NHLs of mass 1.45 GeV from D meson decay, the average momentum was ~ 100 GeV; for the 0.35 GeV NHLs coming mainly from K decay, the average momentum was ~ 140 GeV.

This analysis reports the results of a search for muonic decays of NHLs with masses between 0.25 to 2.0 GeV. We searched for $\mu e \nu$, $\mu\mu\nu$, $\mu\pi$, and $\mu\rho$ final states. In the standard mixing model [1,7], the expected ratio of decay rates for $\mu\pi{:}\mu e\nu{:}\mu\mu\nu$ is 3.5:1.6:1.0. The $\mu\rho$ channel is significant only for NHL masses above 1 GeV, where it is comparable to the $\mu\pi$ mode.

Charged tracks from NHL decays were detected by an instrumented decay channel (shown in Fig. 2) 1.4 km downstream of the production target. A 4.6 m $\times$ 4.6 m array of plastic scintillators vetoed charged particles entering from upstream. The decay channel was 34 m long, interspersed with 3 m $\times$ 3 m multiwire argon-ethane drift chambers positioned at 15.4, 25.2, 35.5, 36.8, and 38.5 m downstream of the veto array. Tracks were reconstructed from drift chamber hits and grouped to form candidate decay vertices. Typically, a vertex from a NHL of mass 1.15 GeV was reconstructed with a resolution of 0.04 cm in the transverse direction and 28 cm in the longitudinal direction. The region between the drift chambers was filled with helium contained in cylindrical plastic bags 4.6 m in diameter.

The Lab E neutrino detector [8], located immediately downstream of the decay channel, provided final state particle identification, energy measurement, and triggering. This detector consisted of a 690-ton iron-scintillator sampling calorimeter followed by a toroidal muon spectrometer. Drift chambers were positioned every 20 cm along the length of the calorimeter, and 2.5 cm-thick liquid scintillator counters were interleaved with 10 cm steel plates along the length of the calorimeter. The trigger selected events with a penetrating muon or at least 6 GeV of hadronic or electromagnetic energy in the calorimeter. Off-line, hits in the calorimeter drift chambers were analyzed to determine if they formed a track (consistent with a muon) or a cluster of hits (consistent with an electron or pion shower).

Tracks found in the decay channel were linked to clusters or tracks in the calorimeter. Pulse height information from the scintillation counters was used to determine hadronic or electromagnetic energy deposition; the hadronic energy resolution of the calorimeter was $\frac{\sigma}{E} = 0.024 \oplus \frac{0.87}{\sqrt{E}}$, and the electromagnetic energy resolution was $\frac{\sigma}{E} = 0.040 \oplus \frac{0.52}{\sqrt{E}}$. Muon energies were determined either by the toroid spectrometer (with 11% resolution) or by range (with a resolution of 155 MeV). The energy of muons which exited through the side of the calorimeter was determined from the track's multiple scattering, with a resolution of 25% for energies lower than 85 GeV.

The following processes were the main backgrounds to this search: (1) neutrino interactions within the helium; (2) neutrino interactions in the material upstream of the decay channel, where a neutral kaon survived to the decay channel and decayed in the fiducial volume; and (3) neutrino interactions in the material surrounding the decay channel. Neutrino interaction backgrounds could arise from low multiplicity resonance production or from deep inelastic scattering (DIS). Resonance production was simulated using the calculations of Belusevic and Rein [9]; such events were characterized by a high-energy muon accompanied by a low-energy pion track. The Lund MC program was used to simulate DIS events [10]. While these were generally of high multiplicity, events with few or poorly reconstructed tracks could contribute to the two-track background. The detector was simulated using the GEANT [11] MC, which produced a hit-level simulation of raw data including beam and cosmic ray related noise hits. These were processed using the same analysis routines as those used for the data.

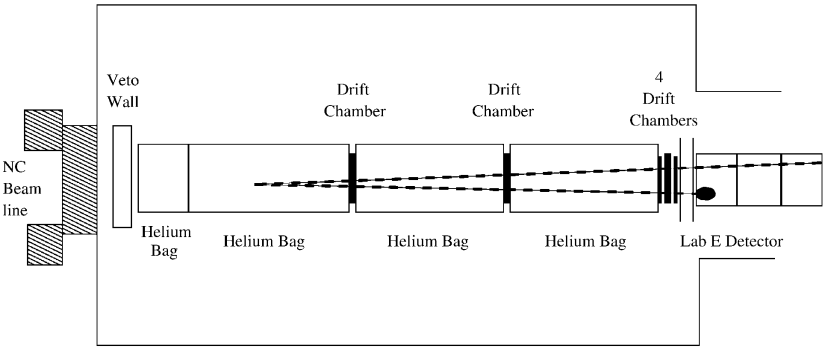

FIG. 2. A schematic diagram of the NuTeV decay channel. The beam enters from the left; at the far right is the Lab E calorimeter. An example NHL decay to $\mu\pi$ is also shown. The event appears as two tracks in the decay channel, and a long muon track and a hadronic shower in the calorimeter.

Backgrounds from cosmic rays were estimated using a sample of cosmic ray muons which interacted in the target calorimeter; an upper limit of 10^{-3} background events was determined. We have therefore ignored cosmic rays in the final background estimate.

Event selection criteria maintained high efficiency for the NHL signal while minimizing known backgrounds. Cuts fell into two broad categories: reconstruction and kinematic.

Reconstruction cuts isolated events with a two-track decay vertex within the decay channel fiducial volume and no charged particle identified in the upstream veto system. The two tracks were required to be well reconstructed, have an accompanying energy measurement, and form a common vertex. Large angle tracks arising from cosmic rays were removed by requiring tracks to form an angle of less than 0.1 rad with the beam direction. Exactly two tracks were required, both projecting to the calorimeter, with at least one of the two identified as a muon. To ensure good particle identification and energy measurement, muons were required to have an energy greater than 2.0 GeV; an energy greater than 10.0 GeV was required for electrons or hadrons. (The latter cut eliminated the low-energy pions associated with resonance production.) The reconstructed two-track decay vertex was required to be at least 1 m from any material in the drift chambers.

The kinematic cuts were designed to remove the remaining DIS and resonance backgrounds. The effective scaling variables x_{eff} and W_{eff} were calculated for each event under the following assumptions: (1) the event was a neutrino charged current interaction ($\nu N \rightarrow \mu N' X$); (2) the highest energy identified muon was the outgoing particle from the lepton vertex; and (3) the missing transverse momentum in the event was carried by an undetected final state nucleon. Specifically, $x_{\text{eff}} \equiv \frac{Q^2_{\text{vis}}}{2m_p \nu_{\text{vis}}}$ and $W_{\text{eff}} \equiv \sqrt{m_p^2 + 2m_p \nu_{\text{vis}}/c^2 - Q^2_{\text{vis}}/c^2}$, where Q^2_{vis} is the reconstructed momentum transfer squared, m_p is the mass of the proton, and ν_{vis} is the reconstructed hadron energy. Requiring $x_{\text{eff}} < 0.1$ reduced backgrounds from DIS; requiring $W_{\text{eff}} > 2.0\ \text{GeV}/c^2$ removed quasielastic and resonance backgrounds. Since we could not reconstruct the true mass of the NHL due to the missing neutrino, a cut was applied on the "transverse mass," $m_T \equiv |p_T| + \sqrt{p_T^2 + m_V^2}$. p_T is the component of the total momentum perpendicular to the beam direction, and m_V is the invariant mass for the two charged tracks. Requiring $m_T < 3.0$ GeV removed additional DIS background.

The NHL and background acceptances and reconstruction efficiencies were calculated from the hit-level MC simulation. For a range of NHL masses from 0.25 to 2.0 GeV, mesons were allowed to decay in the beam line to muons and NHLs. The NHLs from these decays were propagated to the decay channel, weighted by their decay and the meson production probability, and allowed to decay in the decay channel producing hits in the drift chambers and depositing energy in the calorimeter. These simulated raw data were reconstructed with the same programs used for the data including the above reconstruction and kinematic cuts. For NHL decays generated within the decay channel fiducial volume, the average acceptance was 23% for masses between 0.25 and 2.0 GeV. From the background simulation, the calculated background contributions for the full data sample after cuts are listed in Table I.

TABLE I. Backgrounds to the NHL search.

Background source description	Number of events
ν interactions in the helium	0.56 ± 0.15
K^0 punch-through	0.005 ± 0.001
ν interactions in drift chambers	0.002 ± 0.001

Neutrino interactions in the drift chambers were used to cross check the MC calculations of backgrounds and efficiencies. For example, as a check on the two-track reconstruction efficiency, we have compared the fourteen two-track data events with vertices in the drift chambers to the MC prediction of 15 ± 2 events. Figure 3 shows comparisons of distributions for the previously introduced DIS variables, x_{eff}, W_{eff}, Q^2_{eff} as well as m_T and $y_{\text{eff}} \equiv \frac{E_\nu - E_\mu}{E_\nu}$. Data events with >2 tracks also showed good agreement with the MC prediction: 280 events were predicted, and 275 were observed.

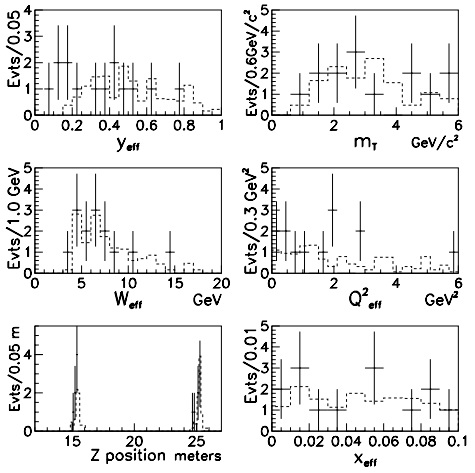

FIG. 3. Kinematic distributions for data (crosses) and MC DIS background (dashed) events with two-track vertices reconstructed in the decay channel drift chambers. MC events are absolutely normalized to the number of protons on target. The DIS reconstructed variables y_{eff}, W_{eff}, Q^2_{eff}, x_{eff} and m_T are defined in the text. Z positions are referenced to the veto array; spikes in the Z distribution correspond to the locations of the decay channel drift chambers.

TABLE II. Systematic uncertainties on the sensitivity of the NHL search.

Source	NHL mass (GeV/c^2) 0.38	0.85	1.45
D production	···	44.6%	44.0%
K production	20.7%	···	···
D_S production	···	5.6%	5.4%
Alignment	1.0%	0.4%	0.02%
Resolution model	9.3%	7.0%	0.8%
Reconstruction eff.	17.0%	19.1%	17.0%
Total Syst.	28.4%	49.3%	47.5%

For the full NuTeV data sample, no data events passed all cuts. This is consistent with the expected background of 0.57 ± 0.15 events. We have set limits from this null result by using the MC prediction for $N_{\mathrm{pred}}(m_{\mathrm{NHL}}, |U|^2)$, the normalized number of NHL events expected in the decay channel as a function of mass and $|U|^2$. The 90% confidence level limit for a given mass was calculated for the null observation by finding the $|U|^2$ value for each mass such that $N_{\mathrm{pred}}(m_{\mathrm{NHL}}, |U|^2) = 2.3$ events.

The statistical 90% confidence level limit was modified by the addition of systematic uncertainties on the NHL sensitivity. These uncertainties are summarized in Table II. Experimental uncertainties on the D production cross section [5] and on the K meson flux MC [4] were the dominant contributions to the systematic error. The systematic uncertainties were incorporated into the 90% confidence level limit by adding in quadrature a fractional error term corresponding to the systematic uncertainty for a given mass. Since the NHL rate was proportional to $|U|^4$, adding the systematic uncertainties increased the $|U|^2$ limit by 4%(14%) at 0.35(1.45) GeV.

Figure 4 shows the limits obtained from this search for the NHL-ν_μ mixing parameter $|U_\mu^2|$ as a function of the mass of the NHL. The limits are for NHL decay modes containing a muon in the standard mixing model presented above. Also shown in Fig. 4 are the results of previous experiments [12–16].

In summary, we have searched for NHLs in the mass range from 0.25 to 2.0 GeV that mix with muon neutrinos. No evidence for NHL production was observed. New limits have been set that are up to an order of magnitude better than previous searches in the lower mass range.

This research was supported by the U.S. Department of Energy and the National Science Foundation. We thank the staff of FNAL for their contributions to the construction and support of this experiment during the 1996–1997 fixed target run.

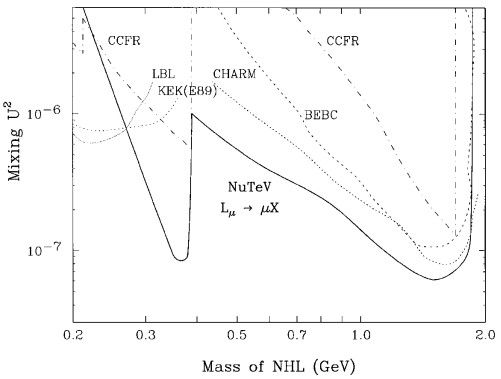

FIG. 4. NuTeV 90% confidence level limit for U_μ^2, the mixing of NHLs to standard model left-handed muon neutrinos, as a function of NHL mass. The solid line in the figure corresponds to the limit with systematic errors included.

[1] M. Gronau, C. N. Leung, and J. L. Rosner, Phys. Rev. D **29**, 2539 (1984).
[2] Particle Data Group, C. Caso *et al.*, Eur. Phys. J. **C3**, 1 (1998).
[3] A. Malensek, FNAL-FN-341, 1981.
[4] D. C. Carey, K. L. Brown, and F. C. Iselin, SLAC-0246, 1982.
[5] R. Ammar *et al.*, Phys. Rev. Lett. **61**, 2185 (1988); K. Kodoma *et al.*, Phys. Lett. B **263**, 573 (1991). [See also S. Frixione *et al.*, Nucl. Phys. **B431**, 453 (1994).]
[6] J. A. Formaggio *et al.*, Phys. Rev. D **57**, 7037 (1998).
[7] L. M. Johnson, D. W. McKay, and T. Bolton, Phys. Rev. D **56**, 2970 (1997).
[8] W. Sakumoto *et al.*, Nucl. Instrum. Methods Phys. Res., Sect. A **294**, 179 (1990).
[9] R. Belusevic and D. Rein, Phys. Rev. D **38**, 2753, (1988).
[10] G. Ingelman *et al.*, Comput. Phys. Commun. **101**, 108 (1997).
[11] CERN CN/ASD, GEANT detector description and simulation library 1998.
[12] S. R. Mishra *et al.*, Phys. Rev. Lett. **59**, 1397 (1987).
[13] A. M. Cooper-Sarkar *et al.*, Phys. Lett. **B160**, 207 (1985).
[14] J. Dorenbosch *et al.*, Phys. Lett. **B166**, 473 (1986).
[15] T. Yamazaki *et al.*, in *Proceedings of Neutrino 84* (World Scientific, Singapore, 1985).
[16] C. Y. Pang *et al.*, Phys. Rev. D **8**, 1989 (1973).

Bibliography

[1] W. Pauli "Letter to the Physical Society of Tubingen", reproduced in Physics Today **31** 9,23 (1971).

[2] R.P. Feynman, M. Gell-Mann, Phys. Rev. **109**, 193 (1958).

[3] B.J. King, *et al.*, Nucl. Instrum. Methods. **A 302**, 179 (1990).

[4] C. Athanassopolous *et al.*, Phys. Rev. Lett. **77**, 3082 (1996).

[5] Y. Fukuda *et al.*, hep-ex/9908049 Phys. Lett **467**, 185-193 (1999)

[6] F. Bohm and P. Vogel, "Physics of Massive Neutrinos" (Cambridge University Press, Cambridge, 1987)

[7] F. Reines and C. L. Cowan Phys.Rev. **90**, 492 (1953).

[8] G. Danby *et al.* Phys. Rev. Lett. **9**, 36 (1962).

[9] M.L.Perl *et al.* Phys.Rev.Lett. **35**, 1489 (1975). Neutrinos" (Cambridge University Press, Cambridge, 1987)

[10] J.Conrad, talks Inner Space/Outer Space and Panic (1999)

[11] D.Buskulic *et al.* Phys. Lett. **D313**, 520-534 (1993)

[12] R.M.Barnett *et al.* "Review of Particle Physics", Phys. Rev. **D54**, 1 (1996)

[13] H.B.Thacker, J.J.Sakurai, Phys.Lett. **B36**, 103-105 (1971).

[14] M. Davier, B.H. Wiik (SLAC), SLAC-TN-71-021

[15] R.S.Hayano, T.Yamazaki *et al.*, Phys.Rev.Lett. **49**, 1305 (1982).

[16] C.Y. Pang *et al.*, Phys. Rev. **D8**, 1989 (1973).

[17] J. Dorenbosch *et al.*, Phys. Lett. **B166**, 473 (1986).

[18] A.M. Cooper-Sarkar *et al.*, Phys. Lett. **B160**, 207 (1985).

[19] G.Bernardi *et al.*, Phys. Lett. **B166**, 479 (1986).

[20] M.Acciarri *et al.*, Phys. Lett. **B462**, 354-364 (1996)

[21] D.Buskulic *et al.*, Phys. Lett. **B384**, 439-448 (1996)

[22] P.Abreu . *et al.*, Z.Phys. **C74**, 57-71 (1997)

[23] C.Oehler . *et al.*, Proc. 6th Topical seminar on Part. Phys. and Astro., Miniato (1999)

[24] B.Armbruster *et al.*, Phys. Lett. **348**, 19-28 (1995)

[25] S.R.Mishra *et al.*, Phys. Rev. Lett. **59**, 1397 - 1400 (1987)

[26] A.Vaitaitis *et al.*, Phys. Rev. Lett. **83**, 4943-4946 (1999)

[27] D. Michael, Conference Proceedings WIN95, (1995)

[28] H.M. Gallagher, M.C. Goodman, "Neutrino Cross Section", Conference Proceedings NuMi-112, Talloires, France (1995)

[29] Rein and Sehgal, Annals Phys. 133:79, 1981.

[30] Tim Bolton, McNuTeV manual, Fermilab, NuTeV internal memo, unpublished (1995), "http://www-e815.fnal.gov/ arturv/mcnutev.ps"

[31] R.Mohapatra and G.Senjanovic, Phys. Rev. **D23**, 165-180 (1981)

[32] M. Gell-Mann, P. Ramond and R. Slansky, in "Supergravity", ed. F. van Nieuwenhuizen and D. Freedman, (North Holland, Amsterdam, 1979) p. 315; T. Yanagida, Proc. of the Workshop on Unified Theory and the Baryon Number of the Universe, KEK, Japan (1979)

[33] P.Langacker "Neutrino Physics", ed. H.V. Klapdor and B. Pohv (Berlin, 1988); P.Langacker "Proceedings of TASI-90", ed. M.Cvetic and P.Langacker (Word Scientific, Singapore, 1991)

[34] E. Witten, Phys. Lett., (**B91**) 81, (1980)

[35] www-e815.fnal.gov/ e815/hardware_memos.html, "E815 SSQT alignment requirements" (1994) ,"Test run for SSQT alignment" (1995)

[36] www-e815.fnal.gov/ e815/hardware_memos.html, NuTeV hardware memoranda "E815 Data aquisition system", (1994)

[37] J.Yu *et al.* (NuTeV Collab.), Submitted to Nucl. Instr. Meth., hep-ex/9908056 (FERMILAB-PUB-99-024-E) (1999)

[38] NuTeV Drift Chamber Log book, Fermilab (1996-1997)

[39] J.Conrad "NHL Limits: Production and Background Studies" Fermilab, NuTeV internal memo, unpublished, "http://www-e815.fnal.gov/ jconrad/nhl/nhl_study.ps" (1995)

[40] L.M. Johnson, D.W. McKay, and T. Bolton, *Phys. Rev.* **D56**, 2970 (1997).

[41] J.Formaggio *et al.*, Phys.Rev. **D57** 7037-7040 (1998).

[42] M. Gronau, C.N. Leung, and J.L. Rosner, *Phys. Rev.* **D29**, 2539 (1984).

[43] A. Malensek, FNAL-FN-341 (1981)

[44] D. Carey, K. Brown, F.C. Iselin Decay TURTLE: A Computer Program for Simulating Charged Particle Beam Transport Systems, SLAC-0246, 71 (1982).

[45] Atherton *et al.* CERN 80-07, (1980)

[46] Paul Quintas, Ph.D. Thesis, Columbia University (1992).

[47] G. Ingelman *et al., Comput. Phys. Commun.* **101**, 108 (1997).

[48] CERN CN/ASD, GEANT detector description and simulation library, CERN Program Library Long Writeups Q123, Cern Geneva (1997),http://wwwinfo.cern.ch/asdoc/geantold/GEANTMAIN.html

[49] J.Botts *et al.*, Phys. Lett. **304**, 159 (1993).

[50] E815 spec files; on labE cluster "*e815_spec/data/dcpos.spec0020*";

[51] Torbjorn Sjostrand *et al.*, CERN CN/ASD, The LUND Monte Carlo for the jet fragmentation (1997).

[52] Private discussion with G.Ingelman, one of the authors of Lepto.

[53] K. Kodama *et al.*(E653 Coll.) Phys. Lett.**B263**, 573 (1991).

[54] G.A. Alves *et al.*, Phys. Rev. Lett. **77**,2388 (1996).

[55] S.Frixione, M.L.Mangano, P.Nason, G.Ridolfi (CERN-TH-97-16) hep-ph/9702287, to be published in "Heavy Flavours II", ed. A.J.Buras, M.Linder, 609-706 (1997).

[56] A. Vaitaitis and NHL group, "the NHL memo", Fermilab, NuTeV internal memo, unpublished (1998), "http://www-e815.fnal.gov/ arturv/nhl_memo/"

[57] S. Koutsoliotas, Efficiency of the Lab F Veto Wall in the Decay Channel, Fermilab, E815 internal memo, unpublished (1998) "http://www-e815.fnal.gov/ arturv/vetowall.ps"

[58] CERN CN/ASD, The ZEBRA system, Cern Program Library Long Writeups Q100/Q101, Cern Geneva (1995) , http://wwwinfo.cern.ch/asdoc/zebra_html3/zebramain.html

[59] CERN CN/ASD, MINUIT, fitting routine, Cern Program Library Long Writeups D506, Cern Geneva (1995)

[60] Bruce J. King, PhD Thesis, Columbia University, Nevis preprint 284, unpublished (1994).

[61] Bill Seligman, PhD Thesis, Columbia University, Nevis preprint 292, unpublished (1997).

[62] J. Formaggio *et al.*, hep-ex/9912062 submitted to Phys. Rev. Lett., (1999).

[63] NuTeV collab., "Software available in CVS" Fermilab, NuTeV internal memo, unpublished (1995), "http://www-e815.fnal.gov/cvs_software.html"